NASA CONTRACTOR REPORT

NASA CR-2617

A STUDY OF AIR-TO-GROUND SOUND PROPAGATION USING AN INSTRUMENTED METEOROLOGICAL TOWER

Peter K. Kasper, Richard S. Pappa,
Laurence R. Keefe, and Louis C. Sutherland

Prepared by
WYLE LABORATORIES
Hampton, Va. 23666
for Langley Research Center

NATIONAL AERONAUTICS AND SPACE ADMINISTRATION • WASHINGTON, D. C. • OCTOBER 1975

1. Report No.	2. Government Accession No.	3. Recipient's Catalog No.
NASA CR-2617		

4. Title and Subtitle
A STUDY OF AIR-TO-GROUND SOUND PROPAGATION USING AN INSTRUMENTED METEOROLOGICAL TOWER

5. Report Date
October 1975

6. Performing Organization Code

7. Author(s)
Peter K. Kasper, Richard S. Pappa, Laurence R. Keefe, and Louis C. Sutherland

8. Performing Organization Report No.

10. Work Unit No.

9. Performing Organization Name and Address
Wyle Laboratories
3200 Magruder Boulevard
Hampton, Virginia 23666

11. Contract or Grant No.
NAS1-12841

13. Type of Report and Period Covered
Contractor Report

12. Sponsoring Agency Name and Address
National Aeronautics and Space Administration
Washington, D. C. 20546

14. Sponsoring Agency Code

15. Supplementary Notes
FINAL REPORT

16. Abstract

This report provides the results of an exploratory NASA study leading toward a better understanding of the effects of meteorological conditions on the propagation of aircraft noise. The experimental program utilized a known sound source fixed atop an instrumented meteorological tower. The basic experimental scheme consisted of measuring the amplitude of sound radiated toward the ground along a line of microphones fixed to a tower guy wire. The experimental results showed the feasibility of this approach in the acquisition of data indicating the variations encountered in the time-averaged and instantaneous amplitudes of propagated sound. The investigation included a consideration of ground reflections, a comparison of measured attenuations with predicted atmospheric absorption losses, and an evaluation of the amplitude fluctuations of recorded sound pressures.

17. Key Words (Suggested by Author(s))		18. Distribution Statement
Aircraft Noise	Meteorological	Unclassified - Unlimited
Propagation	Attenuation Mechanism	
Atmosphere	Fluctuation Spectrum	Subject Category 32
Sound	Excess Absorption	

19. Security Classif. (of this report)	20. Security Classif. (of this page)	21. No. of Pages	22. Price*
Unclassified	Unclassified	94	$4.75

For sale by the National Technical Information Service, Springfield, Virginia 22161

SUMMARY

This report provides the results of a pilot NASA program to develop a greater understanding of the effects of the atmosphere on sound propagation. This exploratory study utilized a known sound source fixed at the top of a 150-meter meteorological tower radiating toward the ground along a linear array of microphones supported by a tower guy wire. Sinusoidal signals were systematically radiated along the fixed propagation path, and resulting sound pressures were recorded at each of the four microphones. The data reduction and analysis of the recorded signals incorporated an examination of both time-averaged and instantaneous sound amplitude fluctuations.

The experimental program, in general, provided a demonstration of the feasibility of using an instrumented tower to study air-to-ground sound propagation. The measured results included data indicating the influence of ground reflections and the degree of amplitude fluctuations in propagated sound. A comparison of time-averaged measured results with predicted atmospheric absorption losses failed to show a consistent trend in attenuation in excess of absorption effects. No evidence of saturation of the instantaneous amplitude fluctuations was found for the propagation distances and turbulent conditions evaluated. Attempted correlation of the sound amplitude fluctuation data with meteorological data indicated a potential relation between the induced sound fluctuation and the meteorological parameter, Richardson number.

CONTENTS

		Page
	SUMMARY	iii
1.0	INTRODUCTION	1
2.0	BACKGROUND.	2
2.1	Spreading Losses	2
2.1.1	Uniform Spherical Spreading	2
2.1.2	Reflection by Boundaries	3
2.1.3	Refraction by Nonuniform Atmosphere	3
2.1.4	Scattering by Nonstationary or Turbulent Atmosphere	3
2.2	Absorption Losses	4
2.2.1	Atmospheric Absorption Losses	4
2.2.2	Absorption Losses by Ground Surface and Ground Cover.	4
2.3	Unsteady Propagation Effects	4
3.0	APPARATUS AND METHODS	5
3.1	Experimental Program	5
3.1.1	Description of Test Site.	5
3.1.2	Test Configuration	5
3.1.3	Field Instrumentation	6
3.1.4	Test Program	7
3.1.5	Experimental Procedure	7
3.2	Data Reduction Equipment and Procedure	8
3.2.1	Time Histories	8
3.2.2	Tone Bursts.	9
3.2.3	Long-Time-Averaged Sound Pressure Levels	9
3.2.4	Sound Pressure Level Amplitude Distribution	9
3.2.5	RMS Fluctuation Amplitudes.	10
3.2.6	Fluctuation Spectra.	10
3.2.7	Weather Data	10
4.0	RESULTS	11
4.1	Effects of Ground Reflections	11
4.2	Analysis of Long-Time-Averaged Sound Levels	14
4.3	Sound Fluctuations Due to Atmospheric Effects	17
4.3.1	Envelope Fluctuations	17
4.3.2	Sound Level Amplitude Histograms.	19
4.3.3	Correlation of Sound Fluctuation Data with Weather Conditions.	20

CONTENTS (Continued)

		Page
5.0	CONCLUDING REMARKS	21
APPENDIX A	Atmospheric Absorption Prediction Model	23
APPENDIX B	Compilation of Measured Sound Pressure Level Histograms	25
REFERENCES		27

TABLES AND FIGURES

Table		Page
I	Tabulation of Meteorological Conditions During Test Runs	31
II	Compilation of Data from 8-Cycle Tone Burst Tests	32
III	Long-Time-Averaged Sound Pressure Levels	33
IV	Calculated Atmospheric Absorption Losses	34
V	Normalized RMS Envelope Fluctuations	35

Figure		Page
1	View of Test Site	37
2	Profile Sketch of Haswell Tower Showing Positions of Microphones Along East Guy Wire	38
3	Close-Up of Microphone Carriage	39
4	View of Top of Tower Showing First Microphone Position	40
5	Block Diagram of Field Instrumentation	41
6	Measured Directivity Pattern of Sound Source	42
7	Sketch of Microphone System Components	43
8	Block Diagrams of Data Reduction Systems	44
9	Instrumentation Diagram for Envelope Fluctuation Analysis	45
10	Illustration of Direct and Ground-Reflected Sound Paths to Microphone Position	46
11	Typical Microphone Signal Oscillograms of 8-Cycle Tone Burst at 1100 Hz	47
12	Illustrative Microphone Signal Tone Burst Oscillograph Trace Showing Overlap of Direct and Reflected Sound Waves	48
13	Microphone Signal Oscillograms of Three Consecutive One-Half Second Duration Tone Bursts at 550 and 1100 Hz	49
14	Calculated Range of Influence of Reflected Wave on Direct-Wave Sound Levels Based on Tone Burst Data	50

TABLES AND FIGURES (Continued)

Figure		Page
15	Correlation of Sound Pressure Level at Microphone Position 1 with Temperature	51
16	Comparison of Normalized Long-Time-Averaged Sound Pressure Levels for CW Test Runs at 550 Hz	52
17	Comparison of Normalized Long-Time-Averaged Sound Pressure Levels for CW Test Runs at 1100 Hz	53
18	Comparison of Normalized Long-Time-Averaged Sound Pressure Levels for CW Test Runs at 2200 Hz	54
19	Comparison of Normalized Long-Time-Averaged Sound Pressure Levels for CW Test Runs at 4400 Hz	55
20	Comparison of Normalized Long-Time Averaged Sound Pressure Levels for CW Test Runs at 8000 Hz	56
21	Comparison of Measured and Calculated Sound Attenuation for CW Tests at 550 Hz	57
22	Comparison of Measured and Calculated Sound Attenuation for CW Tests at 1100 Hz.	58
23	Comparison of Measured and Calculated Sound Attenuation for CW Tests at 2200 Hz.	59
24	Comparison of Measured and Calculated Sound Attenuation for CW Tests at 4400 Hz.	60
25	Comparison of Measured and Calculated Sound Attenuation for CW Tests at 8000 Hz.	61
26	Comparison of Calculated Atmospheric Absorption with Measured Attenuation for Test Runs 21 and 40	62
27	Typical Microphone Signal Oscillograms for CW Test Run at 4400 Hz	63
28	Comparison of RMS Time Histories for Test Runs 21 and 40 at 4400 Hz	64
29	Illustration of Envelope Fluctuation of CW Waveform	65
30	Sound Fluctuation Amplitudes Versus Propagation Distance and Test Frequency	66
31	Spectra of Envelope Fluctuations for Test Run 21.	67
32	Spectra of Envelope Fluctuations for Test Run 40.	68

TABLES AND FIGURES (Continued)

Figure		Page
33	Illustration of RMS Amplitude Histogram	69
34	Measured RMS Sound Pressure Level Histograms for Test Runs 21 and 40	70
35	Trial Correlation of Normalized RMS Value of Sound Pressure Envelope Fluctuations with Wind Speed	71
36	Trial Correlation of Normalized RMS Value of Sound Pressure Envelope Fluctuations with Wind Gradient	72
37	Trial Correlation of Normalized RMS Value of Sound Pressure Envelope Fluctuations with Temperature Gradient	73
38	Trial Correlation of Normalized RMS Value of Sound Pressure Envelope Fluctuations with Richardson Number	74
A1	Comparison of Predicted Atmospheric Absorption Losses at a Frequency of 1000 Hz for a Range of Relative Humidity and Temperature Values Using Four Different Procedures	75
A2	Comparison of Predicted Atmospheric Absorption Losses at a Frequency of 4000 Hz for a Range of Relative Humidity and Temperature Values Using Four Different Procedures	76
A3	Calculated Atmospheric Absorption Loss, 550 Hz	77
A4	Calculated Atmospheric Absorption Loss, 1100 Hz.	78
A5	Calculated Atmospheric Absorption Loss, 2200 Hz.	79
A6	Calculated Atmospheric Absorption Loss, 4400 Hz.	80
A7	Calculated Atmospheric Absorption Loss, 8000 Hz.	81
B1	Measured RMS Sound Pressure Level Histograms for Test Runs 9 and 21	82
B2	Measured RMS Sound Pressure Level Histograms for Test Runs 26 and 29	83

TABLES AND FIGURES (Continued)

Figure		Page
B3	Measured RMS Sound Pressure Level Histograms for Test Runs 33 and 35	84
B4	Measured RMS Sound Pressure Level Histograms for Test Runs 37 and 40	85
B5	Measured RMS Sound Pressure Level Histograms for Test Runs 53 and 57	86

A STUDY OF AIR-TO-GROUND SOUND PROPAGATION USING AN INSTRUMENTED METEOROLOGICAL TOWER

BY

Peter K. Kasper
Richard S. Pappa
Laurence R. Keefe
Louis C. Sutherland

1.0 INTRODUCTION

This report comprises the results of an experimental study of air-to-ground sound propagation conducted for the NASA-Langley Research Center as part of an overall NASA program to further the understanding of the effects of atmospheric conditions on the propagation of sound. The data acquisition phase of the program was accomplished during March of 1974 in conjunction with an atmospheric study conducted by the Wave Propagation Laboratory of The National Oceanic and Atmospheric Administration using the NOAA 150-meter meteorological tower in Haswell, Colorado. The NASA experiment was designed as an exploratory study to evaluate outdoor sound measurement and analysis techniques and to obtain some initial research data. The research aims of this pilot program were:

a. To conduct a measurement of the air-to-ground sound propagation from a known elevated source for a variety of actual atmospheric conditions, and

b. To conduct an interpretive analysis of the data obtained to provide a qualitative as well as quantitative view of the attenuation and variability induced in a propagating sound wave by atmospheric effects.

Section 2.0 of the report provides a brief review of outdoor sound propagation technology. The specific features which influence outdoor sound propagation are outlined. Section 3.0 contains a detailed description of the data acquisition apparatus and experimental procedures used for the measurement program. The special experimental techniques used for analyzing the fluctuating sound data recorded on magnetic tape are also described. A listing of meteorological data for the ten-day period as read directly from weather instrumentation mounted at various stations along the NOAA tower is included for future reference. The experimental results of the program are provided in report section 4.0. The data presented in this section provides a quantitative demonstration of the variability induced in a propagating sound

wave by actual atmospheric conditions. The technical discussion includes an assessment of the effect of ground reflection, a presentation of the sound attenuation in terms of time-averaged values, and an evaluation of the amplitude-fluctuation characteristics of the measured signals.

2.0 BACKGROUND

A major mission of the NASA-Langley Research Center involves evaluation of aircraft noise and its effects on communities near aviation facilities. A significant element of this mission necessarily involves measurement and prediction of the propagation of aircraft noise through the atmosphere. Once the source characteristics of aircraft are known, the resultant noise environment on the ground is determined by the operation of the aircraft and propagation of its noise to the receivers.

Extensive studies have been made of parameters influencing aircraft sound propagation under laboratory conditions to examine, for example, air absorption (refs. 1 through 4). Studies have also been made in the field with actual aircraft to examine the total effect of all the influencing factors on the real, moving source (refs. 5 through 9). Very few studies have been made which allowed air-to-ground propagation effects to be examined in isolation with some precision for a fixed, outdoor noise source (ref. 10).

This program conducted such a study using a fixed sound source at the top of a 150-meter tower directed downward to the ground along a line coincident with one of the tower guy wires. The study thus allowed unique exploratory measurements, under real field conditions, of many of the propagation effects individually.

The sound propagation of aircraft noise is influenced by a variety of loss mechanisms (refs. 11 and 12). The effect of these losses upon the observed signature is dependent upon: a) atmospheric conditions, b) the position of the source relative to the ground, and c) the ground features adjacent to the sound path. The propagation losses can be classified in terms of these factors as spreading losses, and absorption losses. Each of these factors and their effects, any one of which may predominate depending upon atmospheric and ground cover conditions, is reviewed briefly below.

2.1 Spreading Losses

2.1.1 Uniform Spherical Spreading

In an ideal medium, the total sound power radiated from a point source through an expanding spherical wave front remains constant so that sound pressure levels are reduced by 6 dB each time the distance from the

source doubles. Deviations from this rule occur for finite-size sources at small source-to-receiver distances where the physical dimensions of the source region are comparable to the propagation path length. However, for the propagation path lengths considered in this study, this "near-field" effect is not significant, and uniform spreading loss can be computed by the simple 6-dB loss per doubling of distance from the source. This loss is independent of frequency.

2.1.2 Reflection by Boundaries

If the source is sufficiently close to the ground, sound reflection effects will affect propagation characteristics. These include amplifications due to an effective increase in source power when the height is very small compared with a wavelength (not applicable in this study), and reinforcement or reduction due to the interference between the direct and reflected signals. Variations in the far-field sound levels of discrete-frequency sources of up to +6 dB and -10 to -20dB are possible due to these boundary reflection effects (ref. 13).

2.1.3 Refraction by Nonuniform Atmosphere

Atmospheric wind velocity and temperature gradients can change the directional characteristics of a source by bending the sound rays indicated by the source. Although theoretical methods for predicting the effects of refraction are well developed, these require detailed definition of the atmospheric distribution of meteorological parameters and are thus seldom considered for practical studies of aircraft noise signatures. Also, a point of practical significance should be mentioned. That is that refraction effects are not strongly dependent upon frequency and are usually observed to be insignificant for elevation angles of the propagation path greater than about 10 degrees (ref. 14).

2.1.4 Scattering by Nonstationary or Turbulent Atmosphere

Turbulence scattering is another important source of propagation effects on aircraft sound. It probably does not involve a dissipation of sound energy, but rather a constantly varying redirection of its propagation path. The principal effects on a directional sound field are twofold: a) to cause fluctuations in the signal received (ref. 15), and b) to tend to equalize acoustic energy propagation in all directions at large distance from the source (ref. 16), thus adding an apparent excess attenuation which can be attributed to scattering (ref. 17). This latter effect is a direct result of the scattering of the sound field by the nonuniform sound velocity distributions in atmospheric turbulence. Thus, a highly directional sound profile can be gradually rounded out, tending to a nondirectional pattern at great distances from the source. For this program, it was desirable to avoid this latter effect as

much as possible and consider only the fluctuation effects. Hence, the test sound source was selected to have a pattern as nondirectional as possible along the transducer array.

2.2 Absorption Losses

2.2.1 Atmospheric Absorption Losses

Atmospheric absorption losses have two basic forms: a) classical losses associated with the change of acoustical energy (or kinetic energy of molecules) into heat by fundamental gas transport properties of a gas, and b) for polyatomic gases, relaxation losses associated with the change of kinetic or translational energy of the molecules into internal energy within the molecules themselves. A detailed review of current atmospheric absorption loss theory is contained in Reference 18.

Of the two forms of absorption losses, molecular or relaxation loss is far more important at low audible frequencies. This component depends on frequency, temperature, and humidity content, and, in the critical frequency range, is primarily due to vibration relaxation enchanced by the presence of water molecules. Until recently, the significance of nitrogen as a principal contributor to this loss was not recognized so that previous comparisons of theory and experiment, based only on relaxation of oxygen molecules, were in substantial disagreement (refs. 1, 3, 4, and 19). By including relaxation of nitrogen in the theoretical predictions, substantial improvement is obtained in agreement between theory and experiment (ref. 20).

2.2.2 Absorption Losses by Ground Surface and Ground Cover

The vast majority of field measurements of sound propagation losses have been made over horizontal propagation paths with ground surface conditions ranging from hard concrete to dense jungle. As indicated earlier, the effect of refraction on sound propagation is particularly important for near-horizontal propagation paths. Thus, field measurements are not a reliable source of data for isolating effects of ground cover unless great care has been taken in the experiment to remove any effects associated with weather (refs. 21 and 22). Thus, this program made no serious attempt to examine ground absorption effects since emphasis was to be on air-to-ground propagation.

2.3 Unsteady Propagation Effects

In addition to the loss mechanisms described above, the effect of inhomogeneous and time-varying atmospheric conditions impose both amplitude and phase fluctuations on propagating sound waves. The investigation of

these sound fluctuations is important in the overall study of aircraft noise propagation for two reasons: a) the fluctuations impose a character to the propagating sound which influences the aural detection, recognition and general subjective response to the noise, and b) the complete interpretation of aircraft flyover noise signatures requires an accounting for fluctuations induced by atmospheric conditions.

Over the past thirty years, there have been a number of theoretical investigations of sound fluctuations and scattering by velocity and temperature turbulence (refs. 23 through 28). The availability of experimental data related to atmospheric induced sound fluctuation has, however, been more limited (refs. 29 through 32). Data has been included in this report to provide examples of parametric forms useful in evaluating sound fluctuations as well as providing quantitative indications of sound fluctuations measured during the experimental program.

3.0 APPARATUS AND METHODS

3.1 Experimental Program

3.1.1 Description of Test Site

The measurement program was conducted at the site of the NOAA 150-meter tower near Haswell, Colorado. The site is located off state highway 96, about 180 miles southeast of Denver. It is in an area east of the Rocky Mountains with extensive flatlands extending for a distance of approximately 50 miles. The test site is pictured in Figure 1.

3.1.2 Testing Configuration

A sketch showing the dimensional layout of the experiment appears in Figure 2. The sound source was mounted at the top of the tower about 1 meter below the attachment point of the main east guy wire, with the major axis of the mouth positioned parallel to the ground. The sound source was pointed down the wire, making an angle of approximately 35^{o} with the vertical. It was aligned by sighting the axis of the horn along a best straight-line fit through the guy wire microphone positions.

Four microphones, designated 1 through 4, were located along the guy wire at 18.3 (60), 73.2 (240), 109.7 (360), and 146.3 meters (480 feet), respectively, from the sound source. Specially fabricated carriages were used to support the microphones at appropriate positions along the guy wire. A close-up view of a microphone carriage is shown in Figure 3. A view of the top of the tower showing the sound source and first microphone position

appears in Figure 4.

The bottom three microphone positions were chosen to match the elevations of existing meteorological instrument stations which were spaced every 30.5m (100 ft) up the tower. Meteorological data was also available from sensors mounted on the winch-operated tower personnel carriage.

All microphone power supplies, signal-conditioning and recording equipment, and monitoring instruments were located in an underground bunker near the base of the tower.

3.1.3 Field Instrumentation

The basic elements of the acoustic field instrumentation systems are depicted schematically in Figure 5.

The sound source for the experiment consisted of a 40-watt electrodynamic driver mounted to a 300-Hz cutoff frequency, multicellular exponential horn. Free-field directivity measurements of the sound source in five-degree increments along both the major and minor axial planes through the mouth of the horn are presented in Figure 6. These measurements were made at the NASA-Langley Anechoic Facility in still air and with a sound source-to-microphone separation of 5.5m (18 ft).

The components of the four microphone systems were chosen to provide maximum protection from the effects of continuous outdoor weather exposure. The 12.7mm(0.5 in)-diameter condenser microphones were treated with a thin quartz coating on both the diaphragm and backplate to increase resistance to moisture penetration and corrosion. In addition, dessicators were used to dry the air entering the rear of the microphone cartridge for equalizing static pressure. Commercially available nylon mesh windscreens were also used at each microphone position.

Each microphone was provided with an electrostatic actuator (ESA) calibration device which also served as a diaphragm raincover. The ESA was used to electrostatically drive the microphone diaphragm to provide a run-by-run check of the microphone sensitivity. These ESA-raincover units were screwed onto the microphones in place of the standard diaphragm-protecting grids. Each ESA was actuated remotely from the bunker control room. A sketch of an assembled microphone system is shown in Figure 7.

Weather data was obtained from meteorological instrument stations at 30.5m (100 ft) intervals along the height of the tower. Each station provided a continuous indication of temperature, wind speed, and wind direction. Temperature and wind speed data were also available from sensors positioned

on a nearby secondary tower at a height of 2m (6.6 ft). In addition, the traversing tower personnel carriage was instrumented to provide temperature, wind speed, wind direction, and relative humidity data. Atmospheric pressure was recorded from a barometer at ground level.

Continuous analog data was recorded for each test session on an FM instrumentation tape recorder which had a bandwidth of 10 kHz. This data consisted of the following information: the four microphone signals, the voltage and current waveforms of the electrical drive signal to the sound source, the relative humidity and wind speed at the traversing personnel carriage, and the height of the carriage. Accurate time information was kept by recording a standard time-code signal on an additional channel. The time was set to match that of the NOAA continuously recording instruments for possible correlation with additional weather data in the future. A remaining recorder channel was used for voice annotation of the experiments.

3.1.4 Test Program

The sound propagation experiments consisted of 63 separate tests performed during the 10-day measurement program. All tests consisted of producing a series of sinusoidal acoustic signals at the sound source and recording the signals received at the four microphone locations. These sinusoidal signals were chosen to minimize interference with ongoing NOAA echo-sounder experiments and consisted of the following frequencies: 550 Hz, 1100 Hz, 2200 Hz, 4400 Hz, and 8000 Hz.

The primary set of tests used continuous sine wave (CW) acoustic signals. Consistent with the experimental plan to examine both long-time and short-time fluctuations in propagation, these tests were performed for time intervals of either 60 or 120 seconds at standard times of 0200, 0800, 1400, and 2000 hours daily. It was expected that meteorological parameters would change rapidly at dawn and dusk as the transition between inversion and lapse conditions starts to occur. Thus, the test plan allocated the 120-second recording time for tests at these times. The 60-second recording was used at 0200 and 1400 since more stable weather conditions were expected.

Secondary tests using tone bursts at each test frequency were also conducted periodically during the program. These tone-burst experiments were considered important to examine the magnitude of the ground-reflected sound wave and in assessing the use of bursts in future propagation studies.

3.1.5 Experimental Procedure

Preceding each test run, meteorological data consisting of temperature, wind speed and direction, atmospheric pressure, and relative humidity

at meteorological stations along the tower and near the ground was recorded.

Next, sensitivity checks were performed on all microphone systems at 550 and 8000 Hz using the remote electrostatic actuators. All four actuators were activated simultaneously for 15 seconds at each of these frequencies, and the induced microphone signals were recorded onto magnetic tape. The actuator drive signal was obtained by switching the oscillator signal from the sound source to the actuators. A polarization voltage of 300 Vdc for the actuators was provided by a battery-pack power supply.

After the ESA sensitivity checks were complete, the oscillator signal was switched back to the sound source to begin the propagation test. For all tests, the electrical drive voltage to the source was set at a constant value (25 Vac). Each of the standard testing sessions began with sound propagation at 550 Hz and followed successively with 1100, 2200, 4400, and 8000 Hz.

The acoustic tone bursts were produced by a tone-burst generator driven by the signal oscillator. Two durations of tone bursts at each of the five test frequencies were used. Short 8-cycle bursts insured the separation of the direct sound wave from the ground-reflected wave at each microphone position, and bursts of 1/2-second duration allowed overlap between the direct and reflected signals to occur for examination of the interference phenomenon. Each tone-burst test consisted of a series of 20 bursts, spaced approximately 2.5 seconds apart. The same sound source drive voltage as used for the CW tests was maintained.

All microphone signals were recorded on magnetic tape for later processing.

3.2 Data Reduction Equipment and Procedure

3.2.1 Time Histories

Sound pressure level time histories of the microphone signals were obtained with an rms-responding, graphic-level recorder. A time constant of approximately 350 milliseconds was used to display the general character of the fluctuating sound levels over each test period. This response time is roughly equivalent to the "slow" detection characteristic of a standard sound-level meter.

The unprocessed microphone signals were similarly recorded on oscillograph charts. By reproducing the waveform in this manner, the envelope of the sound-pressure amplitude at each microphone was displayed. The instrumentation systems used for time-history analyses of the acoustic data are noted in block diagram form in Figures 8a and 8b.

3.2.2 Tone Bursts

Data reduction of the tone-burst tests was also performed with the instrumentation arrangement shown in Figure 8b. The oscillograph used in the reduction was equipped with galvanometers to follow the instantaneous signal fluctuations up to a frequency of 5000 Hz.

Seven separate testing sessions were conducted using the 8-cycle duration tone burst. Each test consisted of a series of 20 bursts, spaced 2.5 seconds apart, at each test frequency. The amplitudes of the direct and ground-reflected sound bursts received at each microphone position were obtained by graphically measuring the peak-to-peak values of the bursts and converting to sound pressure levels.

3.2.3 Long-Time-Averaged Sound Pressure Levels

A single time-averaged value of sound pressure level for each frequency and microphone position for the CW test runs was obtained using the instrumentation arrangement shown in Figure 8c. The microphone signals were first filtered with a 200-Hz-wide bandpass filter centered at the test frequency to remove background noise and possible harmonic content in the test signals. The rms value of each signal was detected with a thermocouple-type true rms voltmeter having a dc voltage output proportional to the rms amplitude. The time constant of the detector was approximately 300 milliseconds.

This dc voltage output was applied to an integration network which summed the voltage for a specified period of time and displayed the time-averaged value on a digital voltmeter. The integrating times were 20 seconds for the nominally 60-second recordings, and 50 seconds for the 120-second recordings. Using the measured sensitivities of the microphone systems, these long-time-averaged signals were converted to sound pressure levels.

3.2.4 Sound Pressure Level Amplitude Distribution

To provide a convenient presentation of the statistical distribution of sound pressure fluctuations during each test run, the microphone signals were rms-detected and processed by a statistical distribution analyzer. This analyzer essentially presented amplitude histograms representing the percentage of time the rms signal level remained within incremental decibel values of sound pressure level for a given time duration of signal. The instrumentation arrangement is depicted in Figure 8d.

Each histogram was constructed by sampling a 60-second segment of the logarithmic rms output signal at 2000 samples/second. The rms

detection-time constant was approximately equivalent to that of the standard "fast" sound-level meter response. For the 550-, 1100-, and 2200-Hz test frequencies, the histograms were determined in 0.5-dB increments. Because of the greater amplitude variability of the microphone signals at 4400 and 8000 Hz, a 1.0-dB increment was used at these frequencies.

3.2.5 RMS Fluctuation Amplitudes

The signal processing of the rms value of the envelope is clearly shown by the instrumentation diagram shown in Figure 9a. The microphone signal was first bandpass-filtered to remove extraneous noise and signal harmonics and then amplified to maintain a high signal-to-noise ratio. The combination of a full-wave rectifier and a 200-Hz low-pass filter then comprised a demodulation network which transformed the acoustic signal into a fluctuating positive voltage proportional to the amplitude of the envelope of the input signal. A 0.1-Hz high-pass filter served to remove the dc component of the envelope fluctuation. The 0.1-Hz cutoff frequency was chosen based on the requirements imposed by the finite length of recorded signal. The envelope fluctuation signal was then processed with a thermocouple-type true rms voltmeter whose output was averaged over a 50-second segment of the CW test signal. Thus, the integrator permitted an effective averaging time equal to the signal length, to accommodate the predominately infrasonic energy of the envelope fluctuations.

3.2.6 Fluctuation Spectra

The instrumentation arrangement shown in Figure 9b was used to conduct a frequency analysis of the envelope fluctuation signal. The envelope spectra were obtained, with 0.5-Hz resolution, using the 0-to-200-Hz range of a time-compression spectrum analyzer. The output of the analyzer was ensemble-averaged over 32 spectra as limited by the duration of the test signals and the low-frequency analysis range. This reduction scheme was applied to the microphone signals for the set of 10 test runs used for the amplitude fluctuation analysis. In a number of cases, the fluctuation spectrum was indeterminate due to a combination of low-level signal fluctuations and instrumentation noise floor established by the magnetic tape recorder flutter.

3.2.7 Weather Data

A set of weather parameter readings was taken at the beginning of each acoustic testing session. Temperature, wind speed, and wind direction data at each of the 30.5m(100 ft)-spaced weather stations were obtained from NOAA digital readout displays. The wind direction was measured in degrees clockwise from the north. In instances where the wind speed or direction fluctuated, a single averaged value was noted. The relative humidity data,

obtained from a sensor on the traversing personnel carriage, was read directly from a continuous chart-paper printout. For most readings, the carriage was stopped near the top of the tower. The atmospheric pressure was recorded from a wall barometer mounted in the control bunker. A compilation of this data is provided in Table I.

4.0 RESULTS

4.1 Effects of Ground Reflections

An important factor in the study of air-to-ground sound propagation is the resultant effect of ground-reflected sound waves. During the experimental program, it was observed that the reflected-wave sound field had a definite effect on the measured results, particularly for the low-frequency test signals. This section of the report serves to quantify the magnitude and frequency range of measured effects due to the ground-reflected sound.

An illustration of the effect of a plane boundary on a propagating wave is shown in Figure 10 in terms of the propagation paths which reach a given microphone position. As shown in this figure for a measuring point above the plane, the reflected waves appear to be coming from an imaginary source below the boundary. If, in fact, the boundary were rigid and infinite in extent, its effect would be simulated by introducing a mirror image of the actual sound source. If we assume that the source generates a spherically diverging sinusoidal wave of radian frequency ω, the direct and perfectly reflected sound pressure can be expressed as

$$P_d = \frac{A}{R} \cos(\omega t - kR) \qquad (1)$$

$$P_r = \frac{A'}{R'} \cos(\omega t - kR')$$

where
R = Total length of direct path
R' = Total length of reflected path
A, A' = Source strength amplitude factors for direct and reflected waves, respectively.

As discussed in Reference 33, the total sound pressure at a point above the plane, P_t, is given by the instantaneous sum of these direct and reflected waves. The relative sound pressure level change due to ground reflection for this idealized case can be expressed in terms of time-averaged sound

pressure as

$$\Delta SPL = 10LOG\left(\frac{P_t^{rms}}{P_d^{rms}}\right)^2 = 10LOG\left\{1 + \left(\frac{A'/R'}{A/R}\right)^2 + 2\left(\frac{A'/R'}{A/R}\right)\cos(kR - kR')\right\} \quad (2)$$

As shown in this equation, the sound pressure level change due to ground reflection is a function of the relative amplitudes as well as the absolute phase difference between the direct and reflected waves. The table below shows the results of applying this idealized model to the geometry of the experimental configuration.

CALCULATED SOUND PRESSURE LEVEL CHANGE DUE TO REFLECTED WAVE (ASSUMING OMNIDIRECTIONAL SOURCE AND RIGID INFINITE PLANE BOUNDARY)

Test Frequencies	Microphone Positions			
	1	2	3	4
550	-0.54	1.61	3.42	-1.31
1100	0.44	-0.28	3.22	-0.28
2200	0.50	-3.04	3.03	-1.16
4400	0.43	2.24	1.58	-0.55
8000	0.27	0.97	1.88	4.74

In practice, there are a number of factors which modify the results from that expressed by Equation 2. The earth boundary, for example, is not acoustically "rigid" and some acoustic energy loss as well as an additional phase change occurs upon reflection. Atmospheric conditions along the propagation path can introduce additional complications. As shown in Figure 10, the reflected wave travels over a longer path than the direct wave, and therefore, in addition to greater spherical spreading losses, experiences relatively greater influences through atmospheric absorption and scattering mechanisms. The time-varying properties of the atmosphere along the propagation path can induce additional variations in the relative phase between the direct and reflected waves.

The sound directivity pattern of the sound source can also have a strong influence on the amplitude of the reflected wave reaching a point on the original propagation path. From the measured directivity of the sound source (Figure 6), the sound radiation tends to focus in the forward direction for increasing test frequency. Since the ground reflection tends to produce a

mirror-image source, the image radiation will be strongest towards the point where the propagation path intercepts the ground plane. The net result is that, as the sound source becomes more directive at the higher test frequencies, there is a general reduction in the influence of the reflected wave, particularly for the upper microphone positions.

The series of tone-burst experiments provided a direct way of measuring the net effect of the ground reflection for a given set of atmospheric conditions. Figure 11 shows a comparative set of typical microphone signal oscillograph traces using a signal consisting of an 8-cycle duration burst of an 1100-Hz tone. This example shows the time history of a single tone burst as it passes each microphone position. As the tone burst propagates toward the ground, the effects of spherical divergence and atmospheric attenuation combine to reduce the amplitude of the burst. The ground-reflected pulse appears as an echo at each microphone position following a time interval dependent on the particular reflection propagation path.

The use of the 1/2-second tone burst provided additional information about the ground-reflected wave. This tone burst of longer duration allowed sufficient time for the reflected wave to overlap with the direct wave at the two lowest microphone positions. Figure 12 provides an illustration of such a typical tone-burst time trace. As shown, there are three regions of interest. The initial time period, up until the reflected wave reaches the microphone, shows the amplitude of the direct wave. The final period, starting when the direct wave has completely passed the microphone, shows the amplitude of the reflected wave. The period between comprises the time when the direct and reflected waves overlap. This time period of overlap is indicative of conditions existing for a continuous-wave signal in the presence of the ground reflection.

Figure 13 shows oscillograph records of the 1/2-second tone-burst envelopes obtained at the two lowest microphone positions during Test Run 18 for bursts at frequencies of 550 Hz and 1100 Hz. Three consecutive bursts, spaced approximately 2.5 seconds apart, are shown to give indication of the variability of the recorded signals. The change in the amplitude of the pulse overlap region from burst-to-burst is an indication that the relative phase between the direct and reflected wave is changing during the 2.5-second period. The varying phase is particularly significant for the 1100-Hz data where evidence of both constructive and destructive interference occurs within the three consecutive tone bursts. In view of the difficulty in theoretically predicting the relative amplitudes and phases of the direct and reflected waves, it is more practical to rely on the tone-burst test measurements to assess the effect of the ground reflection.

Table II summarizes the results of the 8-cycle tone-burst test runs

taken at various times throughout the field exercise. Each of the tone-burst sound levels shown in this table was determined from nominally averaging twenty consecutive bursts. As indicated in this table, the reflected-wave amplitudes were only determinable above the instrumentation noise floor for the 550- and 1100-Hz data at the two lowest microphone positions. For the other cases, a maximum level established by the instrument noise floor is indicated.

In addition to the amplitude information shown in Table II, it is also necessary to consider the relative phase between the direct and reflected waves. When the relative phase equals an integral multiple of 2π, constructive interference occurs and the total pressure amplitude will be a maximum. Conversely, if the relative phase is equal to an integral multiple of π, there will be a maximum destructive interference and the total pressure amplitude will be a minimum. The actual influence of the ground-reflected wave on the total pressure is then bracketed by these two extremes. This approach was applied to the data shown in Table II. Where necessary, the instrument noise floor levels were used to establish an upper limit for the reflected-wave amplitudes. The relative amplitudes between the direct and reflected waves were determined by averaging over the seven tone-burst test runs. Figure 14 shows the resulting range in sound level at each microphone position derived for the extremes of constructive and destructive interference from the reflected wave. Although not actually derived by calculation, the results for 4400 Hz are included with the 2200-Hz projections since the greater atmospheric attenuation at these higher frequencies further limits the influence of the reflected wave. A conclusion that can be drawn from Figure 14 is that the effect of ground reflections was generally less than ± 1 dB for all the continuous-wave sound-level data except for the two lowest microphone positions at 550 and 1100 Hz. As indicated in Figure 14, the major influence of ground reflection will be in the 550- and 1100-Hz measurements at microphone positions 3 and 4.

4.2 Analysis of Long-Time-Averaged Sound Levels

As described in Section 3.0, the experimental program was designed to provide a systematic measure of the time-averaged and instantaneous variations in the amplitude of a propagating sound wave under a variety of atmospheric conditions. This section comprises an analysis of the data obtained by time averaging the recorded microphone signals over a period on the order of one minute. This duration of averaging time is long enough to allow averaging out the instantaneous sound fluctuations but short enough to permit measurements to be taken during relatively constant macroscopic atmospheric conditions. The long-time-averaged amplitudes can be used as a direct measure of the average sound intensity at a point and thus can define the average propagation loss between successive points along a propagation path.

From each experimental test run, the combination of 5 test frequencies and 4 microphone positions provided a basic sample of 20 acoustic signals which were converted to long-time-averaged sound pressure levels. The total data set chosen for closer study consisted of the time-averaged levels determined from 34 test runs spaced on the average of six hours apart. A compilation of these time-averaged levels is provided in Table III. The time-averaged sound levels measured at microphone position 1, 18.3m (60 ft) from the sound source, were used to define the reference level of the sound source. The variations in this reference sound level for all frequencies at this position were compared with variations in measured values of temperature, temperature gradient, wind velocity, wind direction, wind vector, wind gradient, and barometric pressure. Only the simple correlation with temperature showed any significant relationship. Figure 15 provides the correlation with a temperature plot for the 550-Hz data. As evident in this figure, the general tendency is for the sound levels at microphone 1 to decrease with increasing temperature. In view of the relatively short distance between this microphone and the sound source, the measured sound level variations at this point are believed due in part to variations in sound source power output. To compensate for these source variations, the sound levels for the three lowest microphone positions have been normalized relative to the levels for microphone position 1. These normalized long-time-averaged sound levels, shown in Figures 16 through 20, thus represent the variation in total propagation loss at points 2, 3, and 4 relative to the level at point 1. Since the test runs were generally taken at equally spaced intervals, these figures show a form of time history of sound propagation conditions throughout the experimental program. The run-to-run variations in sound level for each microphone position provide an overall picture of the changing gross sound attenuation characteristics of the atmosphere.

From the discussion in Section 4.1, it is recognized that wave interference from the ground-reflected sound is most significant for the two lower microphone positions at 550 and 1100 Hz. The variations in the long-time-averaged levels for these cases shown in Figures 16 and 17 are likely to have been influenced by weather-induced changes in the ground-reflected wave. For the test frequencies above 1100 Hz, the changes in atmospheric absorption as determined by the relative humidity and temperature are expected to account for a significant part of the observed sound-pressure variations. Values of atmospheric absorption were calculated for the 5 test frequencies based on a new tentative prediction model for air absorption discussed in Reference 20. The calculated results for a range of temperature and relative humidity values are shown in Appendix A. Note that the extreme range of temperature and relative humidity indicated in Appendix A (-10°C to 20°C and 1 to 100%RH) encompasses the range of experimental conditions observed in this study. However, the prediction method in Reference 20 is not necessarily reliable below 0°C and 10% relative humidity.. As is apparent

from the figures in Appendix A, particularly for low relative humidities and the higher frequencies, a small change in temperature or relative humidity results in a large variation in predicted attenuation. Before attempting to account for the measured atmospheric absorption, it is important to consider the accuracy of the relative humidity data. Based on the relative humidity measurement system utilized, it was estimated that the accuracy of the relative humidity data was about $\pm 5\%$. Thus, for this report, a criterion was arbitrarily established to exclude from further analysis of atmospheric absorption, test cases where the predicted absorption varied more than 1dB for a variation of $\pm 5\%$ in relative humidity.

Using this criterion, absorption attenuations were calculated for the propagation paths between microphone position 1 and positions 2, 3, and 4. Available temperature data at 30.5m (100 ft) vertical increments were used in the calculation scheme to refine the absorption-loss prediction. These attenuation values are shown in Table IV. Combining the sound-level decrease due to spherical spreading with the predicted atmospheric absorption values provide a set of calculated total attenuation losses (excluding any reflection or refraction effects) which can be compared directly with measured results. A comparison of these calculated and measured sound level differences is shown in Figures 21 through 25. The diagonal line in these figures provides a reference level representing exact correspondence between calculated and measured sound levels normalized to the sound levels at microphone position 1. The data points above this line correspond to total sound attenuation in "excess" of atmospheric absorption and spherical spreading. This excess attenuation is indicative of acoustic energy refracted or scattered out of the original propagation path. The data points below the diagonal line are indicative of sound energy that was added to the direct wave by reflection or refraction. In general, the scatter of data points for each microphone position indicates the degree of accuracy that sound-level predictions can be made for these distances on the basis of only spherical divergence and atmospheric absorption.

The scatter of the data points in Figures 21 through 25 clearly indicates that these plus-or-minus variations in excess attenuation can be substantial. To further illustrate this point, test runs 21 and 40 were analyzed to show the variation in measured attenuation in excess of spreading loss compared to predicted attenuation due to absorption alone. The results plotted in Figure 26 show that for run 21 made during reasonably stable atmospheric conditions, except for the apparent reflection effects near the ground at 550 Hz and 1100 Hz, the observed and predicted attenuations agree quite well. In contrast, the corresponding observed and predicted attenuations for run 40, for which the atmospheric conditions were relatively unstable, disagree substantially. Further evaluation of the long-time-averaged data tabulated in

Table III could be used to examine atmospheric attenuation effects more completely. However, the influence of the other propagation effects (refraction, reflection, and scattering) and the lack of more precise humidity profile data did not justify such additional evaluation.

4.3 Sound Fluctuations Due to Atmospheric Effects

A sound wave propagating through the real atmosphere is often refracted, diffracted, and reflected by time-varying atmospheric temperature and velocity inhomogeneities. As a result, random fluctuations are induced in the amplitude and phase of the wave. In view of the slow time variations encountered in atmospheric activity, these fluctuations usually fall well within the infrasonic range of the audio spectrum. For a propagating sinusoidal wave, the induced fluctuations can be considered as a combination of amplitude and phase or frequency modulation. Oscillograms of a typical set of instantaneous time histories are shown in Figure 27. In this figure, the fluctuating amplitude of the propagating wave is seen as the modulation envelope of the signal waveform. Amplitude fluctuations are also significant in the rms-detected signals. Examples of rms time histories determined from measurements taken during qualitatively different atmospheric conditions are shown in Figure 28. The rms sound pressure level fluctuations shown in this figure indicate the decibel variations that would have been observed using a sound level meter on "slow" response.

The following subsections serve to quantify and examine the character of imposed amplitude fluctuations for a representative sample of the tape-recorded test signals. The order of presentation starts with an examination of fluctuations of the envelope of the recorded sinusoidal waveforms. Treated next is an investigation of amplitude variations in the rms-detected signals. The final section provides a correlation of the sound fluctuation data with measured weather parameters.

4.3.1 Envelope Fluctuations

The instantaneous pressure amplitude of a sinusoidal sound wave passing a given point in a stationary medium can be described mathematically by the familiar expression

$$P(t) = A \sin (\omega t + \phi) \qquad (3)$$

where A is a constant amplitude factor, ω is the radian frequency and ϕ is an arbitrary phase. The envelope of this simplified signal waveform, as shown in Figure 29a, is represented by the two parallel lines intersecting the peak values of the sine wave at A units above and below the p = 0 axis. The equation for the envelope amplitude e(t) for such a sine wave signal is given by

$$e(t) = \pm A \tag{4}$$

As seen in the example time history oscillogram, the signal waveform of a sinusoidal sound wave propagating in an inhomogeneous time-varying medium, such as the atmosphere, appears more like that illustrated in Figure 29b. In this case, the equation for the instaneous pressure at a given point can be expressed as

$$P(t) = \left[A + e'(t) \right] \sin (\omega t + \phi) \tag{5}$$

where A represents the mean value of the envelope and e'(t) represents the instantaneous variation of the envelope from its mean. The degree of fluctuation of the instantaneous pressure amplitude is thus directly dependent on the behavior of e'(t). The envelope time history is shown in Figure 29c.

The demodulation circuitry described in Section 3.2.5 was used to obtain e'(t) from the instantaneous pressure amplitude signal. The rms value of e'(t) then provides a quantitative measure of the signal fluctuations. In order to compare the degree of fluctuation between signals with different mean amplitudes, e'_{rms} must be normalized to some parameter proportional to the mean amplitude. For this investigation, the long-time-averaged rms value P_{rms}, as defined in Section 4.2, was used as the normalizing parameter. The fluctuation parameter derived in this manner is in the form of a modulation index and is defined simply by the ratio:

$$E = \frac{e'_{rms}}{P_{rms}} \times 100, \ \% \tag{6}$$

A compilation of this fluctuation parameter determined from a selection of the recorded test runs is provided in Table V.

The data in Table V demonstrates the degree of sound amplitude fluctuations caused by atmospheric effects for propagation distances up to 146 meters (480 feet). The general trend in this data is for the fluctuation amplitudes to increase both with frequency and distance. The phenomenon of saturation, in which normalized levels of fluctuation tend to a limiting value with distance, was not observed in this study. Apparently in this experiment, the propagation distance was too short, or the intervening turbulence too weak, for this phenomenon to occur.

Up to the point of saturation, theoretical studies (refs. 23 through 25) indicate that normalized fluctuation amplitudes should increase linearly with frequency and as the square root of the propagation distance. In Figure 30, fluctuation amplitudes from run 40 are plotted against these parameters.

The agreement between predicted and measured frequency dependence is reasonable. Growth of the amplitude fluctuations with distance also shows reasonable agreement with predictions of a $r^{1/2}$ law. The fluctuation amplitudes appear to have slightly greater increase with frequency than predicted at lower frequencies and a lesser one at higher frequencies. The data from other runs show greater deviations from predictions regarding frequency and distance dependence than those found in Run 40 but general trends are similar.

In addition to the determination of rms values, the envelope fluctuation signals e'(t) were also analyzed for spectral content. The resulting frequency spectra obtained for test runs 21 and 40 using the procedure described in Section 3.0 are shown in Figure 31 and 32. In these two figures, the vertical scale corresponds to the value of

$$20 \text{ LOG} \frac{e'^{\text{band}}_{\text{rms}}}{P_{\text{rms}}}$$

where $e'^{\text{band}}_{\text{rms}}$ is the rms envelope fluctuation measured within a 0.5-Hz filter bandwidth and P_{rms} is the long-time-averaged rms sound pressure. The fluctuation spectra display a monotonic decrease in level with increasing frequency. As shown, the greatest amount of fluctuation energy occurs at frequencies less than 10 Hz. All of the spectra have a similar shape which, although not broadband, do not appear to contain discrete frequency components.

4.3.2 Sound Level Amplitude Histograms

As evidenced in the rms time history data previously shown in Figure 28, the measured rms sound pressure levels also exhibited varying degrees of fluctuation. This report section comprises an examination of the statistical characteristics of the rms-detected sound levels for a sampling of test runs. As discussed in Section 3.2.4, the method used to analyze the rms amplitude variations was to determine an amplitude histogram for a specific duration of detected signal. This concept of rms amplitude histogram is illustrated in Figure 33. The upper part of this figure represents the time history of a sample rms-detected sound level. The histogram in the lower figure indicates the percentage of time this rms level remained within each incremental decibel range. The amplitude histogram provides information about both the mean of the analyzed signal as well as the degree of fluctuation about the mean. For a histogram which is approximately symmetrical, the point of symmetry is the mean level. The two extremes at which the histogram goes to zero indicate the maximum and minimum amplitudes achieved by the measured signal during the time period considered by the histogram. In the limit of infinite signal length and infinitely small amplitude resolution, the

amplitude histogram becomes the probability density function of the signal.

The histogram thus provides a qualitative picture of the rms amplitude variability as well as indicating the mean sound level for a specific test run. Figure 34 shows a comparative set of measured histograms determined from Runs 21 and 40. For Run 21, a comparison of the histograms for each microphone position shows the general tendency of the sound fluctuations to increase at the farthest microphone positions. Also from this figure, it is immediately apparent from the broader shaped histograms from Run 40 that sound fluctuations were considerably stronger in this run than in Run 21. A general indication of the range of rms sound amplitude fluctuations encountered during the experimental series can be seen from the set of histograms selected for ten test runs contained in Appendix B.

4.3.3 Correlation of Sound Fluctuation Data with Weather Conditions

In view of the extensive weather data that was available, an attempt was made to relate the sound fluctuation amplitudes directly to measured meteorological parameters. Examples of attempted correlations are shown in Figures 35 through 37, where the linear fluctuation levels in Table V have been compared with wind speed, wind gradient, and temperature gradient. The scatter of data in each case is high particularly in the correlations with wind speed and temperature gradient. Some correlation appears to exist with wind gradient but the erratic behavior of fluctuation levels during low wind shear indicate that additional factors may be significant during such conditions. Because the atmosphere is a stratified fluid, i.e., density gradients exist, most lower atmospheric phenomena, including turbulence, are controlled by a balance between shear and gravitational (buoyancy) forces (ref. 34). Since simple parameters (wind, temperature and their gradients) do not adequately describe this force balance, they cannot be used to predict the intensity and scale of turbulence a wave will encounter during particular atmospheric conditions.

A parameter commonly used by micrometeorologists to describe this balance of shear and buoyancy forces, and the interlocking and often contradictory effects of wind and temperature, is the Richardson number (Ri). This nondimensional parameter is a function both of the wind and temperature gradients, and represents the ratio of energy extracted from atmospheric turbulence by buoyancy forces to the energy input to the turbulence by wind shear forces (ref. 34). Richardson numbers greater than 0.25 generally indicate non-turbulent air flow in the atmosphere. Decreasing Richardson numbers below 0.25 indicate increasing levels of atmospheric turbulence (refs. 34 and 35). In Figure 38, fluctuation levels are plotted versus Richardson number. This correlation is much more striking than in the previous attempts. As expected, large positive values of Richardson number give the lowest values of fluctuation and decreasing values of Richardson

number give greater sound variability. Richardson number can take on negative values, corresponding to what meteorologists call an unstable atmosphere. During such conditions, positive buoyancy forces produced by temperature gradients more negative than $-1^{\circ}C/100$ meters encourage the growth of atmospheric turbulence. This differs from a stable atmosphere (positive Richardson number) where the temperature gradients result in a damping of turbulent disturbances. None of the tests in this experimental program were taken when the atmosphere could be described as unstable all the way to the 150-meter altitude. While additional parameters may be needed to completely specify the scale and intensity of atmospheric turbulence under given conditions, the Richardson number seems to have a potential use in predicting sound amplitude fluctuations due to turbulence during outdoor sound propagation.

5.0 CONCLUDING REMARKS

This experimental program was designed to make systematic measurements of sound along a given air-to-ground propagation path during a variety of atmospheric conditions. The basic experimental scheme of measuring the amplitude of a radiated sinusoidal sound wave at fixed positions along a tower guy wire was found to be a practical means of investigating air-to-ground sound propagation.

The philosophy of the field experiment was to perform the simplest form of sound measurements possible so that the effects of variations in atmospheric conditions would be most evident in the acquired acoustic data. The basic measurement series was repeated at approximately six-hour intervals to provide a periodic measure of sound propagation conditions throughout the field program. The data reduction and analysis procedures were chosen to examine the run-to-run variations in the long-time averaged sound amplitudes as well as instantaneous amplitude fluctuations in the recorded signal.

The limited use of the tone-burst technique provided indication that the ground reflected sound could influence the measured results as high as 66m (200 ft) above the ground for the 550- and 1100-Hz signals. Included among the tone-burst results was data indicating a high degree of phase variability between the direct and ground-reflected waves.

A run-to-run comparison of the long-time averaged sound levels normalized to the levels at the upper microphone position shows a spread in the measured results ranging from 5 dB at 550 Hz for a 73.1m (240 ft) distance to 19 dB at 8000 Hz for a 146.3m (480 ft) distance. The long-time averaged CW measurements also provided a data set by which atmospheric absorption measurements were compared to predicted results. These pre-

dictions were based on a new proposed method (ref. 20) which includes the effect of nitrogen relaxation (see Appendix A). Due to the scatter of data points in this comparison, no conclusion could be made about attenuation in excess of atmospheric absorption and spherical spreading other than noting that no consistent trend in excess attenuation effects was found.

The rms envelope fluctuation data provided a quantitative measure of instantaneous sound amplitude variations encountered for propagation distances of up to 146m (480 ft) under a variety of meteorological conditions. The general trend of the rms envelope fluctuations normalized to the long-time averaged sound pressures was to increase with increasing distance indicating the absence of "saturation"conditions occurring within the range of propagation distances and turbulent conditions studied. From a correlation of the sound fluctuation data with weather conditions, a tentative conclusion, based on the limited data sample, is that the extent of weather-induced sound fluctuation may be predictable from the meteorological parameter, Richardson number.

APPENDIX A

ATMOSPHERIC ABSORPTION PREDICTION MODEL

This appendix contains additional background on the air absorption prediction model utilized in this report. The model, summarized in Reference 20, represents an attempt to account, more accurately, for molecular relaxation effects in air absorption by basing the model on basic physical principles throughout and by including molecular relaxation loss in nitrogen as an added term to previous semi-empirical models. The new method is compared in terms of absorption coefficients in Figure A1 and A2 with the SAE ARP 866 and Harris models (refs. 3 and 5) at frequencies of 1000 and 4000 Hz, respectively. All three models exhibit approximately the same general pattern in changes of loss coefficient with temperature and humidity according to these examples. However, there are clearly substantial differences in absolute values at specific weather conditions. Note that the model in Reference 20 is defined, strictly speaking, for pure tones and can overpredict effective loss coefficients for bands of noise at frequencies above 4000 Hz.

For illustration, Figures A1 and A2 also show the minor influence of a small reduction in atmospheric pressure below standard sea level values. This pressure effect is explicitly accounted for in the new proposed model as are other environmental parameters based on the basic physical principles utilized. Reference 20 provides a comprehensive comparison of the model with a large body of laboratory and field data.

Figures A3 through A7 show a more detailed picture of the variation in air absorption coefficient with temperature and humidity predicted with the new model. Note that Figures A3 and A4, in particular, show that at constant temperature, and hence constant maximum value, the loss coefficient decreases as humidity increases. Unlike the existing models, the loss coefficient shows a small increase, or second absorption peak due to nitrogen for humidities near 70 to 100%.

See pages 75 through 81 for Figures A1 through A7.

APPENDIX B

COMPILATION OF MEASURED SOUND PRESSURE LEVEL HISTOGRAMS

As discussed in report Section 4.3.2 with the aid of Figure 34, the amplitude histograms of the rms-detected sound levels provide a qualitative picture of amplitude fluctuations of sound occuring during a test run. Figures B1 through B4 show measured amplitude histograms for a selection of ten test runs indicating the ranges of sound-level fluctuations encountered for a range of weather conditions. These data are presented as a supplement to the information of Tables I through V.

See pages 82 through 86 for Figures B1 through B5.

REFERENCES

1. Knudsen, V. O.: The Absorption of Sound in Gases. J. Acoust. Soc. America, Vol. 5, 1933, pp. 112-121, also Vol. 6, 1935, pp. 199-204.

2. Evans, E. J.; and Bazley, E. N.: The Absorption of Sound in Air at Audio Frequencies. Acoustica, Vol. 6, 1956, pp. 238-244.

3. Harris, C.M.: Absorption of Sound in Air in the Audio-Frequency Range. NASA CR-647, 1967.

4. Harris, C. M.; and Tempest, W.: Absorption of Sound in Air below 1000 cps. NASA CR-237, 1965.

5. Society of Automotive Engineers: Standard Values of Atmosphere Absorption as a Function of Temperature and Humidity for Use in Evaluating Aircraft Flyover Noise. ARP 866, 1964.

6. Burkhard, M. D.; Karplus, H. B.; and Sabine, H. J.: Sound Propagation Near the Earth's Surface as Influenced by Weather Conditions. WADC TR 57-353, Vol. 1, and Vol. 2, 1958, 1960.

7. Tanner, C. S.: Experimental Atmospheric Absorption Coefficients. Federal Aviation Administration, FAA RD-71-99, 1971.

8. Bishop, D. E.; and Simpson, M. A.: Experimental Atmospheric Absorption Values from Aircraft Flyover Noise Signals. NASA CR-1751, 1971.

9. Parkin, P. H.; and Scholes, W. E.: Air-to-Ground Sound Propagation. J. Acoust. Soc. America, Vol. 26, 1954, pp. 1021-1023.

10. Parkin, P. H.; and Scholes, W. E.: Oblique Air-to-Ground Sound Propagation over Buildings. Acoustica, Vol. 8, 1958, pp. 99-102.

11. Ingard, U.: A Review of the Influence of Meteorological Conditions on Sound Propagation. J. Acoust. Soc. America, Vol. 25, 1953, pp. 405-411.

12. Nyborg, W. L.; and Mintzer, D.: Review of Sound Propagation in the Lower Atmosphere. WADC TR 54-602, 1955.

13. Piercy, J. E.; and Embleton, T. F. W.: Effect of Ground on Near-Horizontal Sound Propagation. Automotive Engineering Congress SAE paper 740211, 1974.

14. Hubbard, H. H.; and Maglieri, D. J.: An Investigation of Phenomena Relating to Aural Detection of Airplanes. NACA TN-4337, 1958.

15. Ingard, U.; and Maeling, G. C.: On the Effect of Atmospheric Turbulence on Sound Propagation over Ground. J. Acoust. Soc. America, Vol. 35, 1963, pp. 1056-1058.

16. Schilling, H. K.; et. al: Ultrasonic Propagation in Open Air. J. Acoust. Soc. America, Vol. 19, 1947, pp. 222-234.

17. Deloach, R.: On the Excess Attenuation of Sound in the Atmosphere. NASA TN D-7823, March 1975.

18. Evans, L. B.; Bass, H. E.; and Sutherland, L. C.: Atmospheric Absorption of Sound: Theoretical Predictions. J. Acoust. Soc. America, Vol. 51, 1972, pp. 1565-1575.

19. Kneser, H. O.: Interpretation of the Anomolous Sound Absorption in Air and Oxygen in Terms of Molecular Collisions. J. Acoust. Soc. America, Vol. 5, 1933, pp. 122-126.

20. Sutherland, L. C.: Review of Experimental Data in Support of a Proposed New Method for Computing Atmospheric Absorption Losses. Wyle Laboratories Report prepared for U. S. Department of Transportation, DOT-TST-75-87, May 1975.

21. Parkin, P. H.; and Scholes, W. E.: The Horizontal Propagation of Sound from a Jet Engine Close to the Ground, at Hatfield. J. Acoust. and Vibration, Vol. 2, 1965, pp. 353-374.

22. Tedrick, R. H.; Polly, R. C.: Sound Propagation of Low Frequency Sound Near the Earth's Surface. NASA TMX-1132, 1964.

23. Tatarski, V. I.: Wave Propagation in a Turbulent Medium. McGraw-Hill, New York, 1960.

24. Brownlee, L. R.: Rytov's Method and Large Fluctuations. J. Acoust. Soc. America, Vol. 53, 1973, p. 156.

25. Mintzer, D.: Wave Propagation in a Randomly Inhomogeneous Medium. J. Acoust. Soc. America, September 1953.

26. Clifford, S. F.; and Brown, E. H.: Acoustic Scattering from a Moving Turbulent Medium. J. Acoust. Soc. America, Vol. 55, 1974, pp. 929-933.

27. Howe, M. S.: Multiple Scattering of Sound by Turbulence and Other Inhomogeneities. J. Sound and Vibration, Vol. 27, 1973, pp. 455-476.

28. Kraichnan, R. H.: Scattering of Sound in a Turbulent Medium. J. Acoust. Soc. America, Vol. 25, 1953, pp. 1096-1104.

29. Kallistratova, M. A.: Experimental Investigation of the Scattering of Sound in the Atmosphere. Proceedings of the Third International Congress on Acoustics, Vol. 1, 1959, pp. 295-298.

30. Baerg, W.; and Schwarz, W. H.: Measurements of the Scattering of Sound from Turbulence. J. Acoust. Soc. America, Vol. 39, 1966, pp. 1125-1132.

31. Suchkov, B. A.: Fluctuations of Sound Amplitude in a Turbulent Medium. Soviet Physics-Acoustics, Vol. 4, pp. 84-90.

32. Knudsen, V. O.: The Propagation of Sound in the Atmospheric--Attenuation and Fluctuations. J. Acoust. Soc. America, Vol. 18, 1946, pp. 90-96.

33. Skudrzyk, E.: The Foundations of Acoustics. Springer-Veriag, New York, 1971.

34. Lumley, J. L.; and Panofsky, H. A.: The Structure of Atmospheric Turbulence. John Wiley and Sons, New York, 1964.

35. Kaimal, J. C.; Wyngaard, J. C.; Izumi, Y.; and Cote, O. R.: Spectral Characteristics of Surface-Layer Turbulence. Quarterly Journal of the Royal Meteorological Society, Vol. 98, 1972, p. 563.

TABLE I. TABULATION OF METEOROLOGICAL CONDITIONS DURING TEST RUNS

Run	Time	Temperature, °C						Wind Speed, m/sec						Wind Direction, deg.					Rel. Hum. at Carriage, %	Carriage Position: T, Top B, Base	Atmospheric pressure, mm Hg
		2m 6.6ft	†31m 100ft	61m 200ft	†91m 300ft	†130m 400ft	†152m 500ft	2m 6.6ft	†31m 100ft	61m 200ft	†91m 300ft	†130m 400ft	†152m 500ft	†31m 100ft	61m 200ft	†91m 300ft	†130m 400ft	†152m 500ft			
1	1930	6.7	7.0	7.1	-	-	7.1	-	8.3	9.7	-	-	10.6	-	-	-	-	-	-	-	-
2	0810	-7.2	-7.9	-8.3	-	-	-9.2	8.0	10.0	10.7	-	-	11.5	-	-	-	-	-	99	-	646.9
3	1410	-1.3	-2.7	-3.2	-	-	-3.8	3.6	6.0	7.5	-	-	5.5	002	000	-	-	013	83	T	654.6
4	2030	-4.0	-4.5	-4.7	-	-	-5.6	2.8	4.5	6.3	-	-	5.5	000	357	-	-	014	68	T	655.8
5	0150	-7.6	-6.3	-6.0	-	-	-6.7	1.2	4.2	5.2	-	-	6.3	174	181	-	-	182	71	T	655.8
6	0330	-7.9	-7.4	-6.7	-	-	-6.2	2.8	6.6	9.3	-	-	11.3	182	186	-	-	182	74	-	653.3
7	0730	-5.6	-6.3	-6.6	-	-	-7.4	3.4	5.0	6.3	-	-	6.6	154	155	-	-	158	86	T	652.3
8	1400	7.5	6.0	5.8	5.4	-	4.8	5.5	8.3	8.0	7.5	-	9.0	053	046	128	112	057	32	T	651.8
9	1930	2.6	5.3	5.7	5.4	-	5.0	2.6	7.2	8.1	-	-	8.3	122	123	-	-	122	6	T	651.8
10	0210	-1.8	0.2	0.0	-0.9	-	-0.4	0.7	1.1	0.3	0.3	-	0.3	323	371	-	-	222	18	T	-
11	0750	3.5	4.3	5.2	6.4	-	6.2	1.1	3.4	6.7	8.7	-	10.5	007	002	-	-	036	4	T	646.2
13	1400	6.0	3.3	3.6	2.0	-	2.0	0.7	11.0	11.0	10.5	-	10.6	055	046	044	-	054	29	T	647.7
14	1950	-3.0	-3.8	-4.0	-4.6	-	-5.1	6.0	10.0	9.5	10.0	-	10.3	059	048	047	-	056	37	T	649.5
16	0150	-7.4	-8.1	-8.5	-8.9	-	-9.3	-	6.4	6.5	6.2	-	6.4	109	102	094	110	090	68	T	649.5
19	0730	-9.1	-9.6	-9.9	-10.3	-	-10.8	4.0	3.9	5.5	6.3	-	6.1	030	012	010	-	037	93	T	649.5
20	1400	-4.7	-6.4	-7.1	-7.4	-	-8.0	3.0	2.9	4.7	4.4	-	3.9	039	038	019	-	033	93	T	653.5
21	2000	-6.4	-6.8	-7.0	-7.4	-	-7.8	1.5	3.6	3.2	3.2	-	3.1	117	112	109	-	104	90	T	654.3
23	0150	-6.8	-8.0	-7.5	-6.8	-	-6.8	1.4	4.6	6.2	7.1	-	6.7	143	150	167	-	173	90	T	654.1
24	0440	-8.6	-8.3	-7.0	-6.2	-	-6.2	1.3	3.9	5.3	5.6	-	6.6	147	174	196	-	206	87	T	653.3
25	0700	-7.0	-7.2	-6.6	-6.4	-	-5.6	1.5	3.5	4.0	4.2	-	2.8	132	164	187	-	182	86	T	652.3
26	0730	-5.9	-7.0	-6.9	-7.1	-	-6.4	1.6	1.4	1.7	2.9	-	3.8	055	109	143	-	199	91	E	653.0
27	1400	6.1	4.5	4.1	3.3	-	3.4	1.2	2.5	0.7	1.5	-	1.0	059	003	087	-	188	45	B	649.5
28	1920	4.1	7.1	7.3	7.0	6.7	6.6	2.3	7.6	8.5	8.7	8.3	8.6	079	072	073	086	081	47	B	649.5
29	1950	4.3	5.2	5.8	5.7	6.2	6.2	5.0	10.0	10.5	12.3	12.0	12.0	095	100	105	120	113	70	B	650.0
30	2040	3.1	3.9	4.6	4.9	5.4	5.5	6.6	11.6	12.0	13.6	13.8	14.0	105	106	115	133	126	53	B	650.5
31	0150	-3.2	-2.7	-2.6	-2.4	-2.6	-2.6	2.8	5.3	6.4	7.2	7.0	7.1	101	114	124	140	131	52	T	651.3
32	0410	-4.8	-4.2	-3.8	-4.0	-3.0	-3.1	2.0	5.1	4.8	4.4	1.8	1.4	038	046	062	101	104	87	T	651.3
33	0650	-6.5	-4.6	-4.3	-4.2	-2.6	-1.9	0.9	3.1	2.9	2.0	2.2	3.3	035	024	350	314	309	82	T	651.5
34	1410	16.8	14.0	13.8	12.8	12.4	13.6	2.8	3.7	4.6	3.8	3.2	4.0	202	200	195	209	206	20	B	650.7
35	1810	19.5	18.7	18.6	18.2	17.6	17.6	2.5	3.0	3.5	2.9	2.9	3.3	200	200	200	213	198	15	B	649.7
36	1840	13.8	17.9	18.0	17.8	17.4	17.2	2.2	5.1	5.6	5.7	5.3	5.8	139	143	145	155	145	15	B	649.0
37	2010	10.7	17.1	17.3	17.2	17.0	16.9	3.6	9.0	8.5	8.0	7.0	7.3	117	116	117	155	125	6	B	650.5
38	0130	1.4	5.3	5.9	6.5	8.1	8.2	1.6	2.9	1.7	1.5	1.3	2.0	114	075	015	335	310	6	T	652.5
39	0230	0.1	4.1	5.2	5.4	6.6	7.2	1.1	3.4	3.9	3.7	1.5	1.4	196	201	194	189	169	10	T	652.8
40	0650	-1.8	5.6	10.0	9.9	12.4	13.4	1.4	1.4	2.4	2.5	4.1	5.3	313	323	300	295	274	3	T	652.8
41	1410	22.7	20.0	19.9	19.6	19.0	19.0	2.0	3.0	2.0	2.0	4.0	3.5	280	290	270	280	270	1	B	651.8
42	1910	13.7	19.8	19.9	19.5	19.2	19.0	2.6	5.9	5.9	5.6	5.5	5.7	125	125	123	138	126	20	T	649.0
43	1950	12.6	19.3	19.5	19.3	19.2	19.0	2.7	4.9	4.8	4.8	4.4	4.5	110	113	124	146	135	11	B	649.2
44	2040	-	18.3	18.9	18.9	18.8	18.7	3.0	8.3	7.6	7.2	6.2	6.4	116	116	115	128	116	12	T	649.5
45	0200	5.3	12.7	13.0	13.1	13.5	13.6	1.7	5.5	6.3	7.3	7.2	6.2	295	298	280	275	259	12	T	648.7
46	0320	1.7	11.2	14.0	14.1	16.5	16.3	.7	2.0	4.1	5.5	7.2	7.9	307	255	241	269	257	12	T	648.5
47	0500	0.1	3.9	8.7	10.6	12.4	13.3	1.5	2.3	3.1	6.1	9.0	10.7	283	232	237	258	246	12	T	649.0
48	0550	3.9	9.4	10.9	12.6	14.3	14.3	1.4	4.6	6.0	8.7	10.0	8.2	284	293	269	270	263	32	B	649.0
49	0740	6.4	7.6	10.5	12.2	12.8	14.0	0.0	2.0	5.1	8.2	8.9	9.3	292	311	292	284	275	12	T	650.0
50	1100	22.9	21.0	21.0	19.9	19.1	19.5	1.7	1.9	3.0	2.9	3.7	2.7	165	175	160	180	180	18	T	650.2
52	1930	16.1	18.9	19.8	19.5	19.1	19.0	3.2	8.3	9.0	8.8	8.3	8.7	112	114	110	125	119	10	B	647.4
53	2010	16.1	18.2	19.7	19.4	19.0	18.9	4.5	9.0	11.2	10.8	10.0	10.5	112	115	109	121	116	10	B	647.2
54	0200	3.4	8.2	11.6	11.5	11.8	12.1	1.6	2.0	3.3	2.7	3.9	4.3	313	350	328	340	312	12	T	647.2
55	0420	4.3	7.1	10.0	10.5	11.1	11.4	0.0	4.1	7.4	5.3	10.6	8.9	290	329	316	327	314	13	T	647.2
56	0730	6.7	7.3	9.9	10.5	12.4	12.2	2.0	6.0	9.0	7.5	7.2	10.0	290	335	320	331	315	13	T	648.2
57	0750	10.1	9.3	9.5	9.8	11.2	11.5	1.7	3.8	7.0	6.0	11.0	-	310	330	320	330	320	12	T	648.2
58	1440	22.0	19.6	19.3	18.9	18.5	18.4	1.7	6.0	7.0	8.0	8.5	9.0	230	220	210	235	210	4	B	646.2
59	1630	21.8	20.6	20.1	19.9	19.1	19.2	2.5	4.0	2.8	3.8	5.2	7.5	230	225	215	236	225	15	B	645.4
60	2020	18.2	18.8	18.9	18.6	18.3	18.3	7.6	14.0	16.5	19.0	16.5	20.0	280	290	270	285	280	14	B	644.9
61	0410	7.3	7.5	7.5	7.3	7.2	6.9	8.9	10.8	15.3	13.5	17.3	18.0	318	324	309	319	363	14	B	649.2
62	0640	5.3	5.4	6.3	6.5	7.1	7.1	7.5	12.9	18.0	16.9	19.6	22.0	309	313	304	311	300	15	B	650.5

† Metric Units Rounded to Nearest Whole Unit.

TABLE II. COMPILATION OF DATA FROM 8-CYCLE TONE BURST TESTS

Test Freq., Hz	Run	Microphone Position 1		Microphone Position 2		Microphone Position 3		Microphone Position 4	
		Direct SPL(dB)	Reflected SPL (dB)	Direct SPL(dB)	Reflected SPL (dB)	Direct SPL(dB)	Reflected SPL (dB)	Direct SPL(dB)	Reflected SPL (dB)
550	6	94.6		80.8		77.8	70.7	75.0	70.5
	10	95.3		81.6		78.3	68.9	75.3	69.7
	17	94.7		80.8		77.9	70.5	75.3	69.6
	24	96.1	< 56	82.2	< 62	78.9	70.7	76.4	71.1
	30	95.6		-		-	-	75.3	-
	32	95.8		81.6		78.9	69.5	76.1	68.9
	44	94.9		80.4		77.5	70.2	74.9	70.0
1100	6	105.0		91.7		88.7	74.4	85.1	77.9
	10	105.0		90.8		87.7	74.3	84.7	78.0
	17	105.8		92.0		88.8	75.0	85.9	73.9
	24	106.7	< 58	93.0	< 62	89.8	76.3	87.0	80.1
	30	102.6		88.4		85.4	75.0	82.4	74.5
	32	106.4		92.4		89.3	73.2	86.1	74.6
	44	-		-		-	-	-	-
2200	6	100.5		84.5		81.1		77.3	
	10	101.2		85.0		81.2		78.0	
	17	100.8		86.5		82.8		78.1	
	24	101.6	< 55	87.3	< 63	83.6	< 57	78.7	< 57
	30	98.6		83.0		80.0		76.2	
	32	101.5		87.3		82.9		78.4	
	44	96.8		81.5		77.6		72.9	
4400	6	94.7		80.1		74.4		69.9	
	10	93.1		78.6		72.9		67.4	
	17	95.5		78.5		74.0		69.3	
	24	96.5	< 54	80.7	< 60	74.5	< 55	69.2	< 56
	30	92.2		-		-		-	
	32	95.4		80.1		74.3		69.3	
	44	95.7		81.4		-		-	

TABLE III. LONG-TIME-AVERAGED SOUND PRESSURE LEVELS

	550 Hz				1100 Hz				2200 Hz				4400 Hz				8000 Hz			
	Microphone				Microphone				Microphone				Microphone				Microphone			
Run	1	2	3	4	1	2	3	4	1	2	3	4	1	2	3	4	1	2	3	4
5	96.8	84.7	82.6	72.2	103.4	91.5	87.3	87.7	98.1	81.1	78.9	76.3	93.4	80.4	74.4	69.2	88.2	67.9	57.2	59.9
7	96.2	83.0	77.9	72.3	103.7	91.8	87.9	87.2	99.0	83.3	79.9	76.4	94.4	79.3	72.7	67.4	86.0	68.4	54.5	57.4
8	96.2	83.4	80.7	80.1	102.9	90.7	86.8	83.9	97.6	83.2	78.6	74.9	92.6	76.7	69.7	64.4	82.4	63.6	53.7	54.6
9	94.6	83.8	73.7	79.5	103.3	90.3	87.4	81.2	97.9	83.2	77.0	71.3	90.1	75.5	70.3	64.4	81.5	69.9	60.1	49.7
10	96.2	84.2	77.2	80.5	104.4	91.3	86.4	88.3	99.2	83.7	80.7	77.4	92.7	78.4	73.0	67.9	84.3	63.1	53.0	51.7
11	95.7	83.3	78.9	72.3	102.7	90.7	86.0	84.8	96.9	82.1	77.8	75.7	91.7	76.6	70.1	63.4	81.2	62.7	51.7	47.7
13	98.1	83.5	80.5	77.6	105.1	90.5	88.1	85.2	100.1	82.5	82.9	78.8	96.6	78.7	73.1	69.4	88.1	64.5	55.5	55.9
15	98.2	84.2	82.6	77.5	105.5	91.8	89.1	85.8	100.3	85.7	81.8	77.3	96.8	77.2	72.7	69.4	80.4	67.1	59.9	60.1
16	96.9	84.3	79.3	81.1	103.2	91.0	87.8	82.9	98.4	85.0	80.9	75.2	94.9	76.9	72.1	68.8	86.4	63.6	57.2	56.5
19	97.1	84.3	80.3	78.4	103.4	90.8	87.6	82.2	96.9	84.0	80.0	74.7	93.9	79.4	73.1	67.7	84.7	66.8	57.5	55.2
20	96.7	83.3	82.4	76.4	103.7	91.6	87.5	85.9	98.0	84.5	81.1	75.1	93.6	78.5	71.8	66.9	89.1	68.8	57.7	56.0
21	97.4	85.0	79.9	74.0	103.9	91.7	89.0	88.3	98.5	85.0	80.6	79.4	94.0	79.3	72.6	67.2	87.3	66.2	57.9	56.2
23	97.8	82.8	82.1	82.0	104.5	92.5	87.9	83.8	99.0	84.8	81.3	76.3	94.3	79.4	73.4	68.0	86.1	67.2	56.7	55.7
26	98.3	84.5	84.7	84.1	104.8	92.9	88.3	84.2	99.1	85.7	81.8	76.5	95.4	80.0	73.3	68.2	90.0	68.8	58.7	56.0
27	97.1	84.5	84.0	80.8	103.9	91.9	88.5	84.7	98.7	85.6	81.5	76.9	93.1	76.0	69.8	65.1	87.0	61.1	52.0	51.1
29	96.3	83.4	81.0	77.3	103.4	89.4	87.7	83.0	97.8	82.4	79.9	76.4	89.0	72.0	65.7	63.7	82.3	58.0	54.6	54.9
31	96.2	81.3	81.3	76.8	103.5	91.0	88.3	85.5	98.9	85.0	80.1	75.2	94.3	74.9	69.1	65.9	87.6	61.2	52.1	50.4
33	98.2	85.3	84.6	80.7	104.9	92.3	87.0	85.9	99.9	86.4	82.8	77.8	95.3	78.0	74.8	68.2	89.3	66.7	55.8	54.6
34	96.3	83.3	80.8	77.4	103.4	90.5	87.1	83.6	97.8	83.3	78.5	73.5	92.0	73.0	65.9	63.7	85.1	63.8	58.3	59.1
35	96.0	84.5	77.2	78.2	102.8	89.8	86.1	82.6	96.5	81.8	76.6	72.7	90.0	70.5	62.9	58.6	84.5	59.0	48.6	51.2
37	95.7	82.8	75.6	71.3	103.2	90.1	84.8	84.6	97.5	83.0	77.3	71.8	92.6	70.9	64.1	64.4	82.0	60.1	53.4	53.9
38	95.9	82.8	77.7	71.8	103.5	89.8	87.1	82.5	99.7	85.3	81.6	76.0	93.6	75.5	69.6	65.1	83.9	58.5	50.9	50.9
40	95.1	81.5	80.9	77.9	103.5	91.2	88.1	83.9	98.6	84.2	81.0	76.7	92.5	74.3	68.8	65.5	85.3	59.4	51.3	52.1
41	95.5	80.9	75.8	70.6	102.4	89.3	86.2	83.2	97.1	82.0	77.0	72.1	92.0	71.2	62.6	59.1	81.9	58.4	47.8	50.4
43	95.6	81.9	80.1	78.2	103.3	89.9	85.6	83.3	96.6	82.3	77.3	68.9	89.8	73.2	64.3	56.6	82.6	57.8	56.4	54.4
45	94.9	82.0	80.1	78.4	102.9	90.7	89.0	84.3	97.6	83.7	78.6	74.7	91.6	73.7	66.7	63.4	83.3	58.3	46.4	44.2
46	95.0	82.9	82.1	74.3	103.3	90.7	86.8	84.1	98.3	83.8	79.7	74.5	86.7	73.6	66.5	61.4	81.4	58.5	53.1	51.1
48	95.4	79.6	78.6	74.4	102.2	85.6	83.5	79.0	98.5	84.2	78.2	75.8	92.8	73.3	67.6	63.2	81.9	56.5	46.9	46.9
49	95.7	84.8	83.2	81.4	103.9	91.2	87.6	82.2	97.9	87.1	82.8	77.7	94.0	73.0	66.7	63.9	80.8	57.1	48.4	48.8
53	95.7	83.7	79.8	78.9	102.9	89.6	86.9	81.6	97.1	83.2	79.4	73.5	91.0	70.9	65.3	61.4	81.1	56.5	56.5	51.7
54	95.4	81.3	78.5	71.5	103.4	91.1	88.3	81.7	97.6	85.1	80.4	78.8	91.3	75.8	70.9	66.9	82.5	58.4	50.0	47.4
57	96.6	81.1	81.0	75.4	103.5	90.1	87.7	85.1	99.5	84.8	81.3	75.7	94.6	78.0	68.6	66.5	83.3	63.8	53.1	54.0
58	96.3	81.8	79.5	77.9	102.7	88.3	85.2	81.3	97.6	81.8	77.4	69.4	93.4	75.2	63.6	59.9	84.3	67.8	57.8	53.3

TABLE IV. CALCULATED ATMOSPHERIC ABSORPTION LOSSES

Run	Absorption Loss (dB) Between Microphone Positions 1 and 2					Absorption Loss (dB) Between Microphone Positions 1 and 3					Absorption Loss (dB) Between Microphone Positions 1 and 4				
	550 Hz	1100 Hz	2200 Hz	4400 Hz	8000 Hz	550 Hz	1100 Hz	2200 Hz	4400 Hz	8000 Hz	550 Hz	1100 Hz	2200 Hz	4400 Hz	8000 Hz
5	0.1	0.3	1.2	3.8	7.5	0.2	0.6	2.0	6.2	12.6	0.2	0.8	2.8	8.7	17.6
7	0.1	0.3	1.0	3.4	7.5	0.2	0.5	1.7	5.6	12.6	0.2	0.7	*	7.8	17.7
8	0.1	0.4	1.5	4.7	9.5	0.2	0.7	2.5	*	*	0.3	1.0	*	*	*
9	0.6	*	*	*	*	1.0	*	*	*	*	1.4	*	*	*	*
10	0.3	1.0	2.1	*	*	0.6	1.7	3.6	*	*	0.8	2.4	*	*	*
11	0.6	*	*	*	*	1.0	*	*	*	*	1.4	*	*	*	*
13	0.2	0.6	1.9	4.8	*	0.3	0.9	3.2	8.1	*	0.4	1.3	*	11.3	*
15	0.2	0.7	1.9	3.9	*	0.3	1.1	3.2	6.6	*	0.4	1.5	4.5	*	*
16	0.1	0.4	1.5	3.8	6.4	0.2	0.7	2.4	6.4	10.8	0.3	1.0	3.3	8.9	*
19	0.1	0.3	1.2	3.5	6.8	0.2	0.5	1.9	5.8	11.5	0.2	0.7	2.7	8.1	16.2
20	0.1	0.3	1.0	3.3	7.4	0.1	0.5	1.6	5.4	12.4	0.2	0.6	2.2	7.5	17.4
21	0.1	0.3	1.0	3.3	7.5	0.1	0.5	1.7	5.5	12.5	0.2	0.6	2.3	7.7	17.5
23	0.1	0.3	1.0	3.3	7.5	0.1	0.5	1.6	5.4	12.6	0.2	0.6	2.3	7.7	17.5
26	0.1	0.3	1.0	3.2	7.5	0.1	0.4	1.6	5.4	12.5	0.2	0.6	2.2	7.6	17.6
27	0.1	0.3	1.2	3.9	9.2	0.2	0.5	1.9	*	15.3	0.3	0.8	2.6	*	21.4
29	0.1	0.2	0.6	2.3	6.8	0.2	0.4	1.1	3.8	*	0.2	0.5	1.5	5.4	*
31	0.1	0.4	1.4	4.1	8.1	0.2	0.6	2.3	6.9	13.4	0.3	0.9	3.2	9.6	*
33	0.1	0.2	0.9	3.0	7.8	0.1	0.4	1.5	5.2	13.0	0.2	0.6	2.1	7.3	18.2
34	0.2	0.5	1.7	*	*	0.3	0.8	*	*	*	0.4	1.1	*	*	*
35	0.2	0.5	*	*	*	0.3	0.9	*	*	*	0.4	1.2	*	*	*
37	0.5	*	*	*	*	0.7	*	*	*	*	1.0	*	*	*	*
38	0.6	*	*	*	*	1.0	*	*	*	*	1.5	*	*	*	*
40	0.7	*	*	*	*	1.1	*	*	*	*	1.5	*	*	*	*
41	0.5	*	*	*	*	0.9	*	*	*	*	1.2	*	*	*	*
43	0.2	*	*	*	*	0.4	*	*	*	*	0.5	*	*	*	*
45	0.2	*	2.6	*	*	0.4	*	*	*	*	0.6	*	*	*	*
46	0.2	*	*	*	*	0.4	*	*	*	*	0.6	*	*	*	*
48	0.1	0.3	1.0	*	*	0.2	0.5	1.7	*	*	0.3	0.8	2.5	*	*
49	0.3	*	2.7	*	*	0.4	*	*	*	*	0.6	*	*	*	*
53	0.2	*	*	*	*	0.4	*	*	*	*	0.5	*	*	*	*
54	0.3	*	2.7	*	*	0.5	*	*	*	*	0.6	*	*	*	*
57	0.3	*	2.7	*	*	0.5	*	4.5	*	*	0.7	*	*	*	*
58	0.6	*	*	*	*	1.0	*	*	*	*	*	*	*	*	*

* uncertainty greater than 1 dB

TABLE V. NORMALIZED RMS ENVELOPE FLUCTUATIONS, E (%)

Run	Microphone Position	Test Frequency, Hz				
		550	1100	2200	4400	8000
9	1	-	-	1.51	2.26	4.13
	2	-	-	2.04	3.64	6.03
	3	-	2.86	3.09	4.44	11.47
	4	-	6.28	12.10	7.44	28.44
21	1	-	0.30	0.58	0.90	1.92
	2	-	0.91	1.68	1.78	2.65
	3	-	1.47	2.27	3.36	4.94
	4	-	1.71	2.93	4.82	7.74
26	1	0.43	1.25	1.89	3.05	2.27
	2	3.63	4.38	4.45	8.46	14.07
	3	2.98	8.27	8.55	14.57	28.90
	4	3.20	13.00	20.90	21.30	40.30
29	1	-	0.64	1.11	-	-
	2	-	8.37	8.53	-	-
	3	12.13	12.51	16.47	-	-
	4	13.30	17.53	22.73	-	-
33	1	-	1.20	2.90	4.34	8.33
	2	-	0.93	2.45	5.94	10.61
	3	-	1.87	2.98	4.51	12.93
	4	-	2.67	4.46	9.96	18.93
35	1	0.69	1.17	1.57	1.86	2.98
	2	1.53	3.27	4.43	5.33	8.11
	3	3.71	7.20	7.05	10 85	-
	4	4.11	7.60	8.57	15.33	-
37	1	-	0.49	-	-	-
	2	-	1.49	-	-	-
	3	-	3.17	-	-	-
	4	-	2.97	-	-	-
40	1	0.73	2.62	5.12	5.67	13.00
	2	1.48	5.00	9.86	20.13	29.10
	3	1.90	5.23	9.42	17.94	20.37
	4	2.21	6.15	10.68	22.85	30.83
57	1	-	-	-	-	-
	2	5.84	8.30	16.94	14.59	40.64
	3	6.08	13.93	19.90	27.79	-
	4	10.07	12.56	27.79	33.80	-

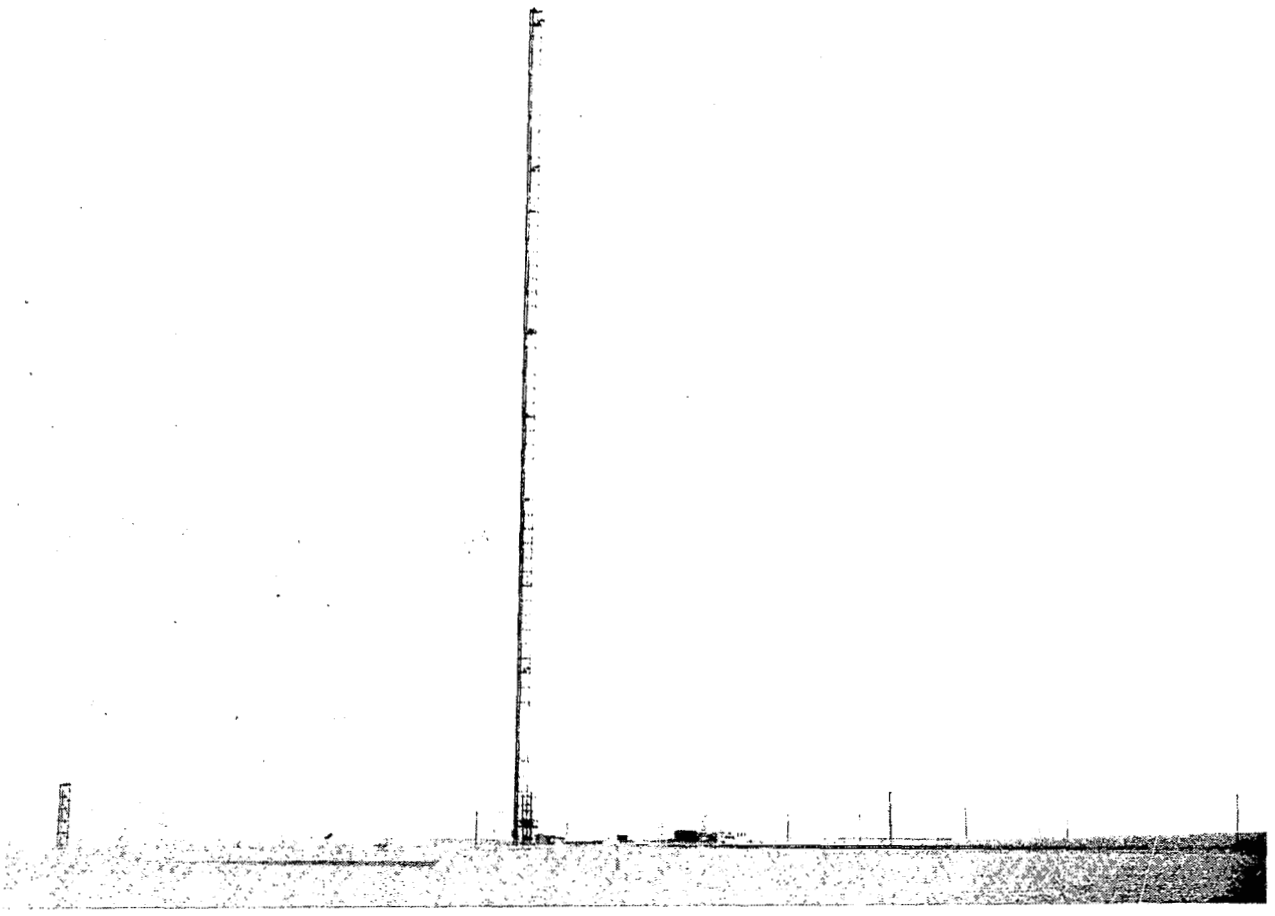

Figure 1. View of Test Site.

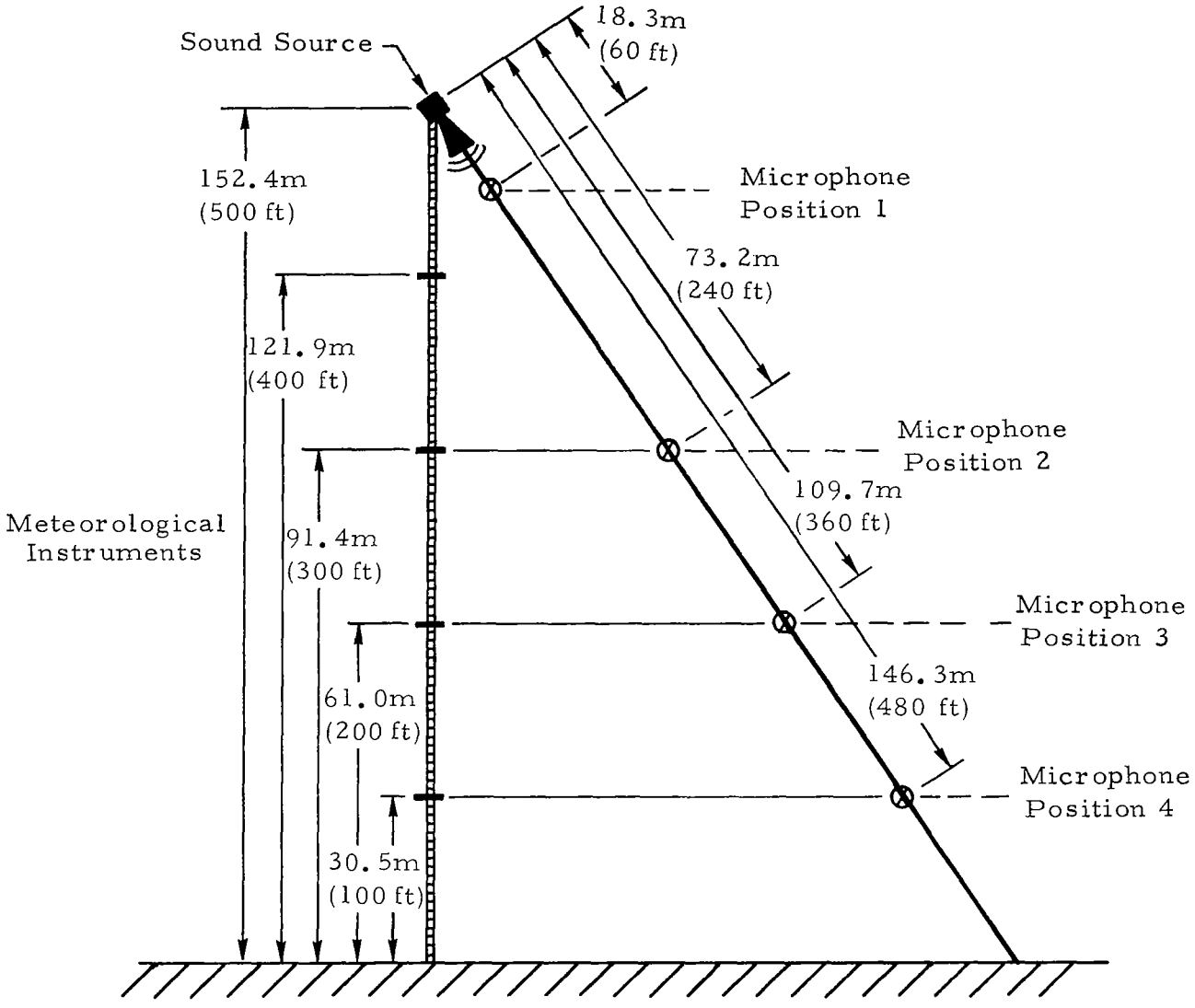

Figure 2. Profile Sketch of Haswell Tower Showing Positions of Microphones Along East Guy Wire.

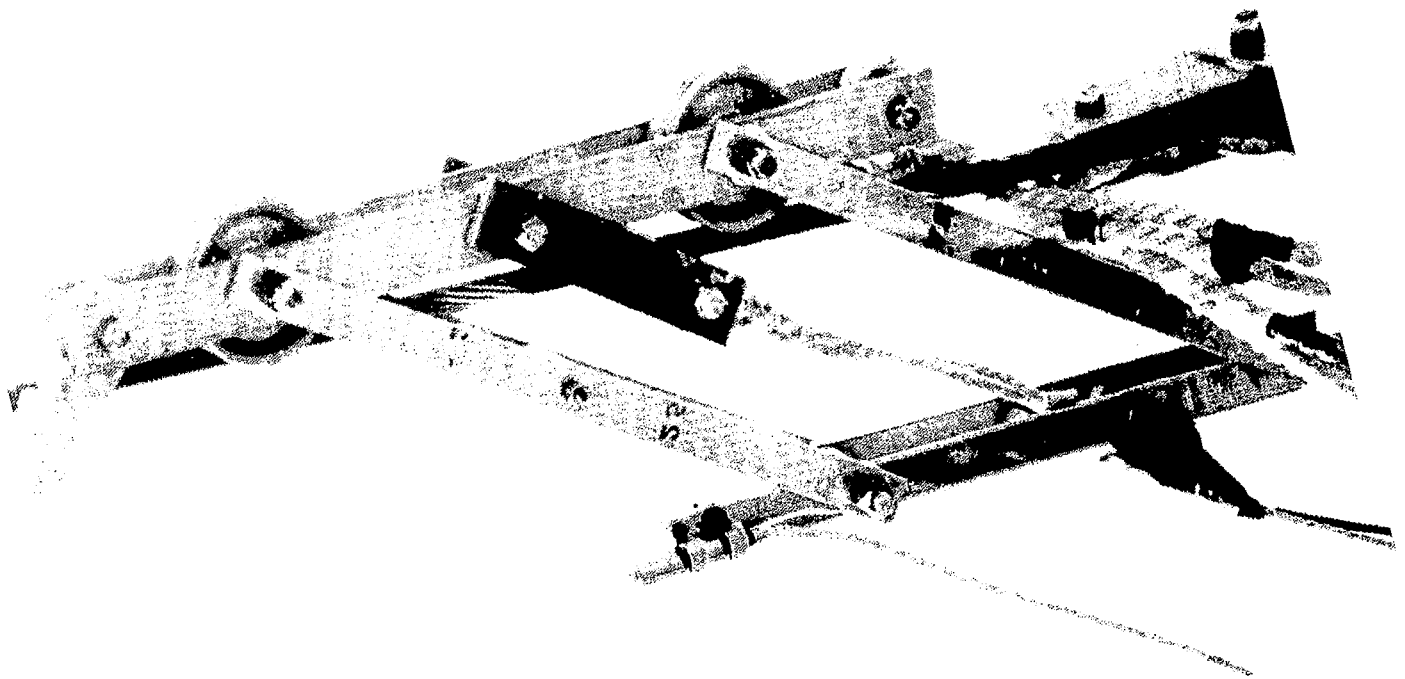

...ophone Carriage.

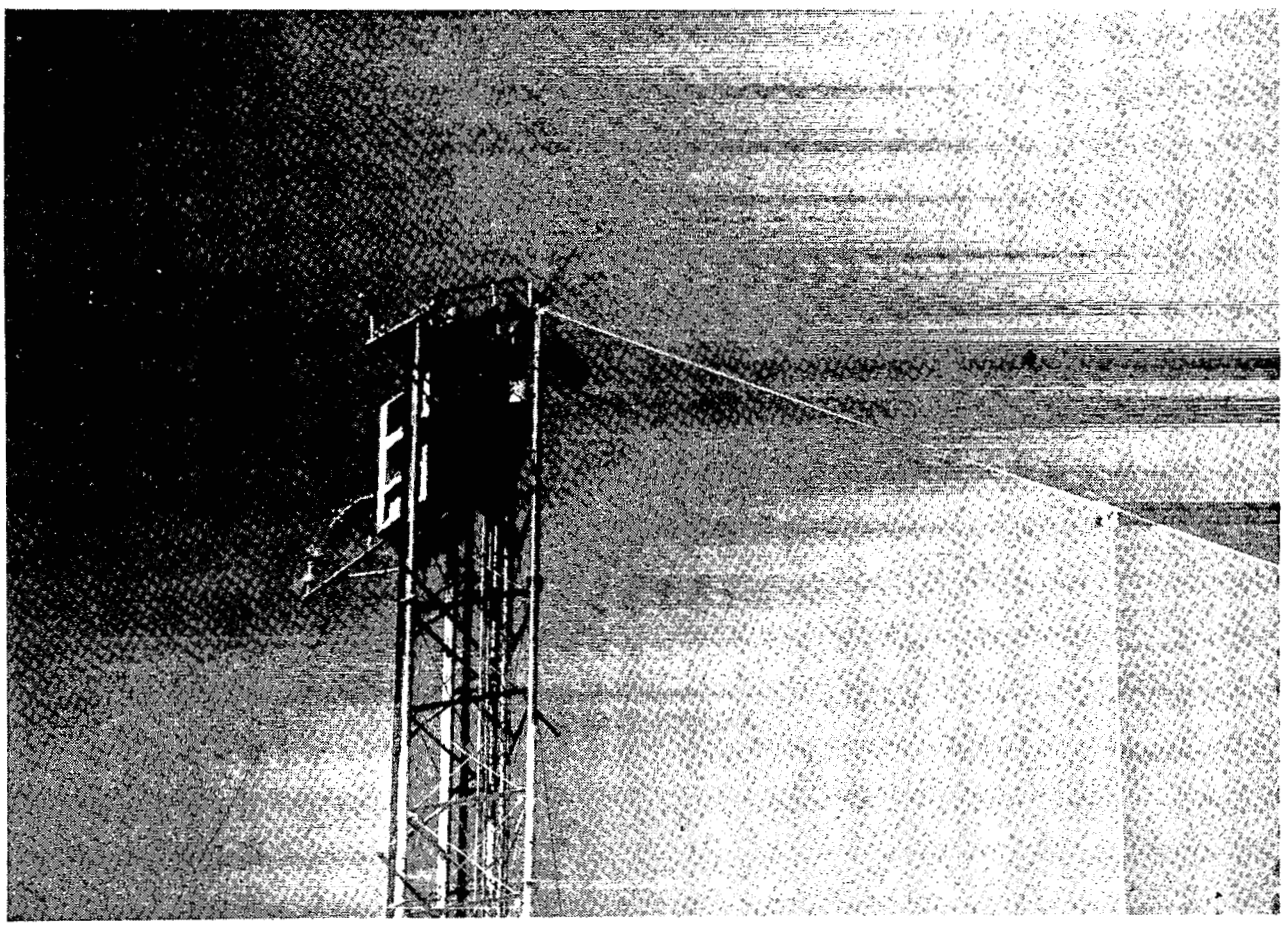

Figure 4. View of Top of Tower Showing First Microphone Position.

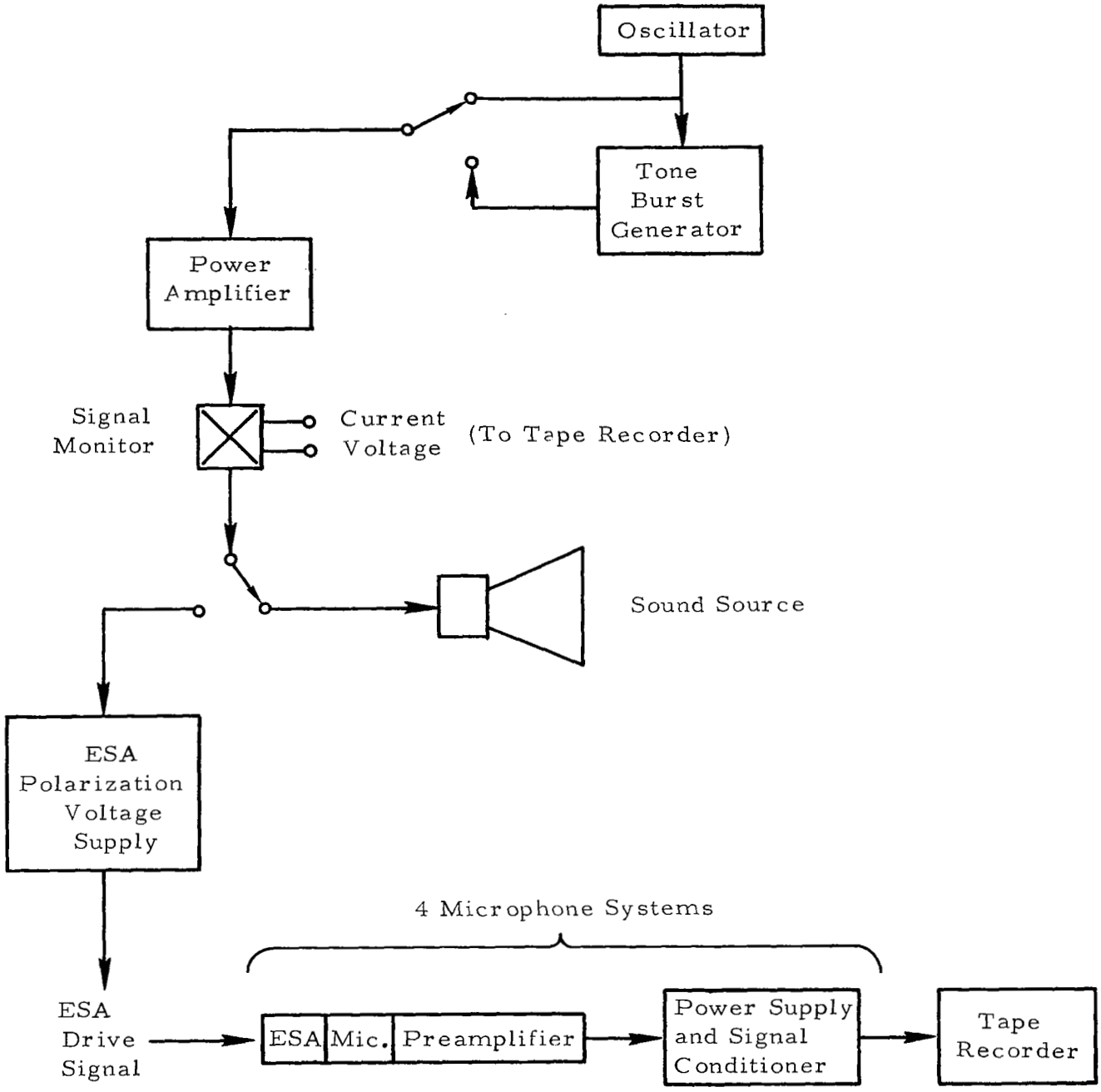

Figure 5. Block Diagram of Field Instrumentation.

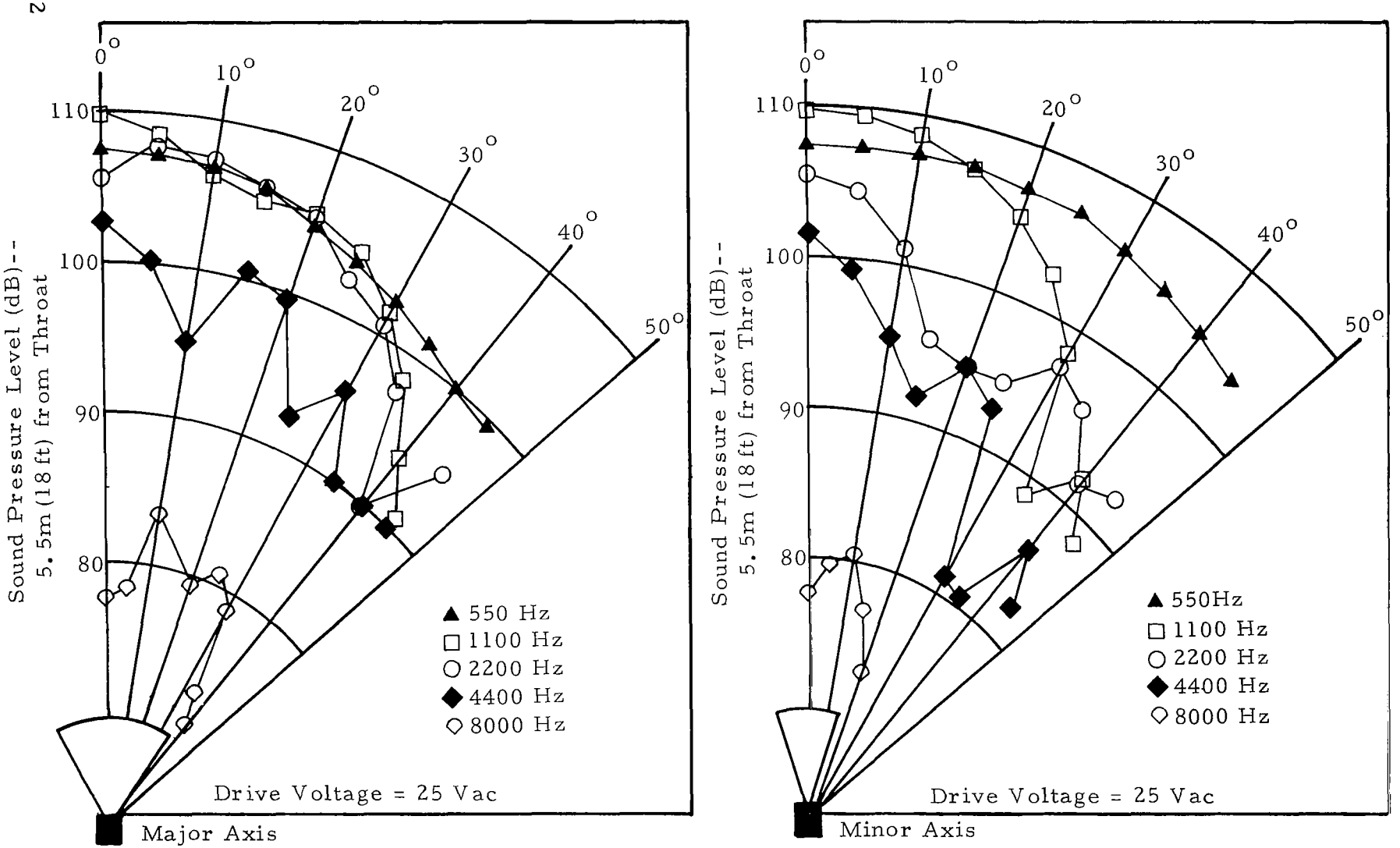

Figure 6. Measured Directivity Pattern of Sound Source.

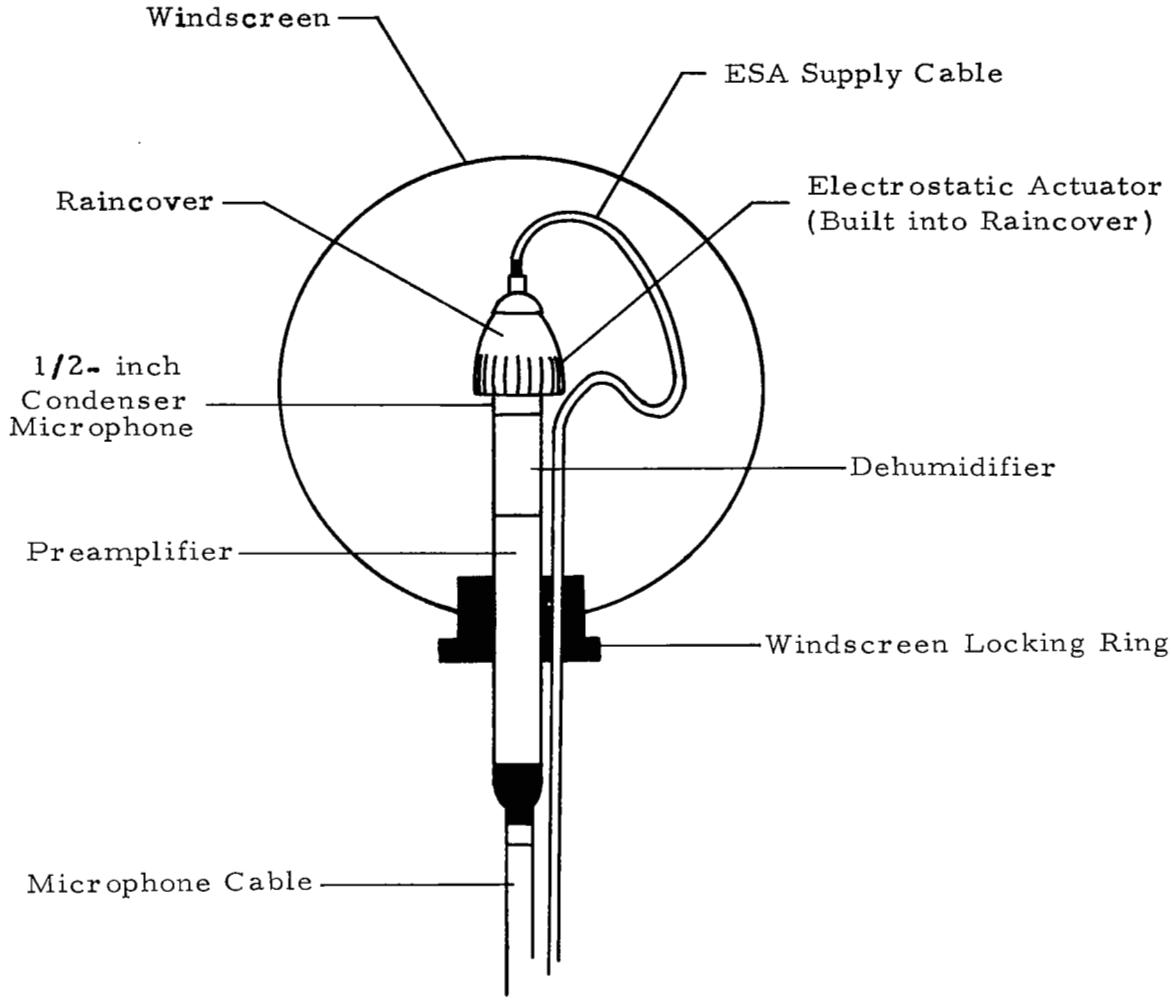

Figure 7. Sketch of Microphone System Components.

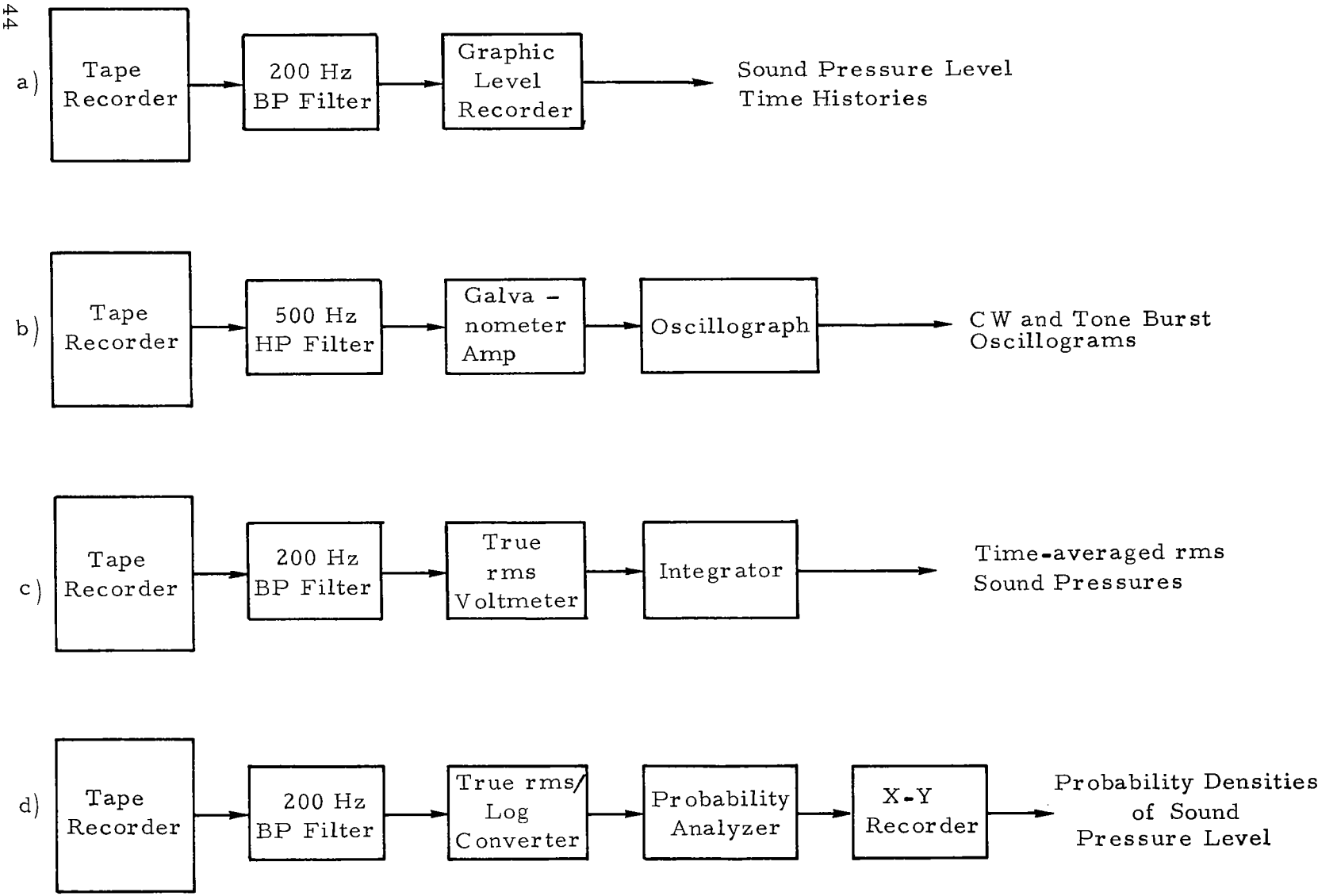

Figure 8. Block Diagrams of Data Reduction Systems.

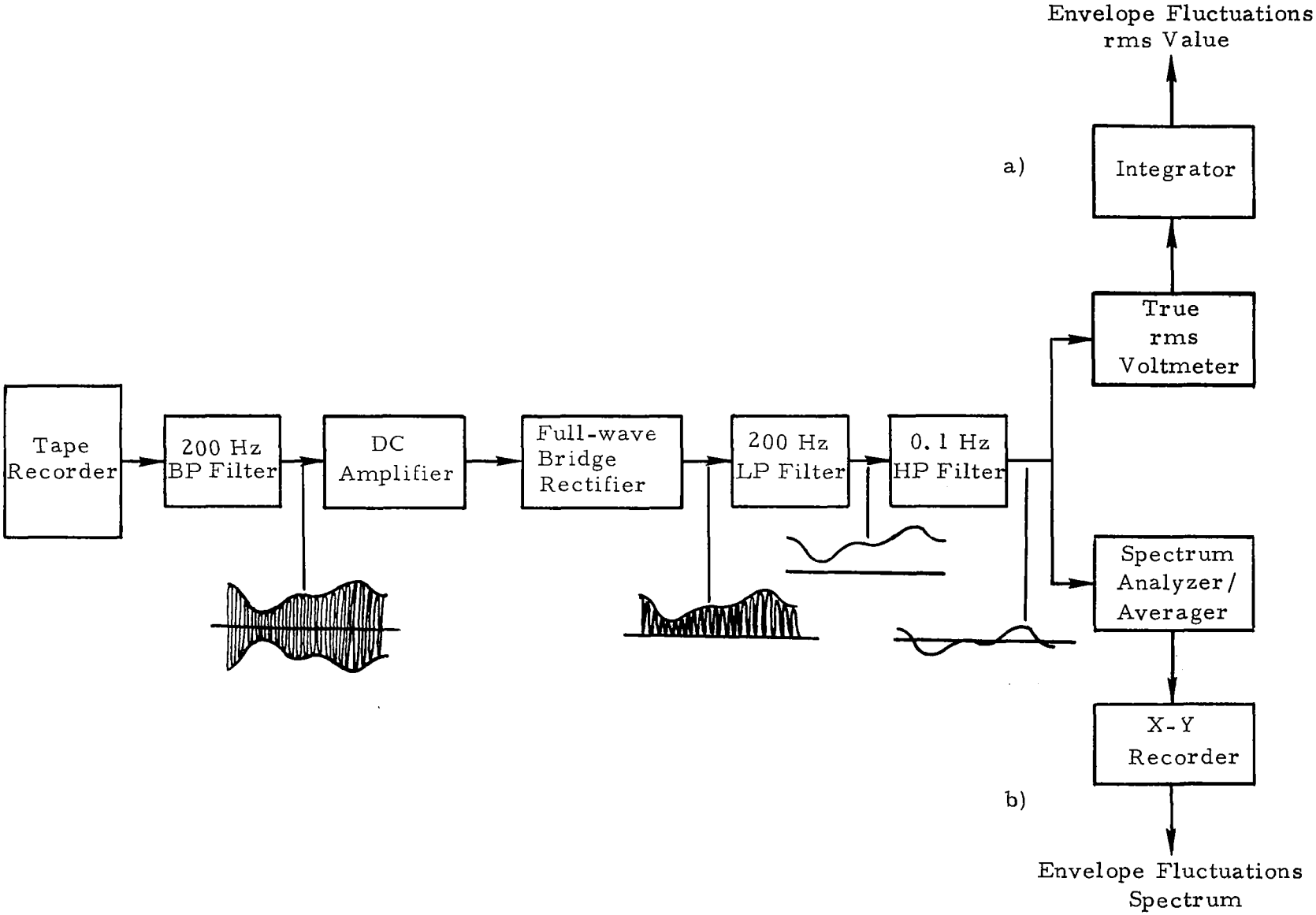

Figure 9. Instrumentation Diagram for Envelope Fluctuation Analysis.

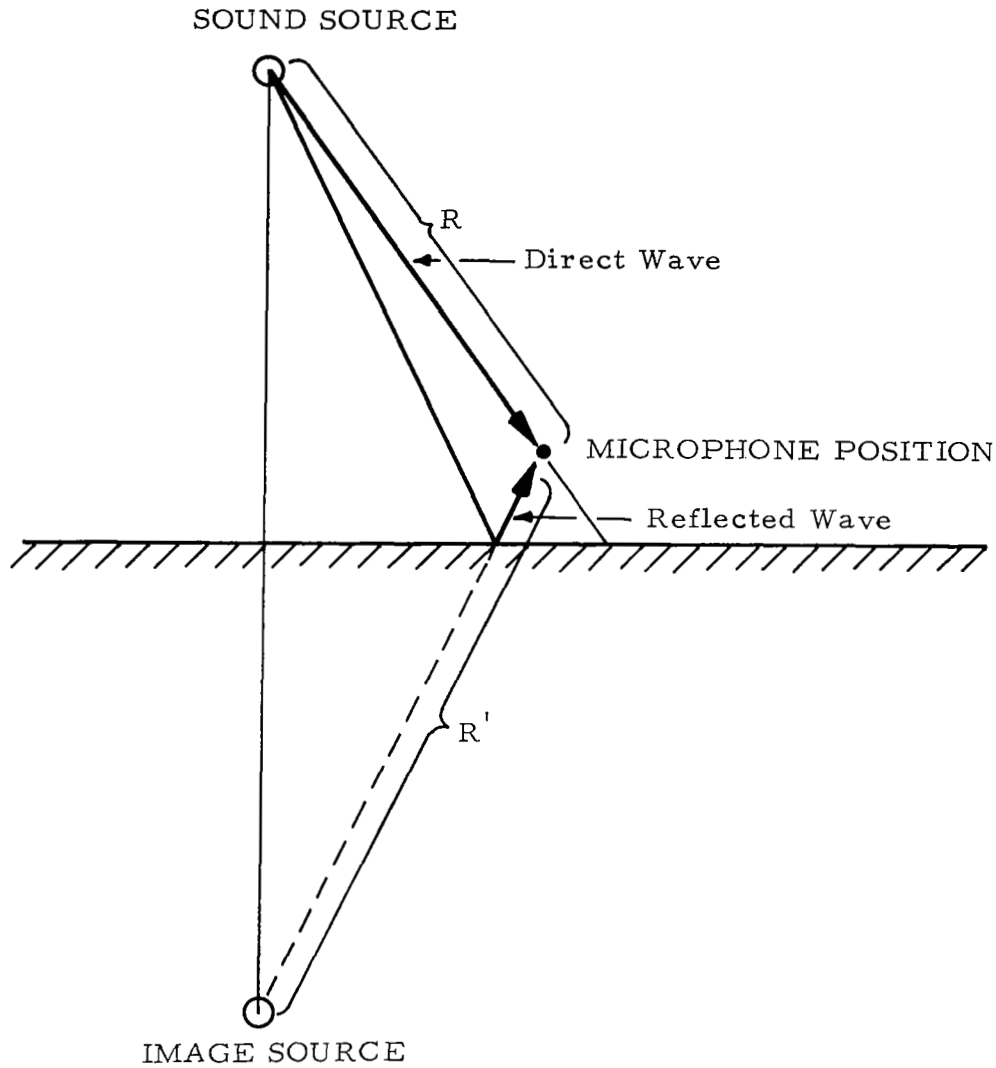

Figure 10. Illustration of Direct and Ground-Reflected Sound Paths to Microphone Position.

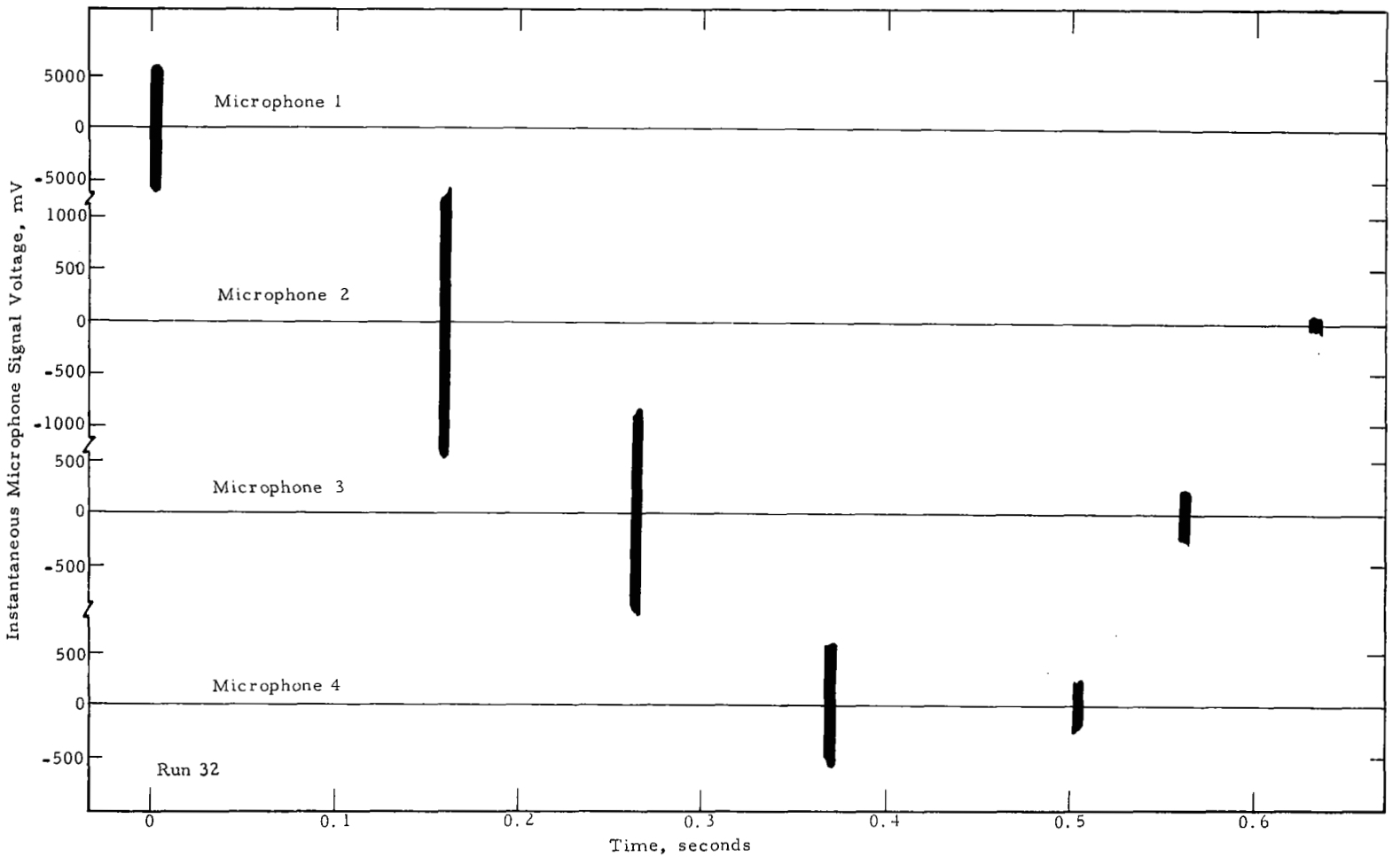

Figure 11. Typical Microphone Signal Oscillograms of 8-Cycle Tone Burst at 1100 Hz.

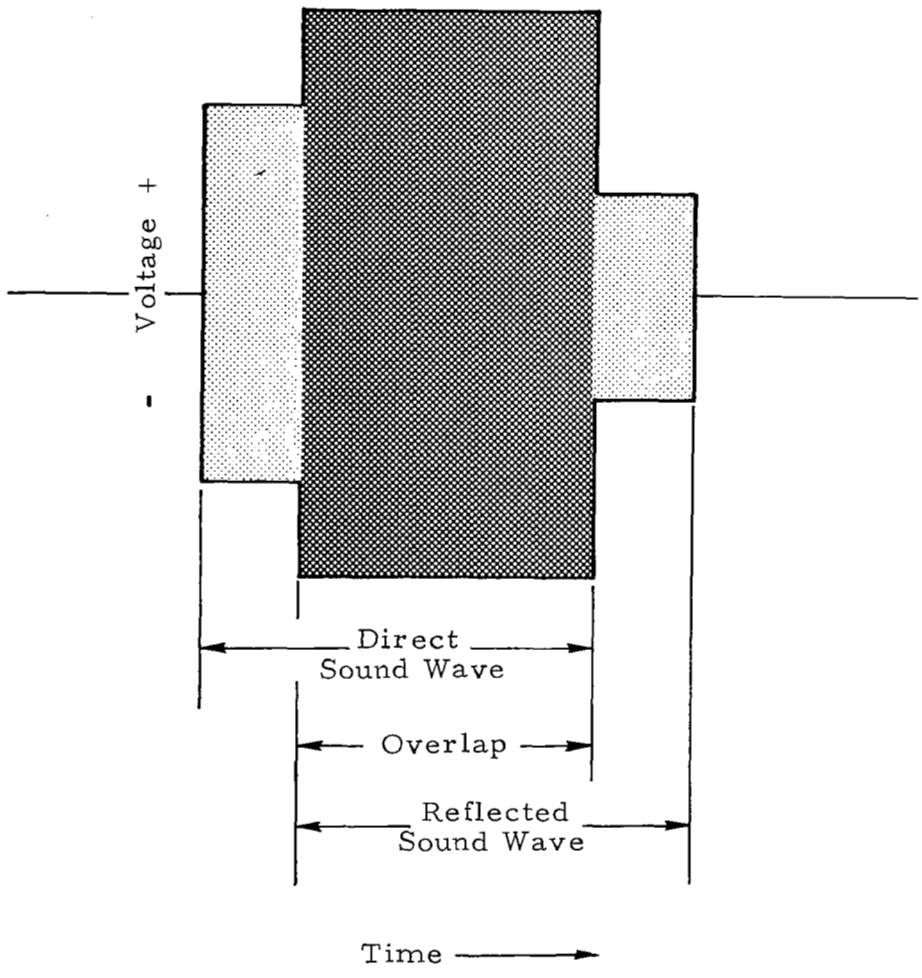

Figure 12. Illustrative Microphone Signal Tone Burst Oscillograph Trace Showing Overlap of Direct and Reflected Sound Waves.

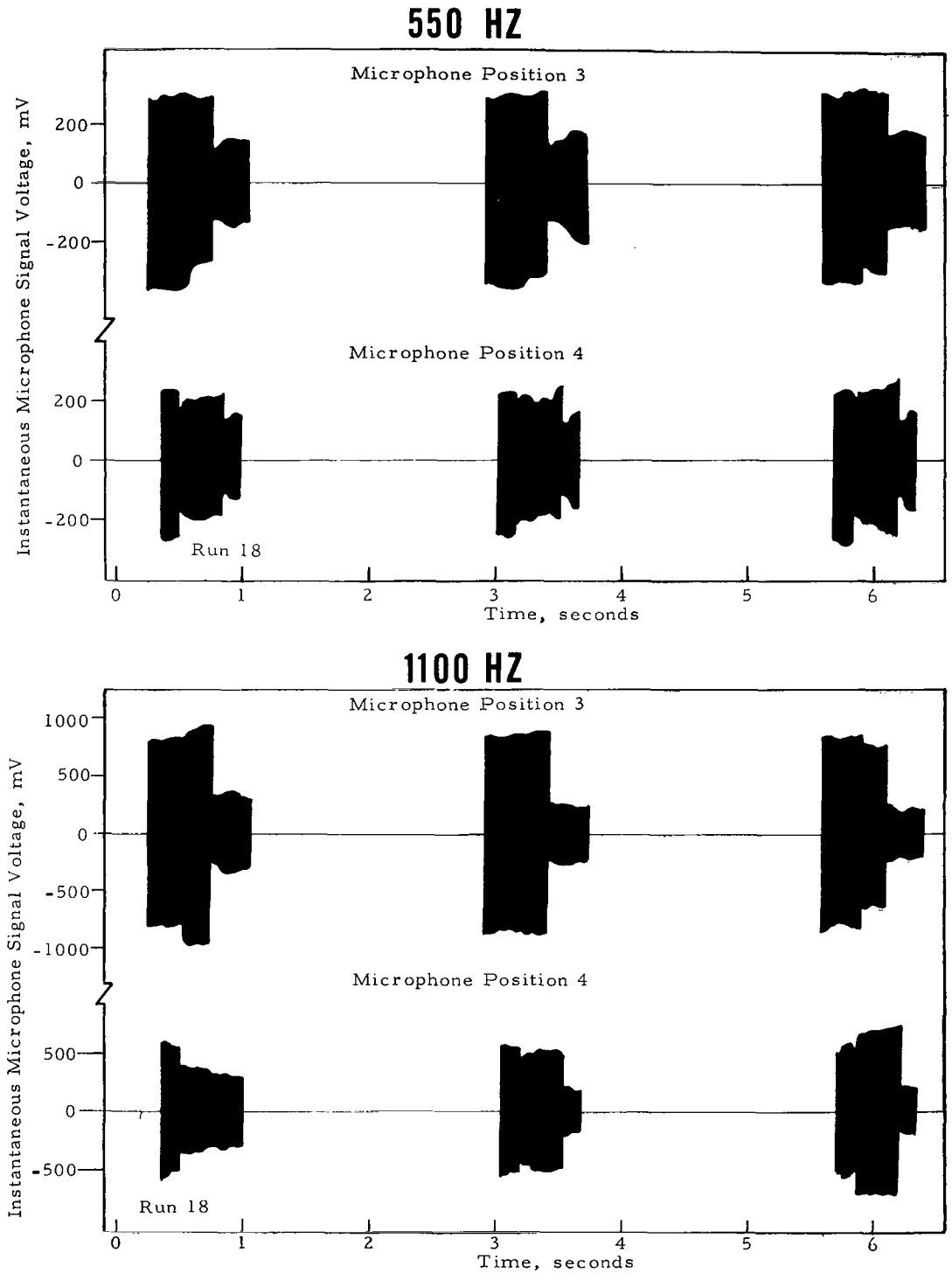

Figure 13. Microphone Signal Oscillograms of Three Consecutive One-Half Second Duration Tone Bursts at 550 and 1100 Hz.

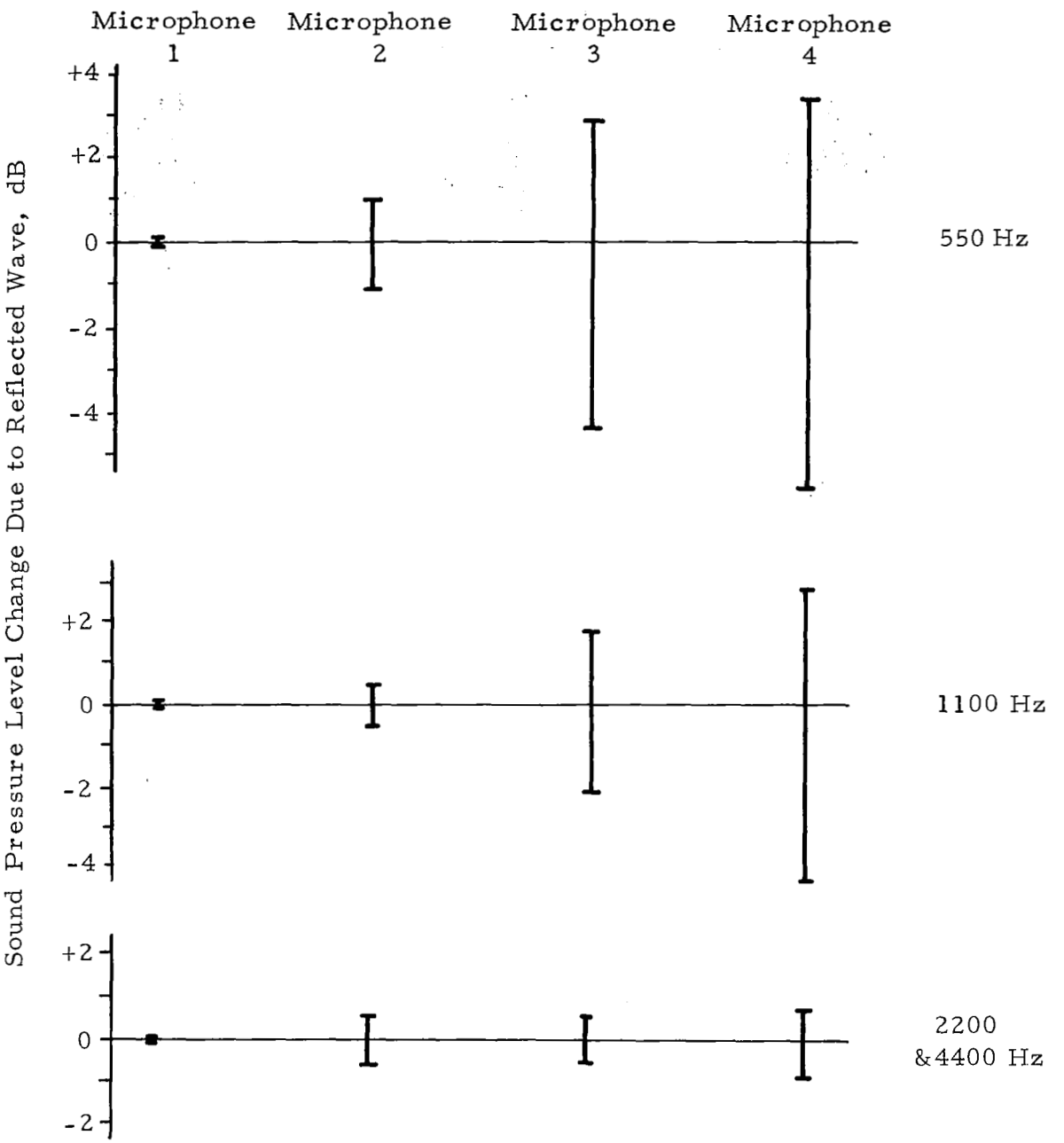

Figure 14. Calculated Range of Influence of Reflected Wave on Direct-Wave Sound Levels Based on Tone Burst Data.

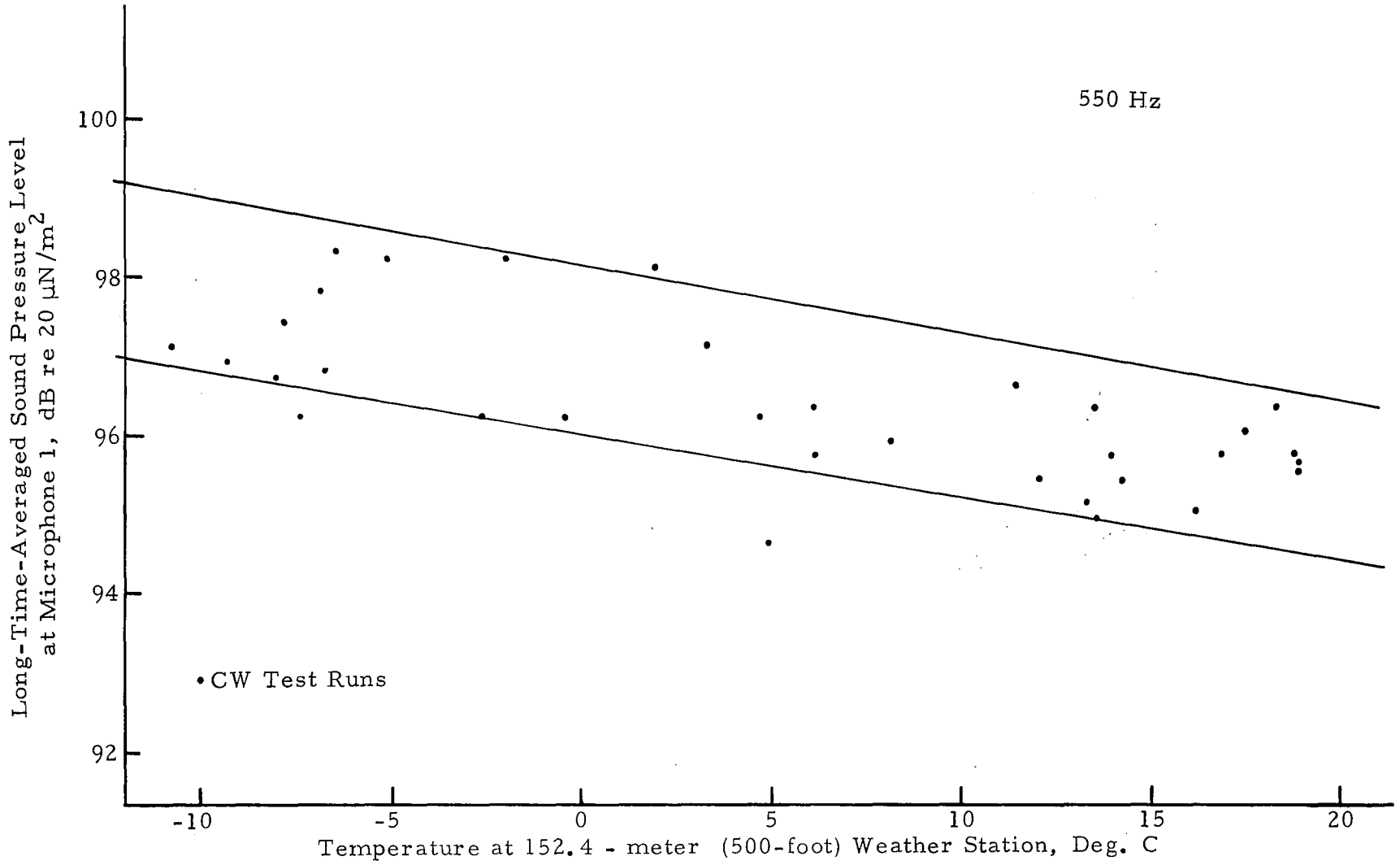

Figure 15. Correlation of Sound Pressure Level at Microphone Position 1 with Temperature.

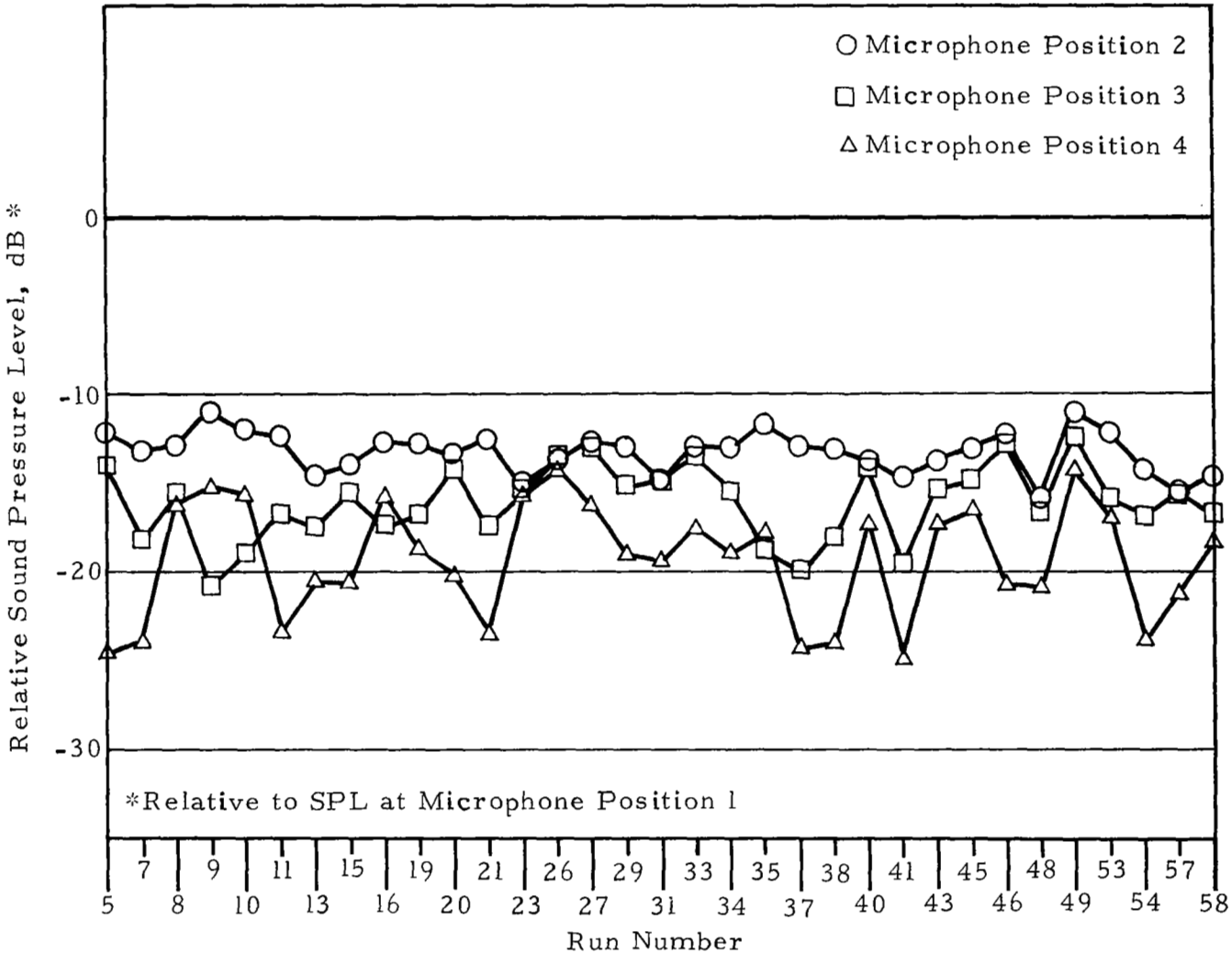

Figure 16. Comparison of Normalized Long-Time-Averaged Sound Pressure Levels for CW Test Runs at 550 Hz.

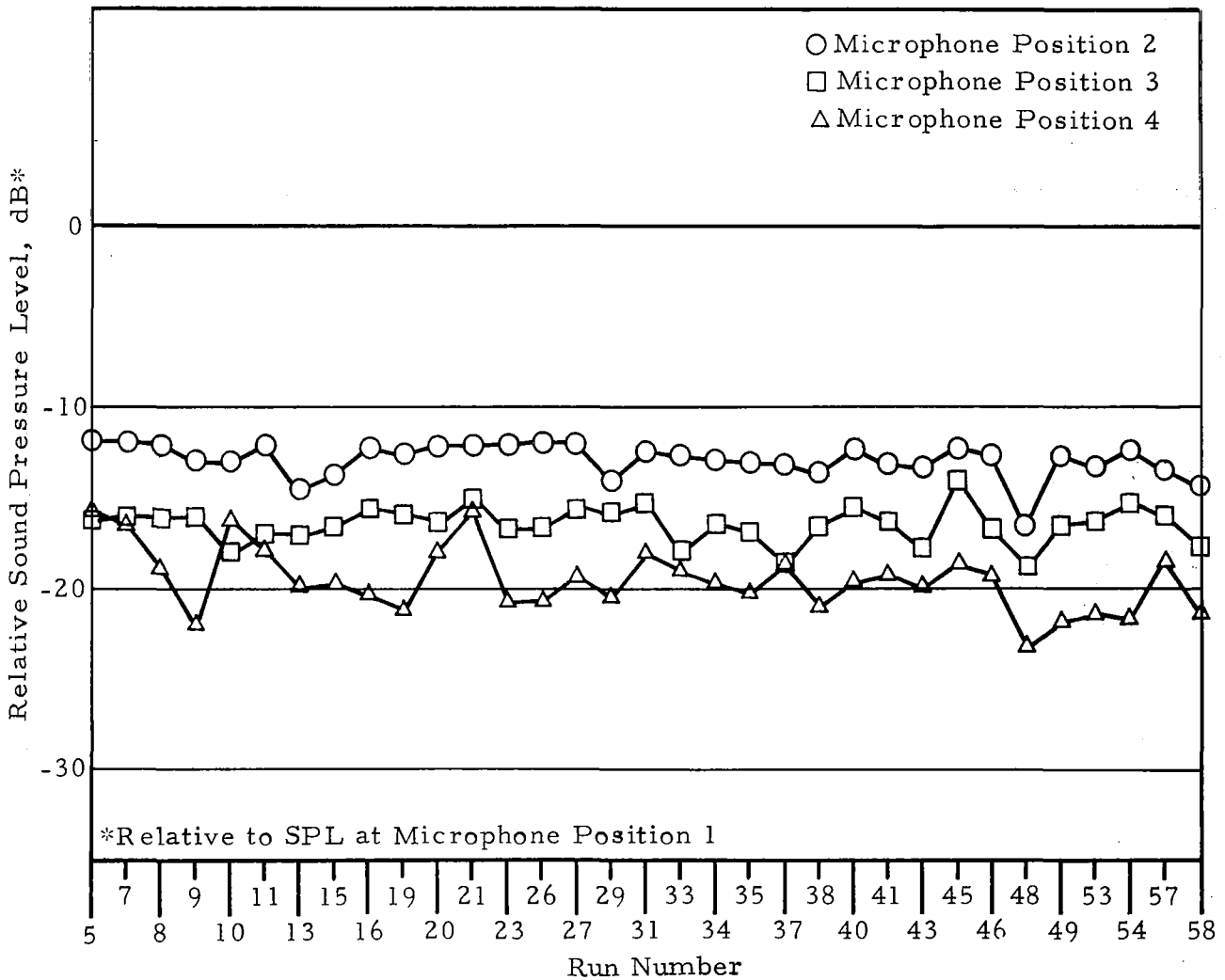

Figure 17. Comparison of Normalized Long-Time-Averaged Sound Pressure Levels for CW Test Runs at 1100 Hz.

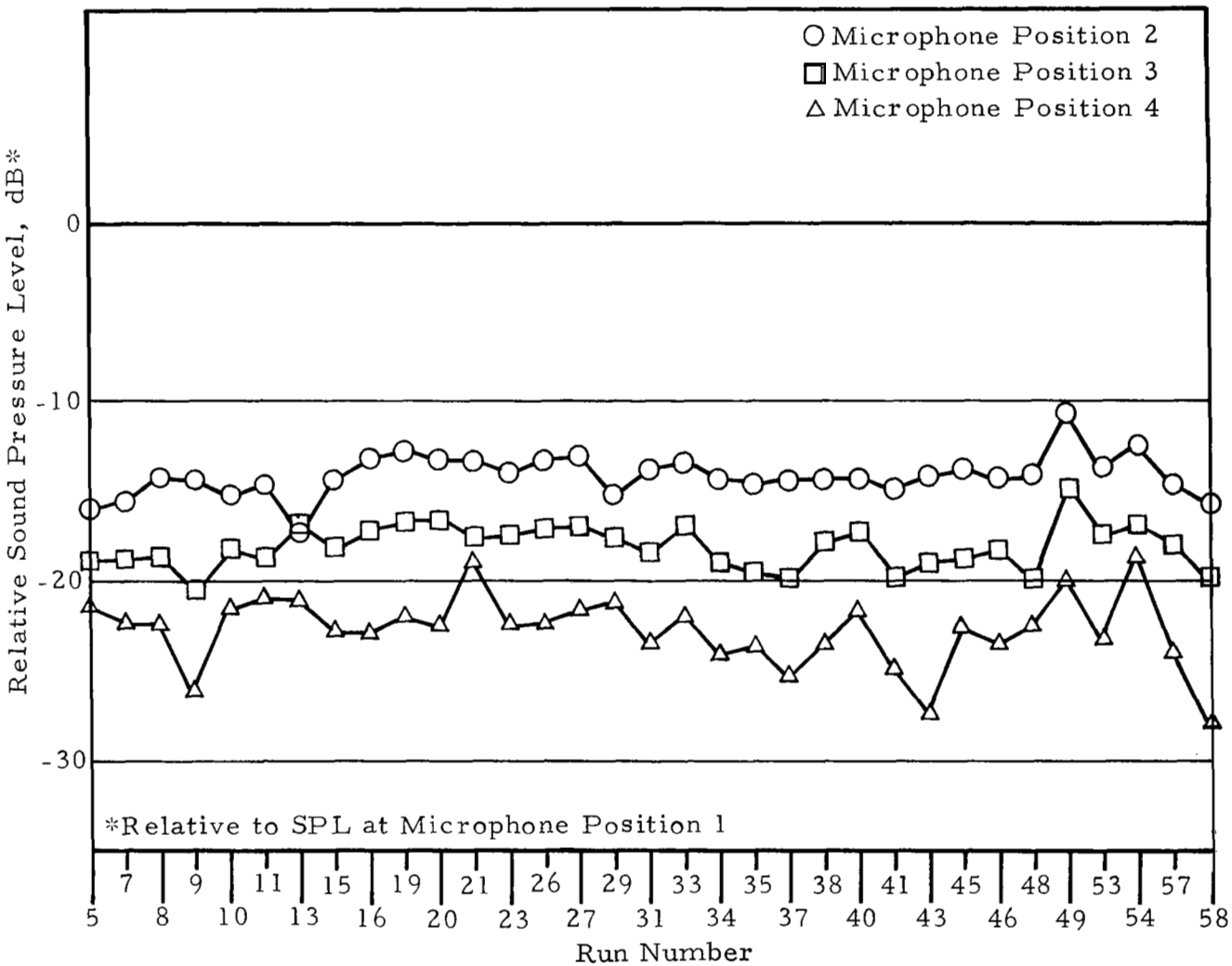

Figure 18. Comparison of Normalized Long-Time-Averaged Sound Pressure Levels for CW Test Runs at 2200 Hz.

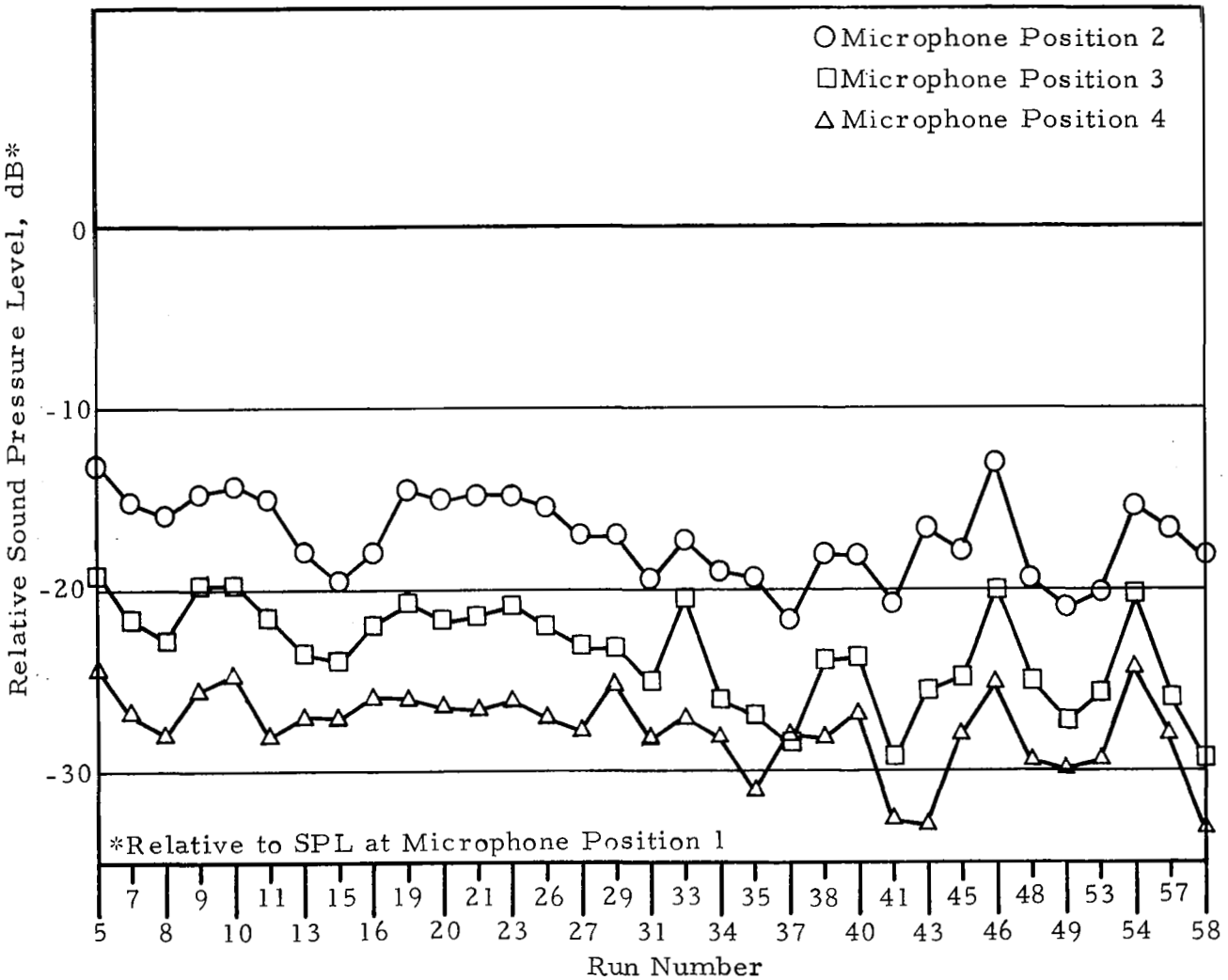

Figure 19. Comparison of Normalized Long-Time-Averaged Sound Pressure Levels for CW Test Runs at 4400 Hz.

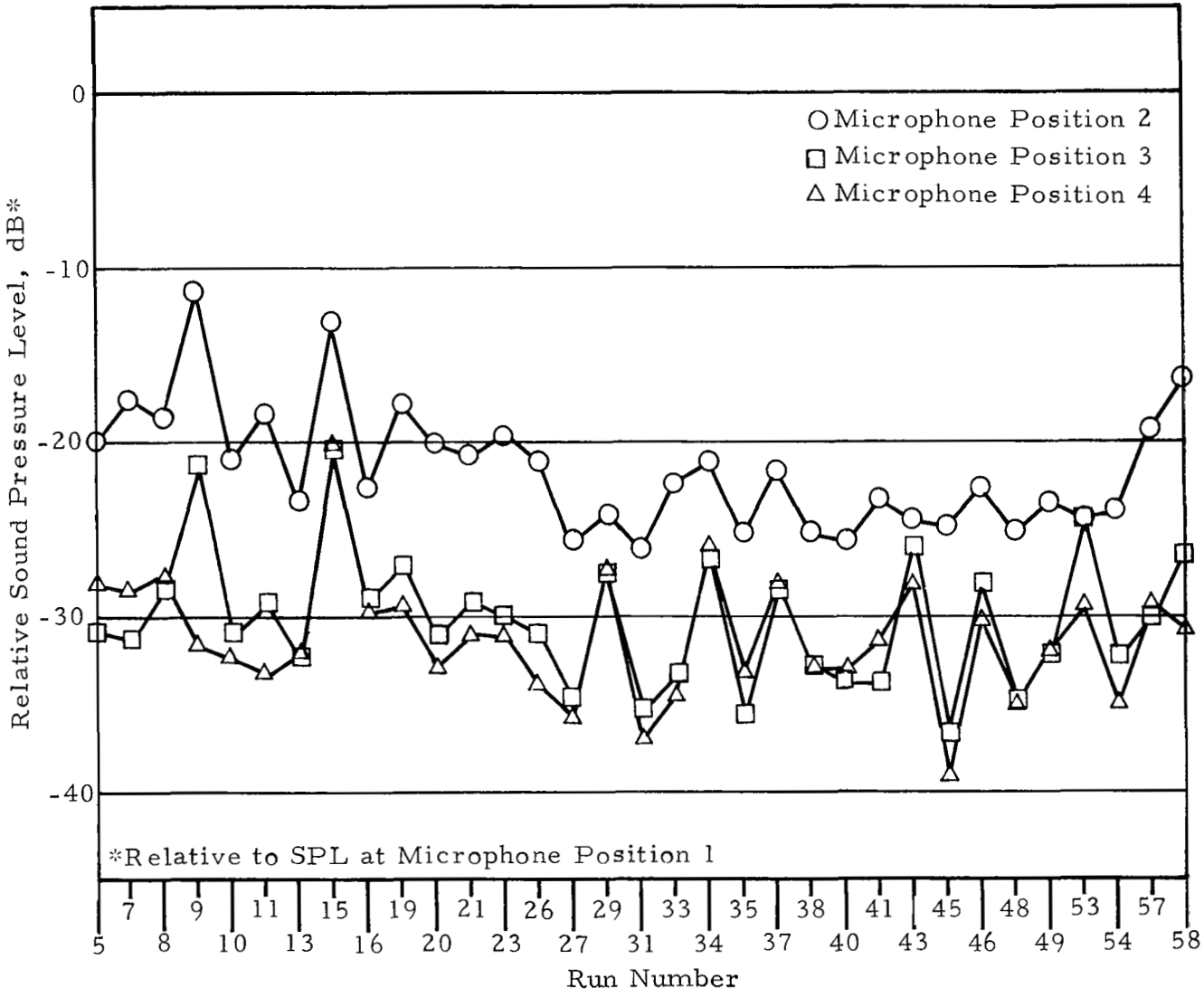

Figure 20. Comparison of Normalized Long-Time-Averaged Sound Pressure Levels for CW Test Runs at 8000 Hz.

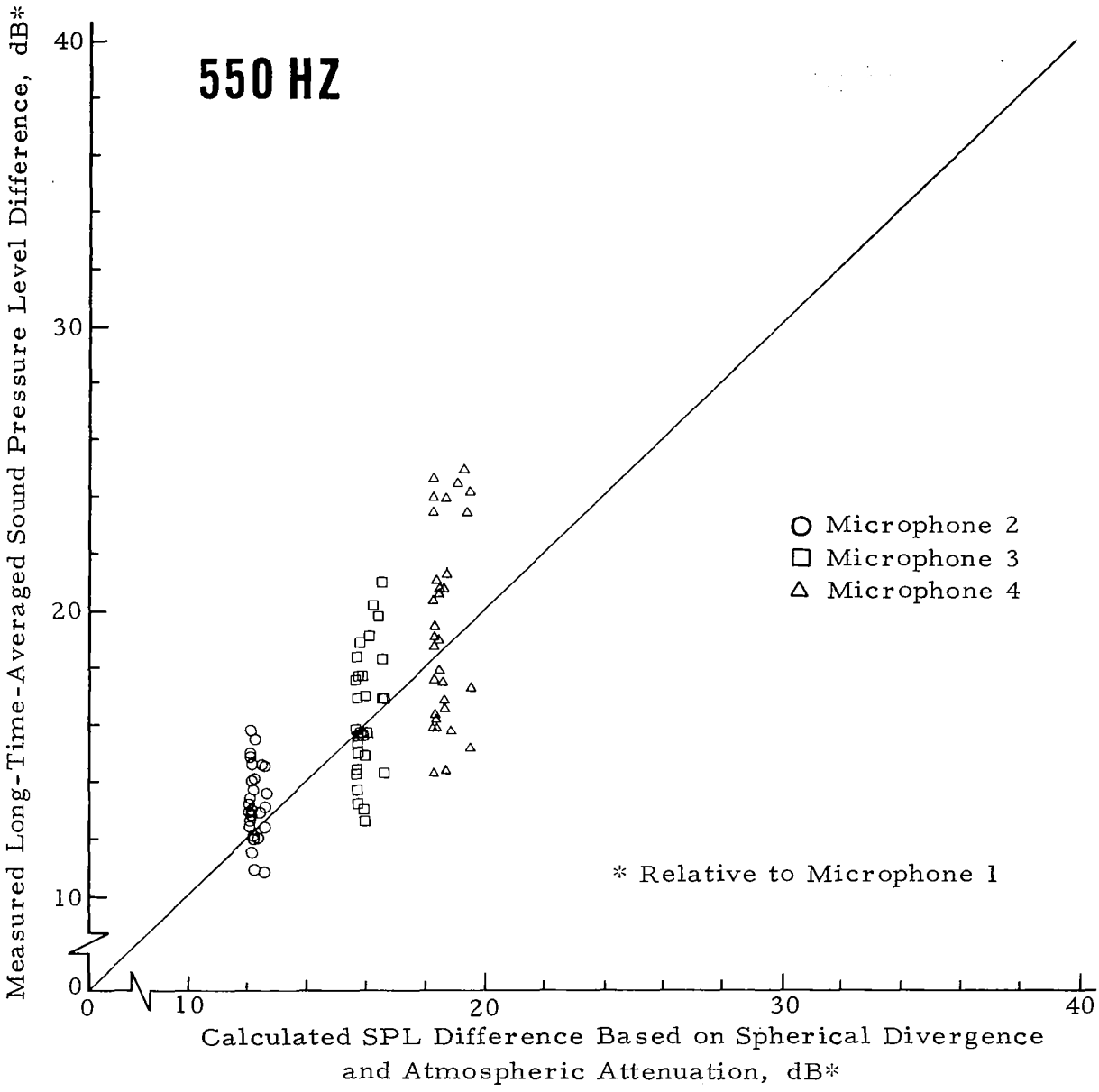

Figure 21. Comparison of Measured and Calculated Sound Attenuations for CW Tests at 550 Hz.

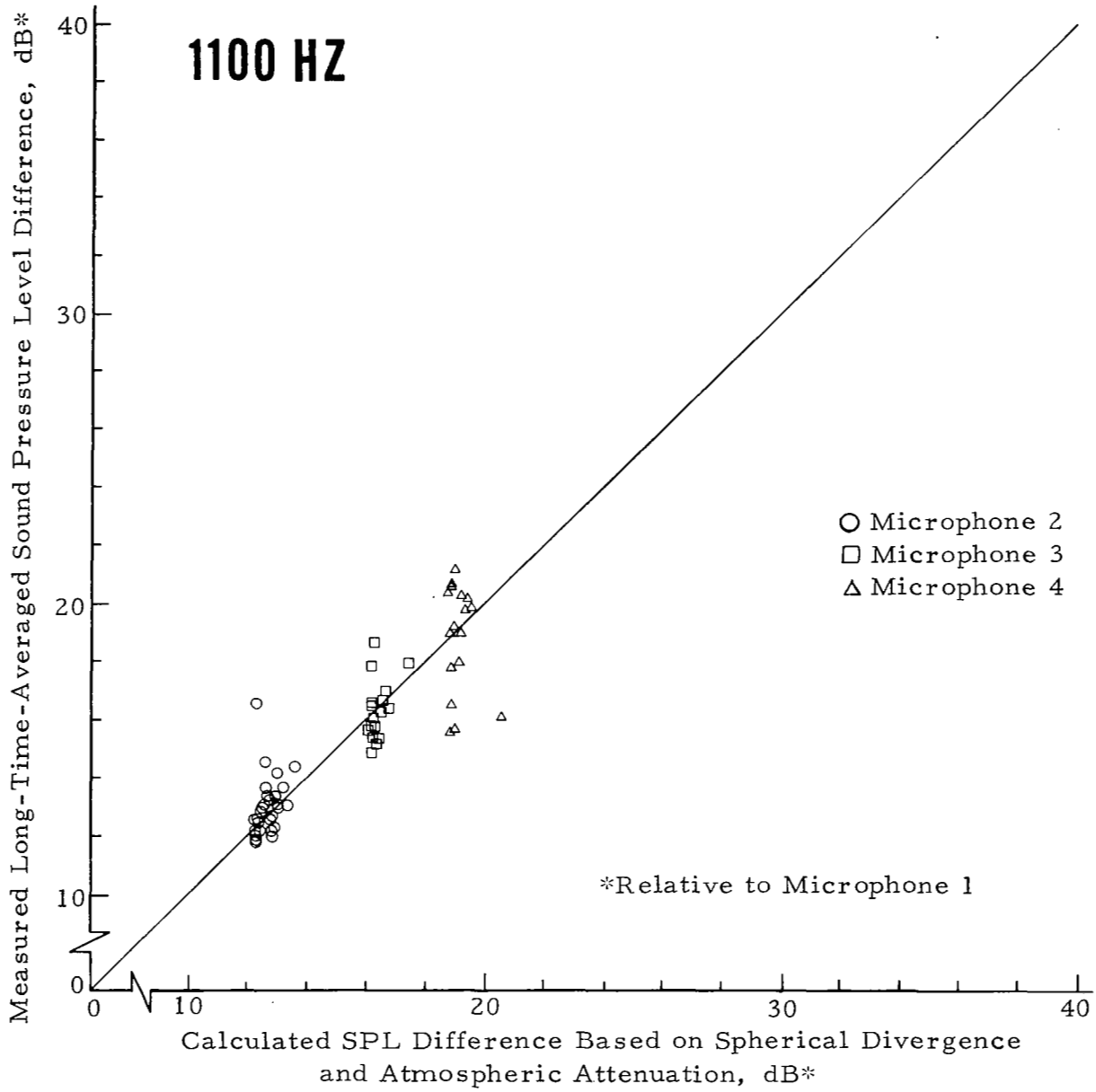

Figure 22. Comparison of Measured and Calculated Sound Attenuations for CW Tests at 1100 Hz.

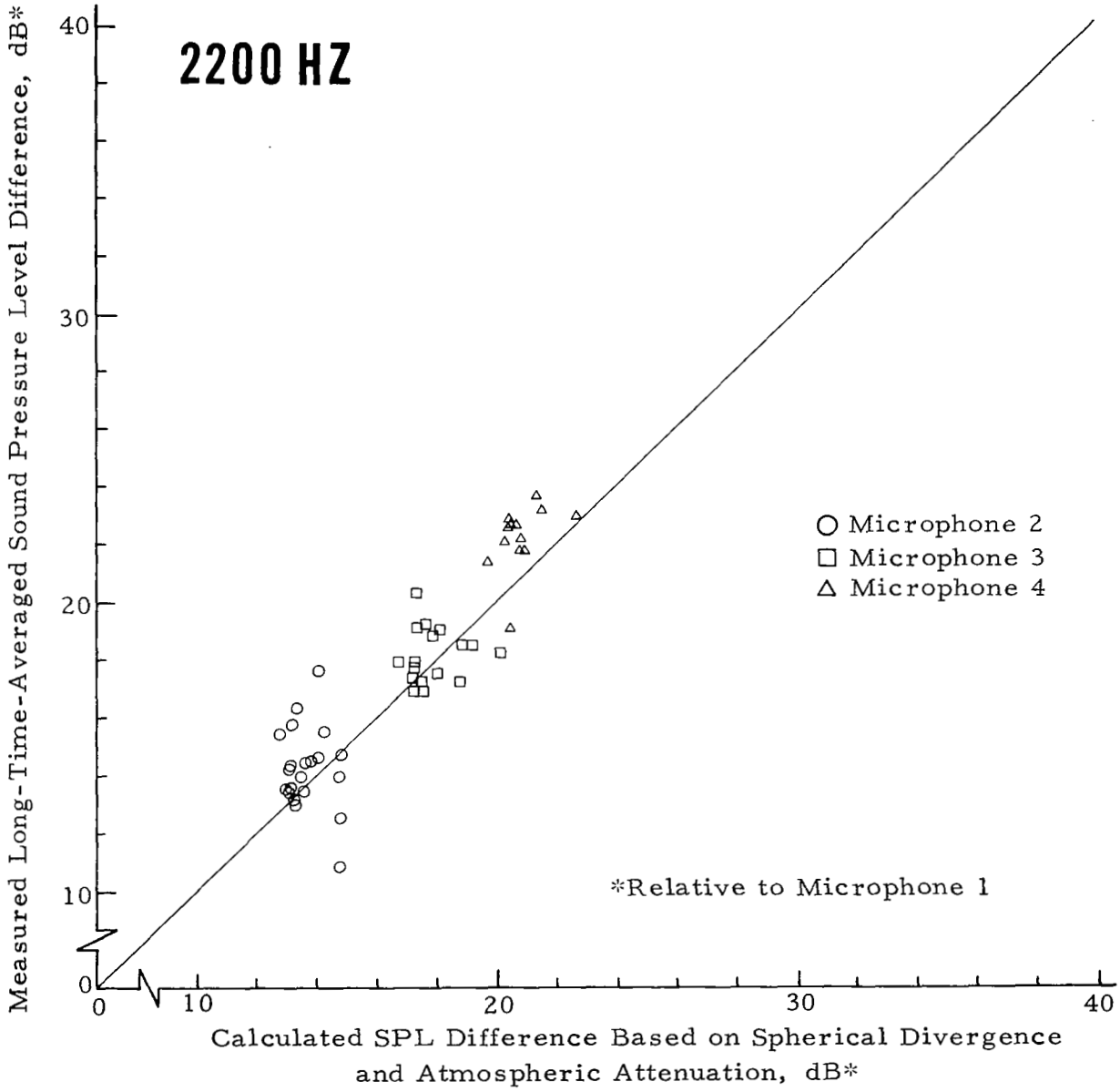

Figure 23. Comparison of Measured and Calculated Sound Attenuations for CW Tests at 2200 Hz.

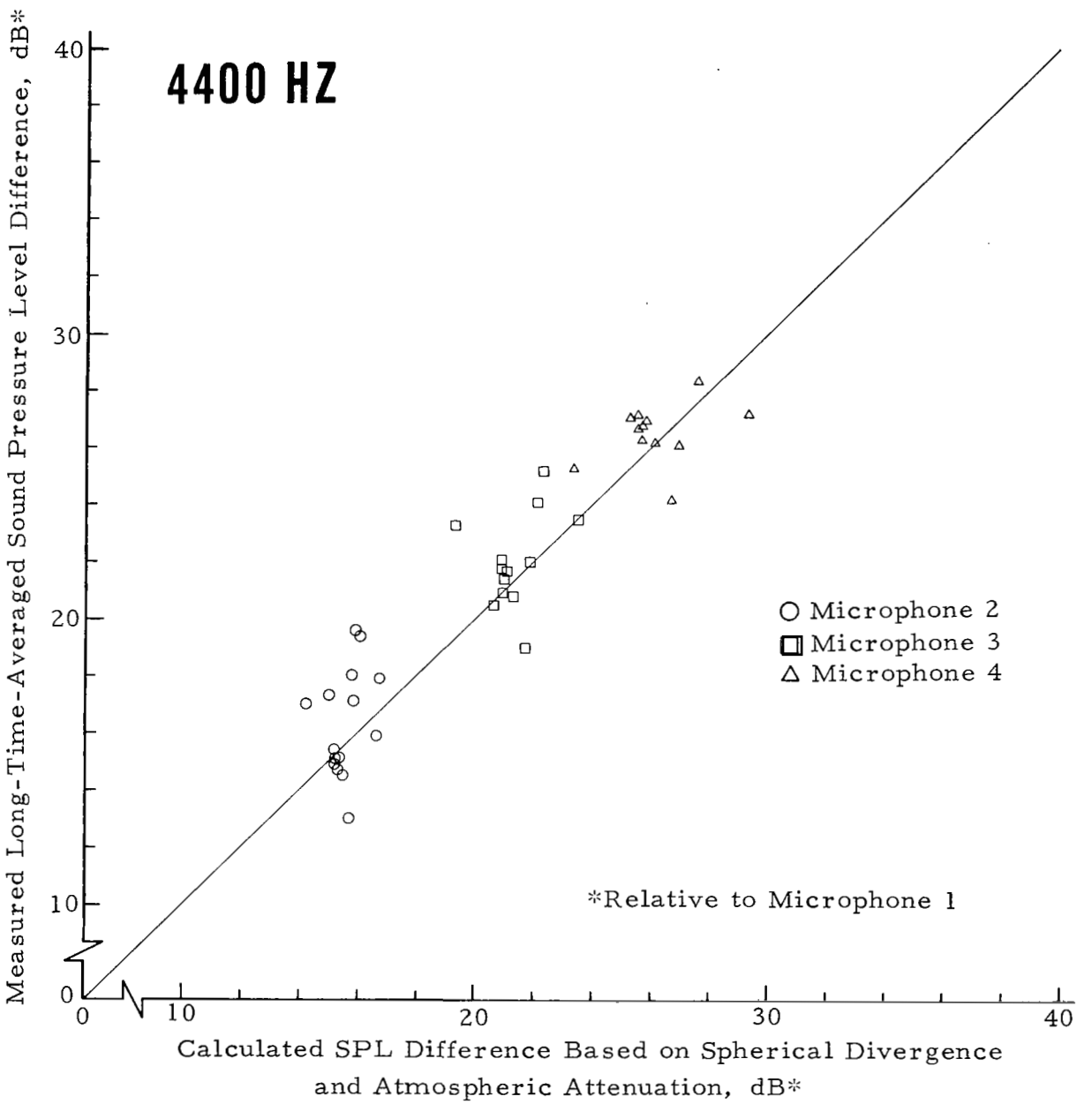

Figure 24. Comparison of Measured and Calculated Sound Attenuations for CW Tests at 4400 Hz.

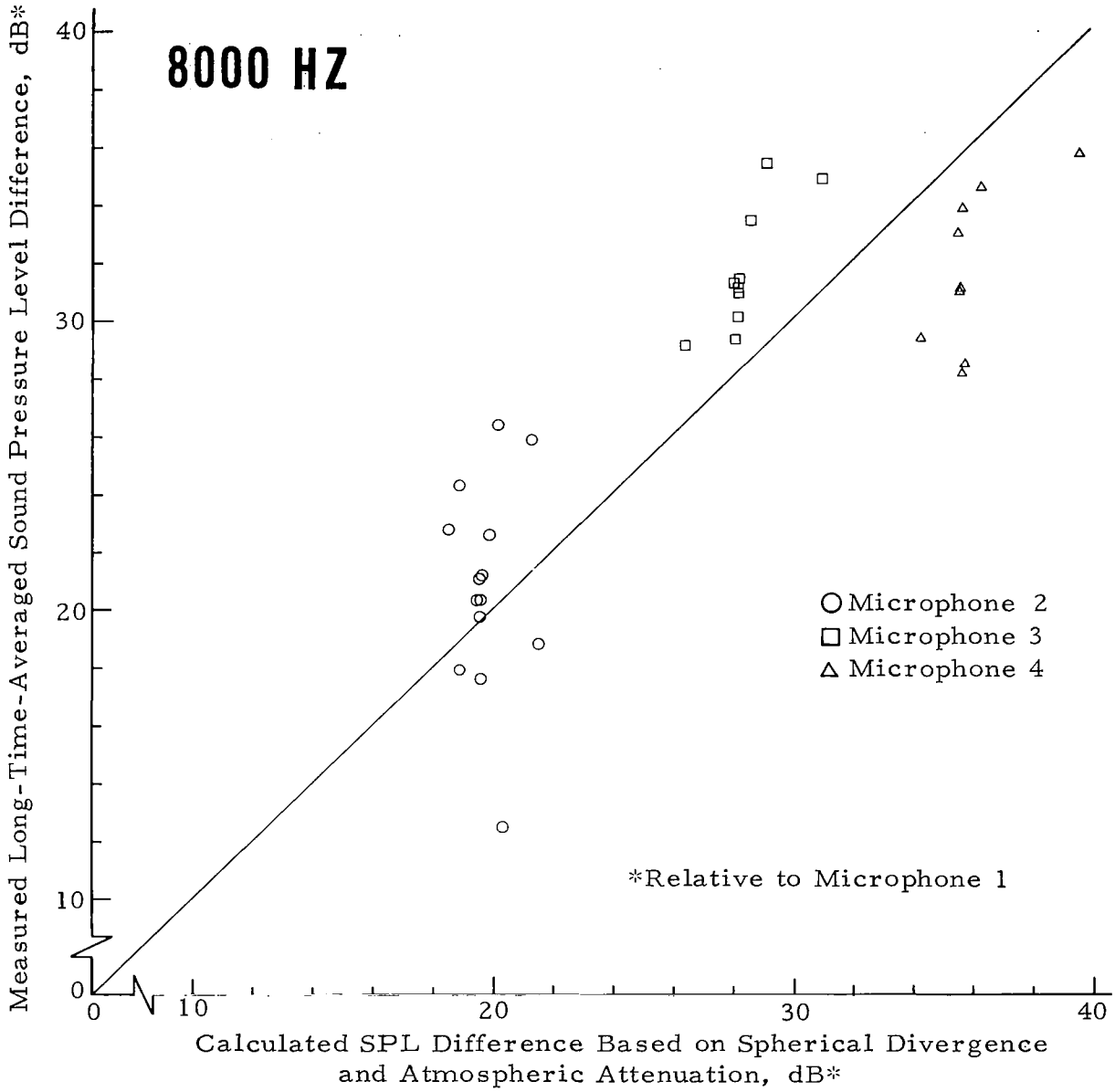

Figure 25. Comparison of Measured and Calculated Sound Attenuations for CW Tests at 8000 Hz.

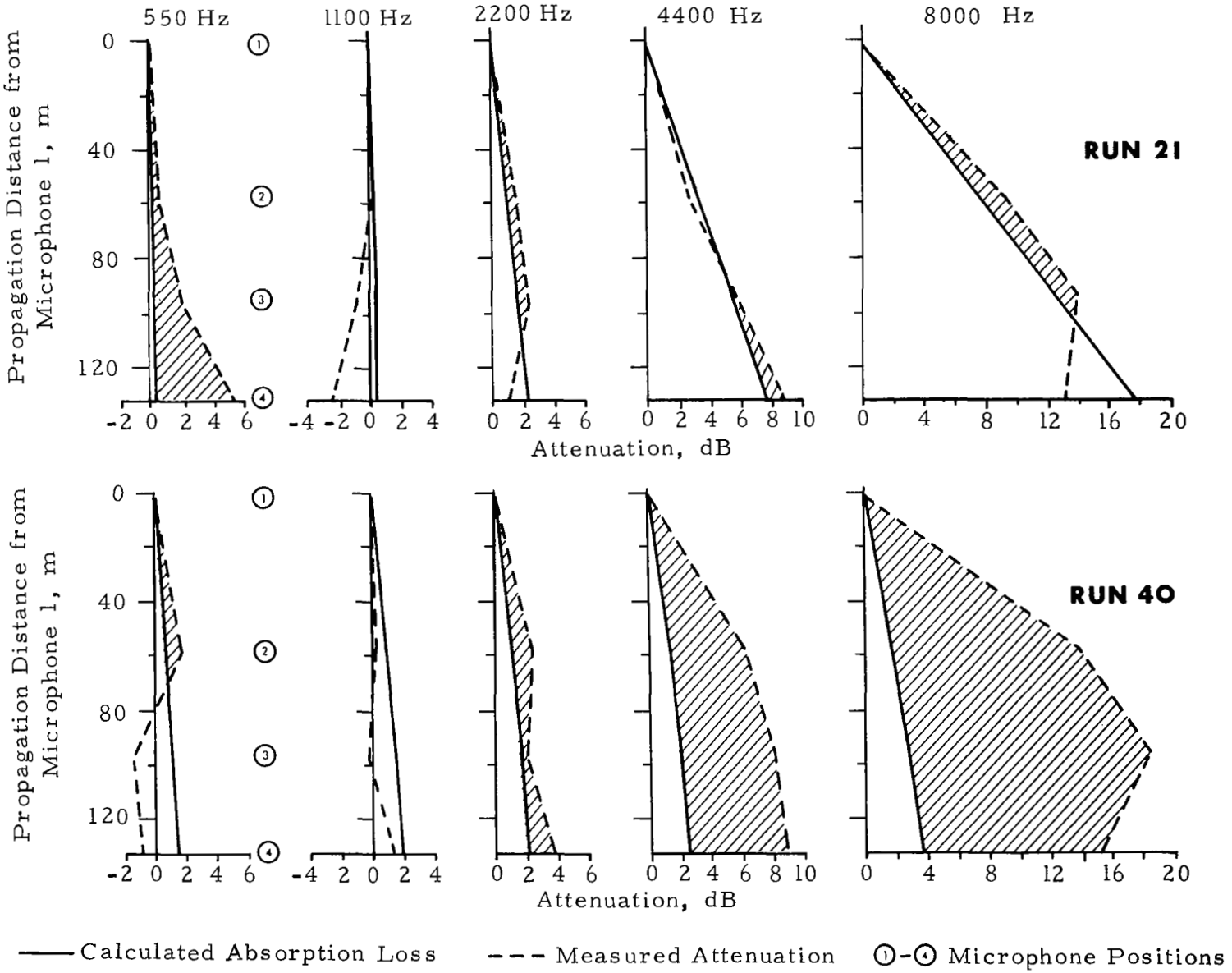

Figure 26. Comparison of Calculated Atmospheric Absorption With Measured Attenuation for Test Runs 21 and 40.

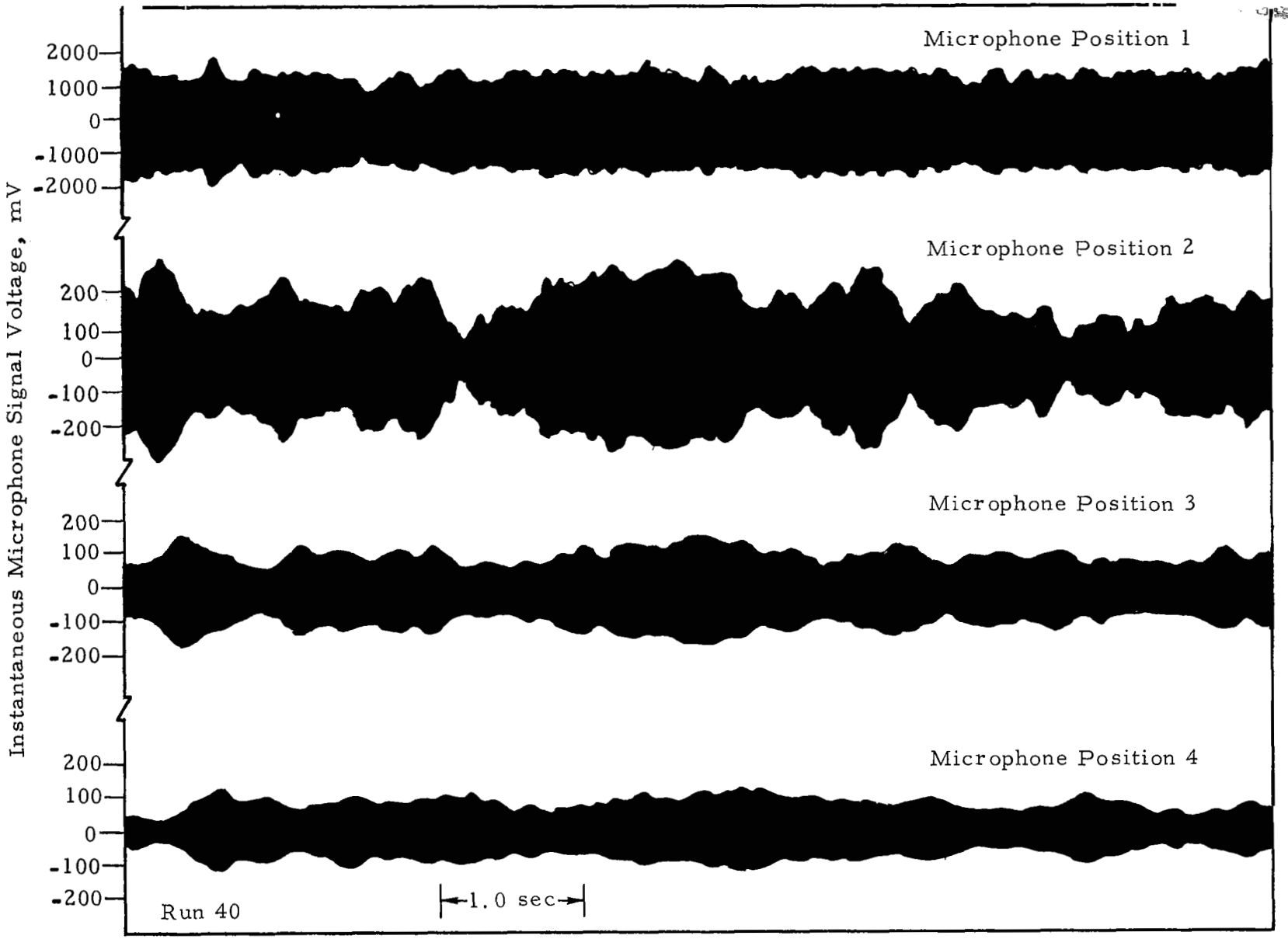

Figure 27. Typical Microphone Signal Oscillograms for CW Test Run at 4400 Hz.

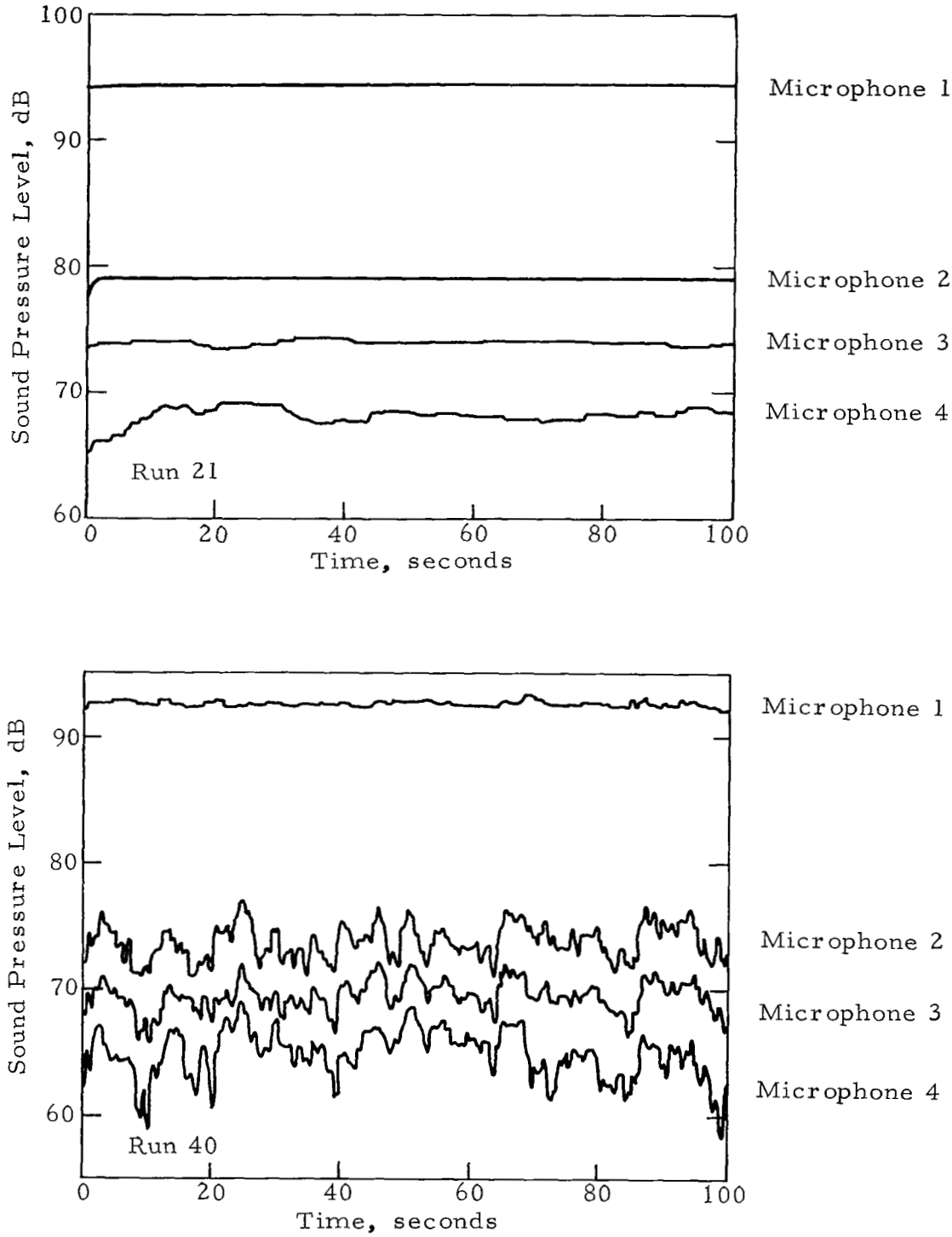

Figure 28. Comparison of RMS Time Histories for Test Runs 21 and 40, at 4400 Hz.

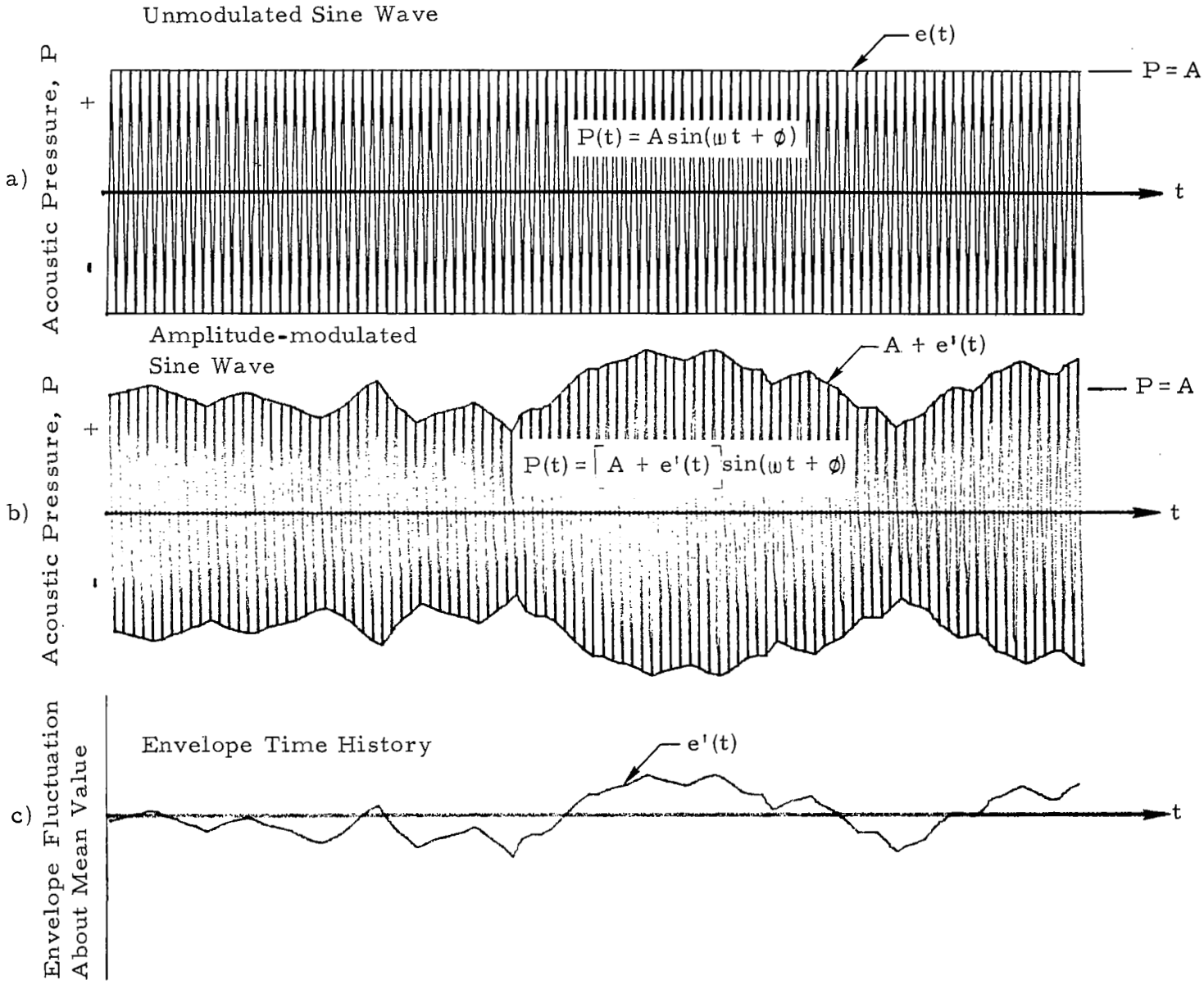

Figure 29. Illustration of Envelope Fluctuation of CW Waveform.

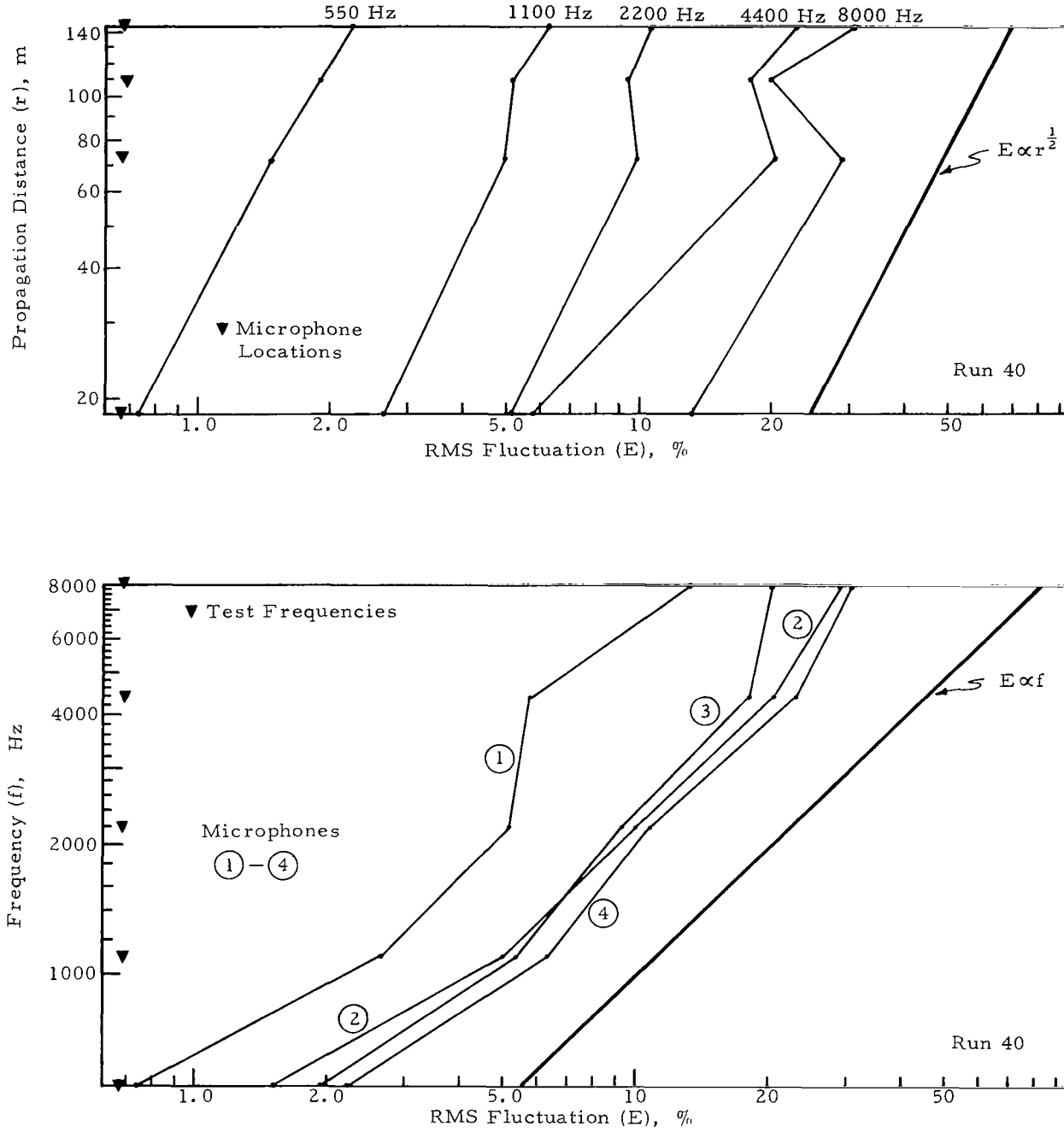

Figure 30. Sound Fluctuation Amplitudes Versus Propagation Distance and Test Frequency.

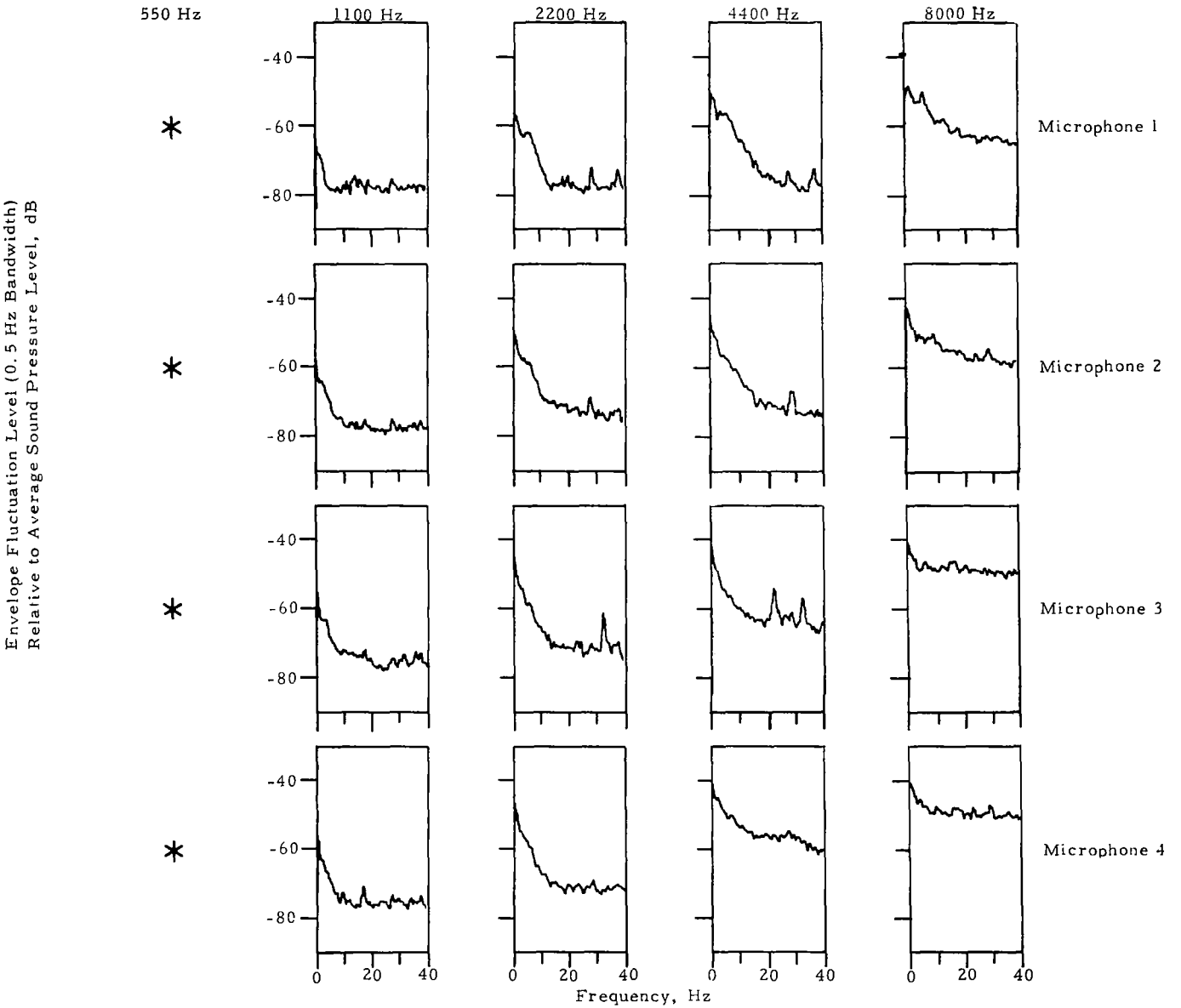

Figure 31. Spectra of Envelope Fluctuations for Test Run 21.

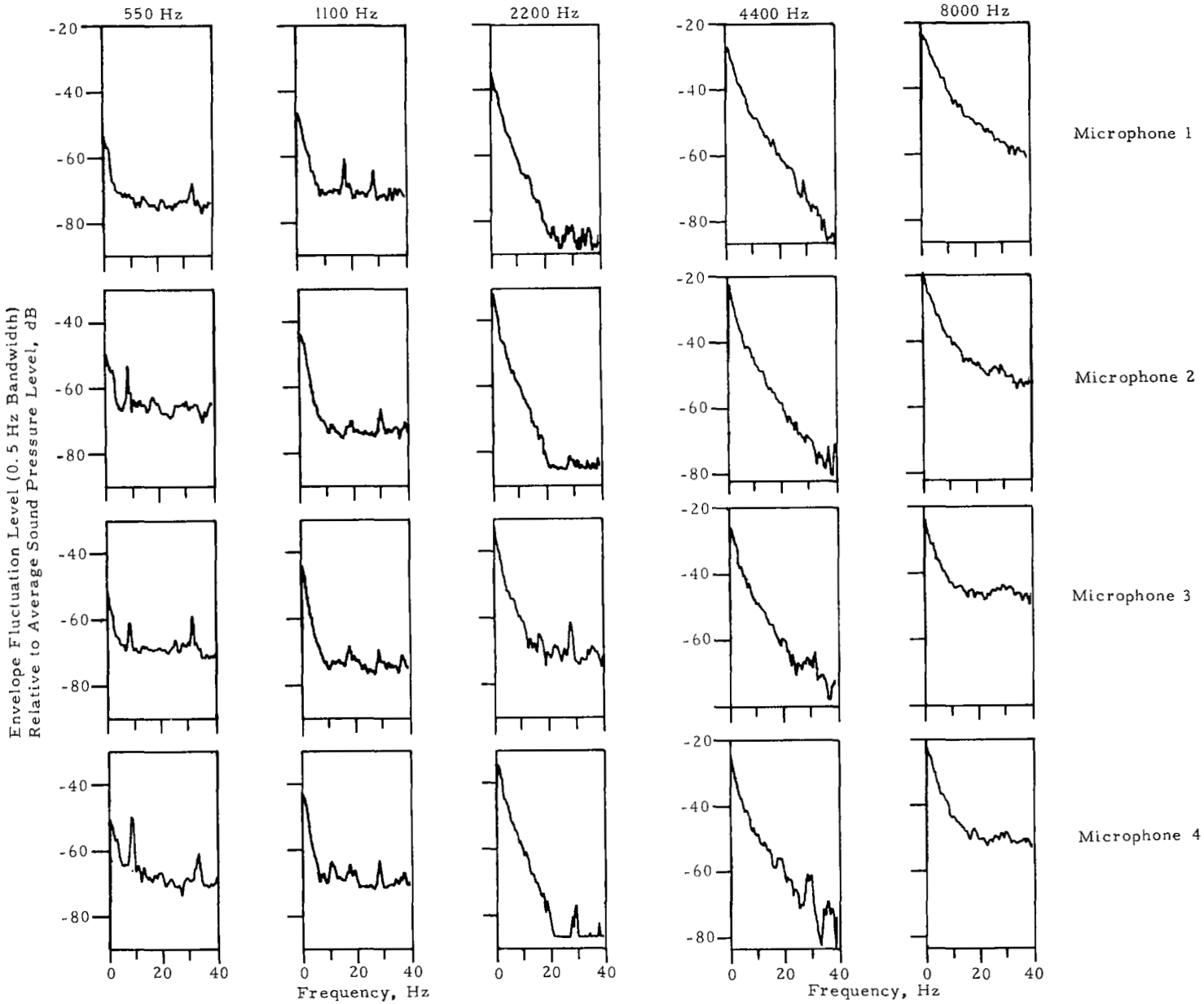

Figure 32. Spectra of Envelope Fluctuations for Test Run 40.

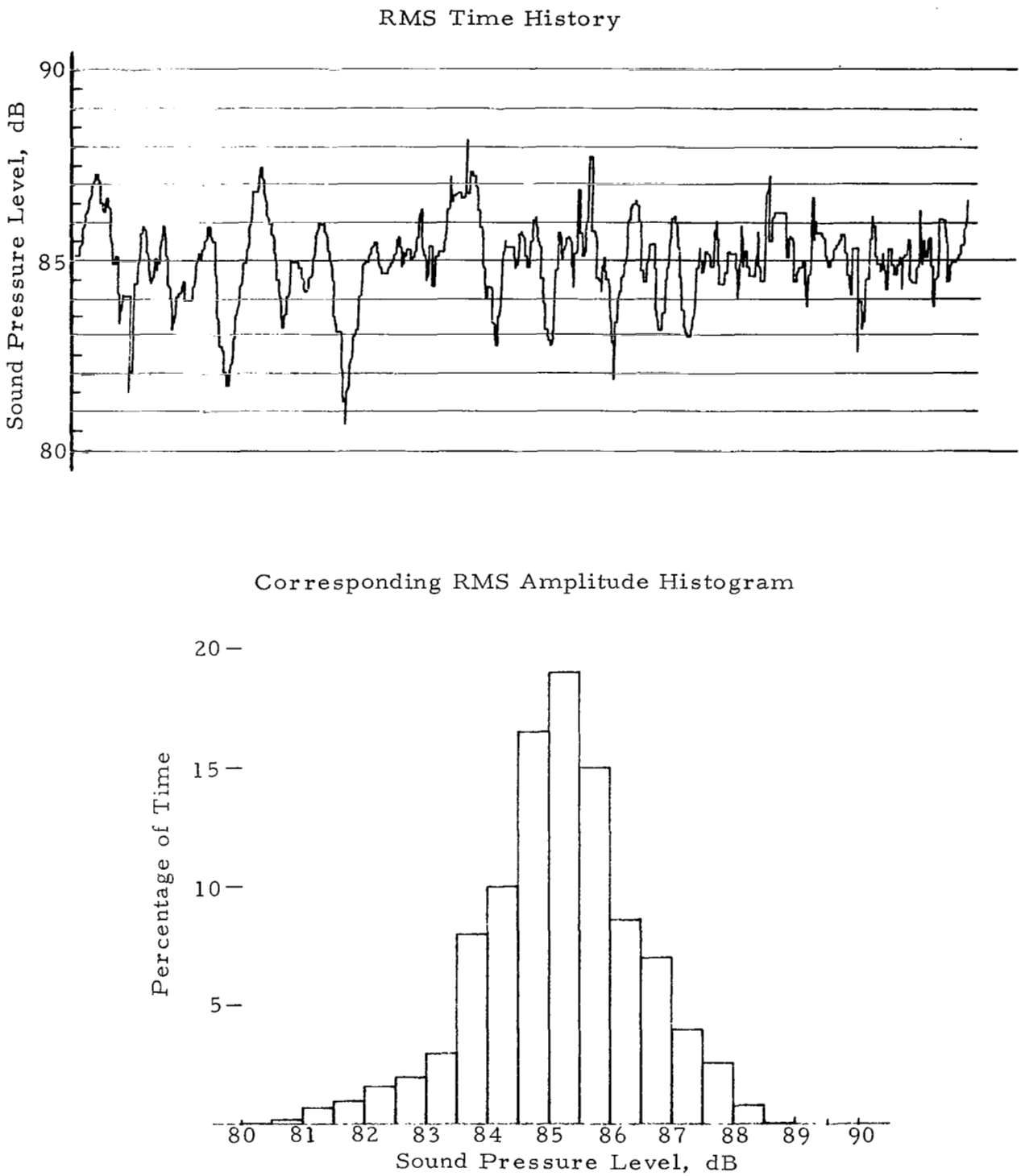

Figure 33. Illustration of RMS Amplitude Histogram.

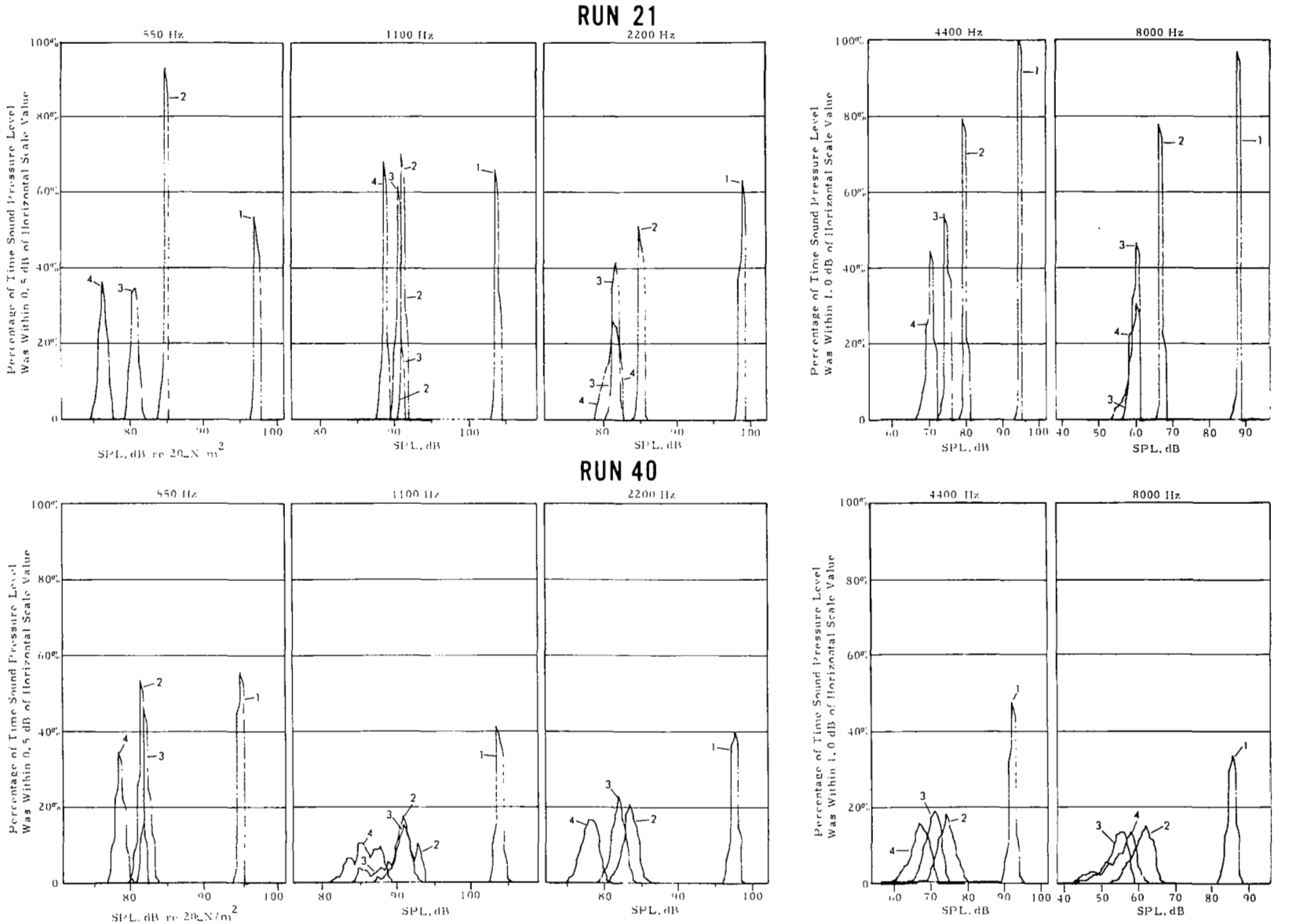

Figure 34. Measured RMS Sound Pressure Level Histograms for Test Runs 21 and 40.

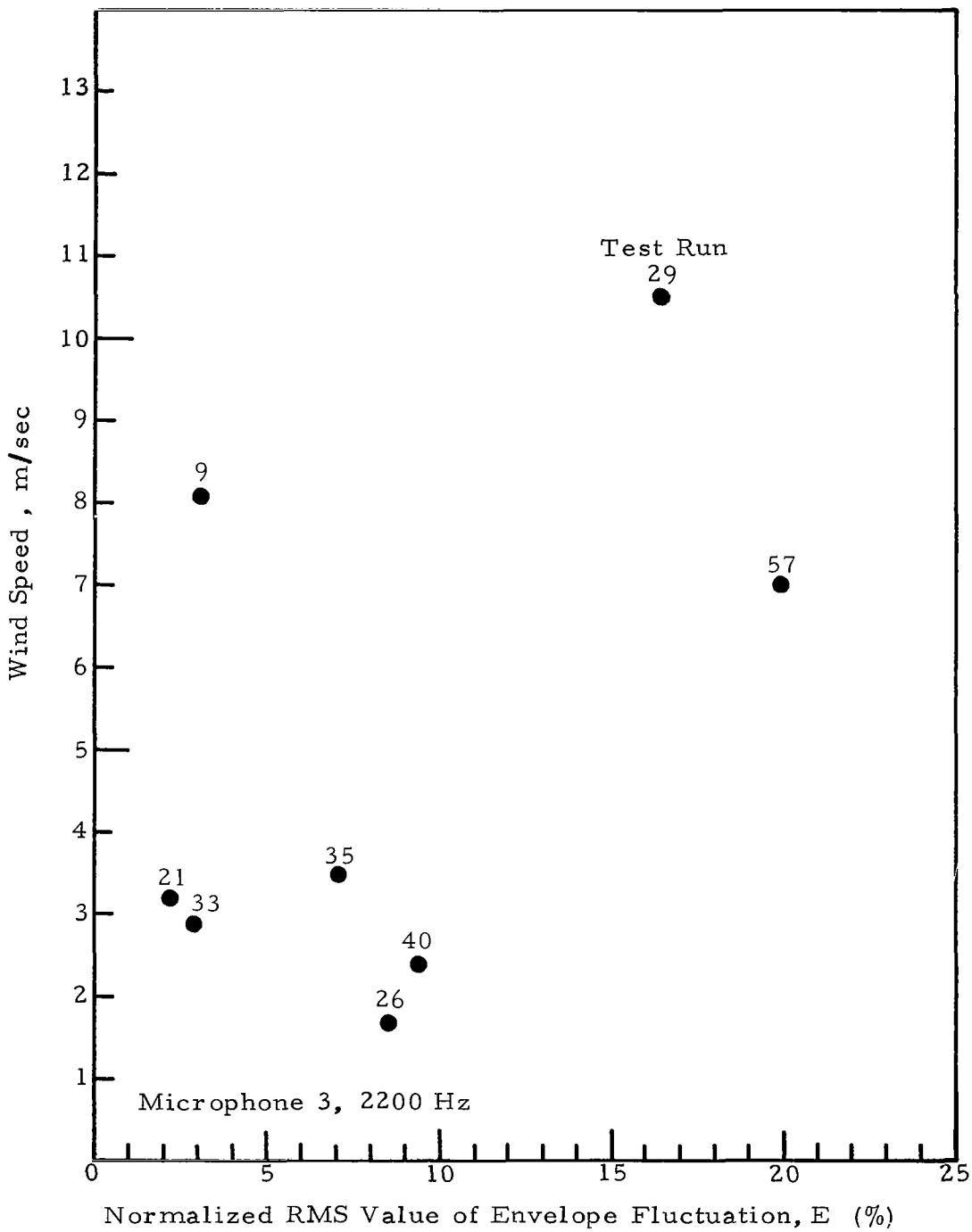

Figure 35. Trial Correlation of Normalized RMS Value of Sound Pressure Envelope Fluctuations with Wind Speed.

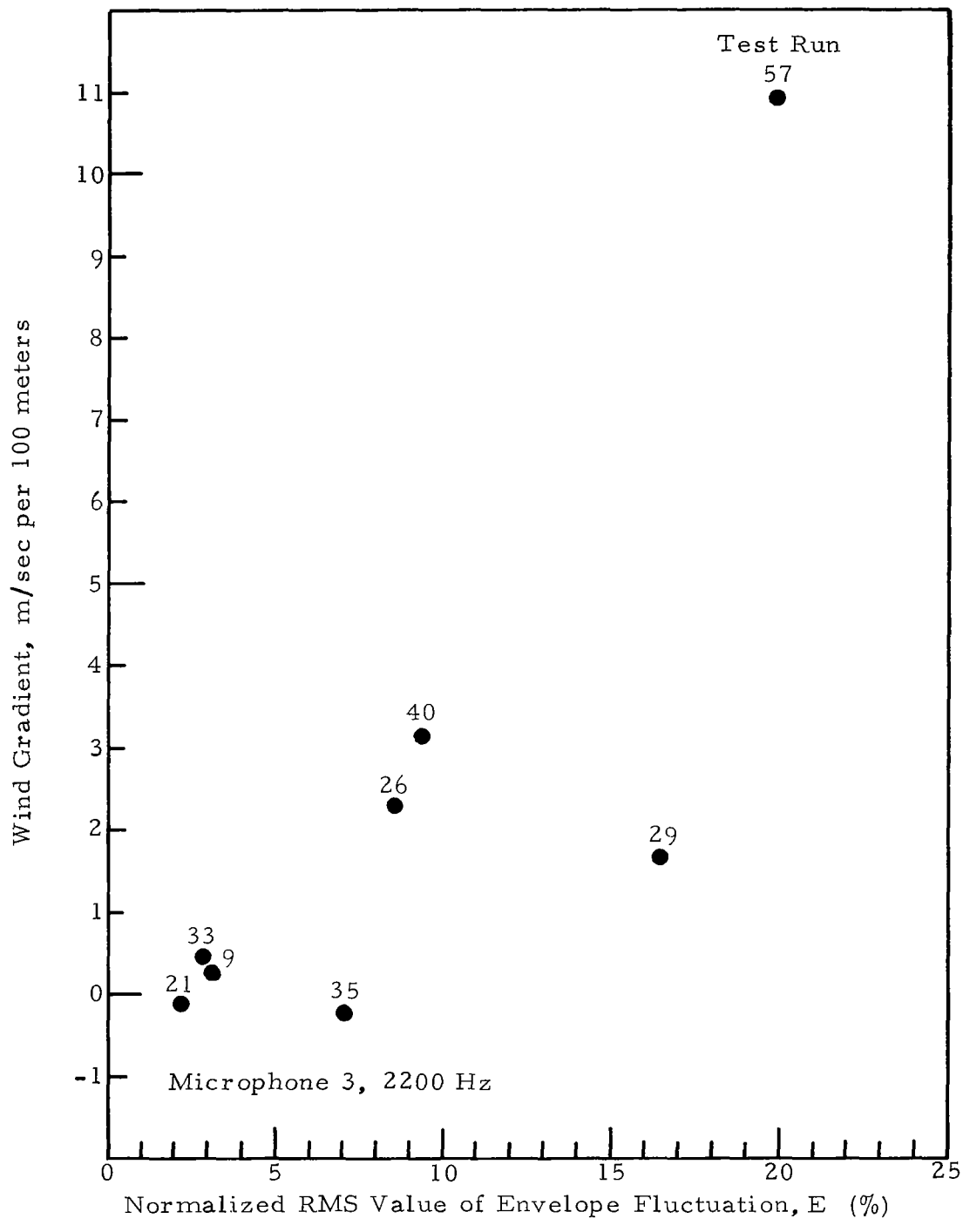

Figure 36. Trial Correlation of Normalized RMS Value of Sound Pressure Envelope Fluctuations with Wind Gradient.

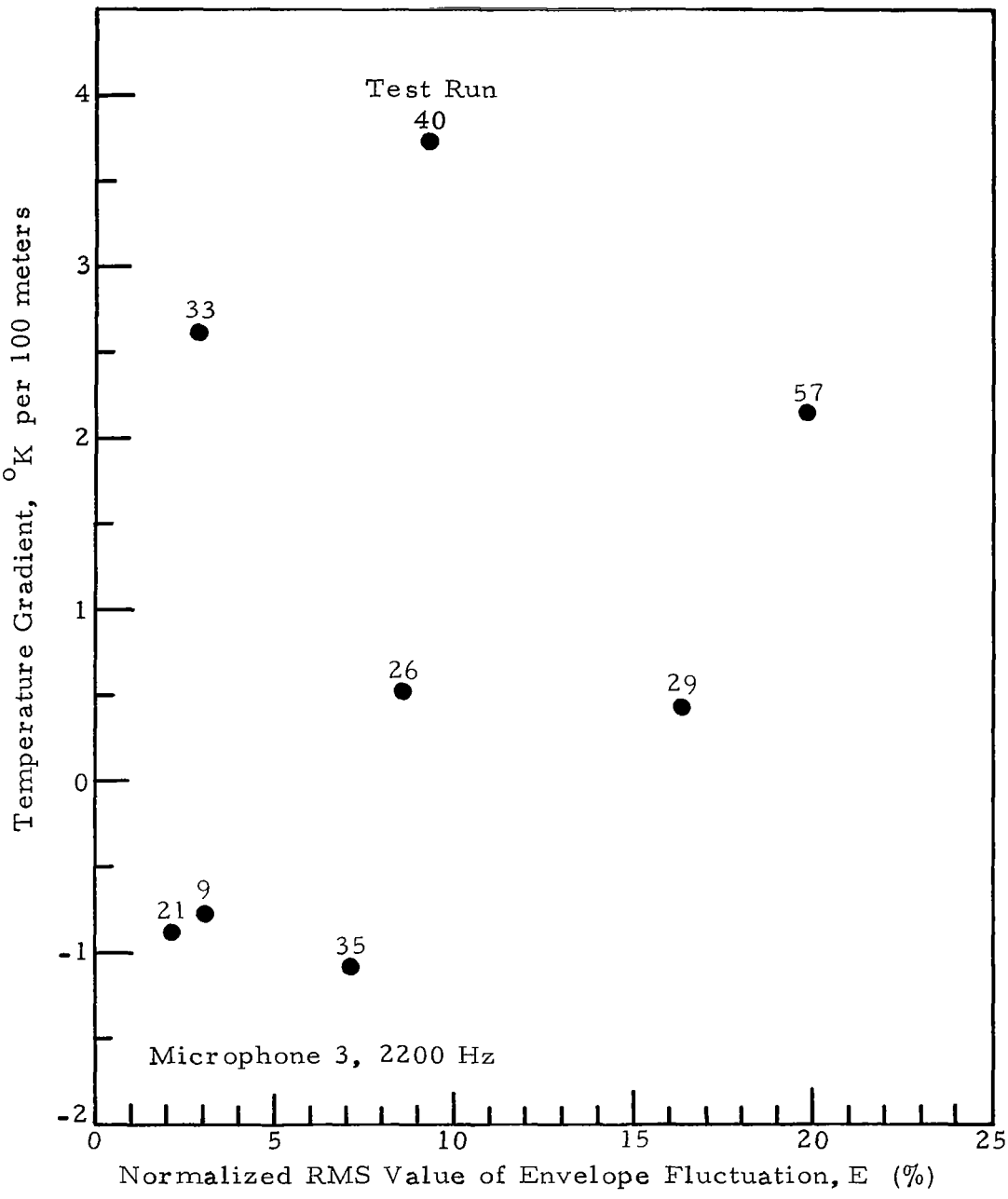

Figure 37. Trial Correlation of Normalized RMS Value of Sound Pressure Envelope Fluctuations with Temperature Gradient.

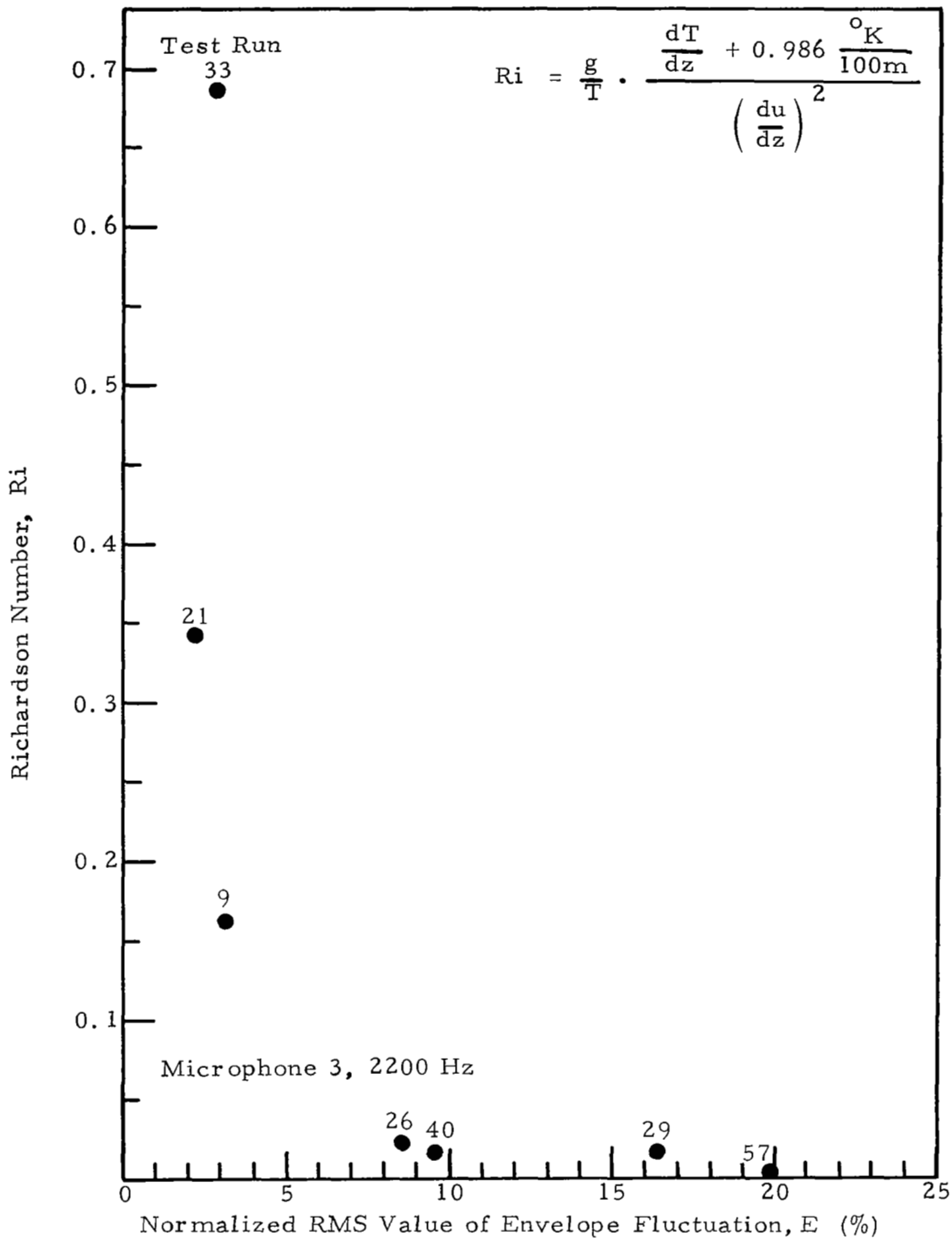

Figure 38. Trial Correlation of Normalized RMS Value of Sound Pressure Envelope Fluctuations with Richardson Number.

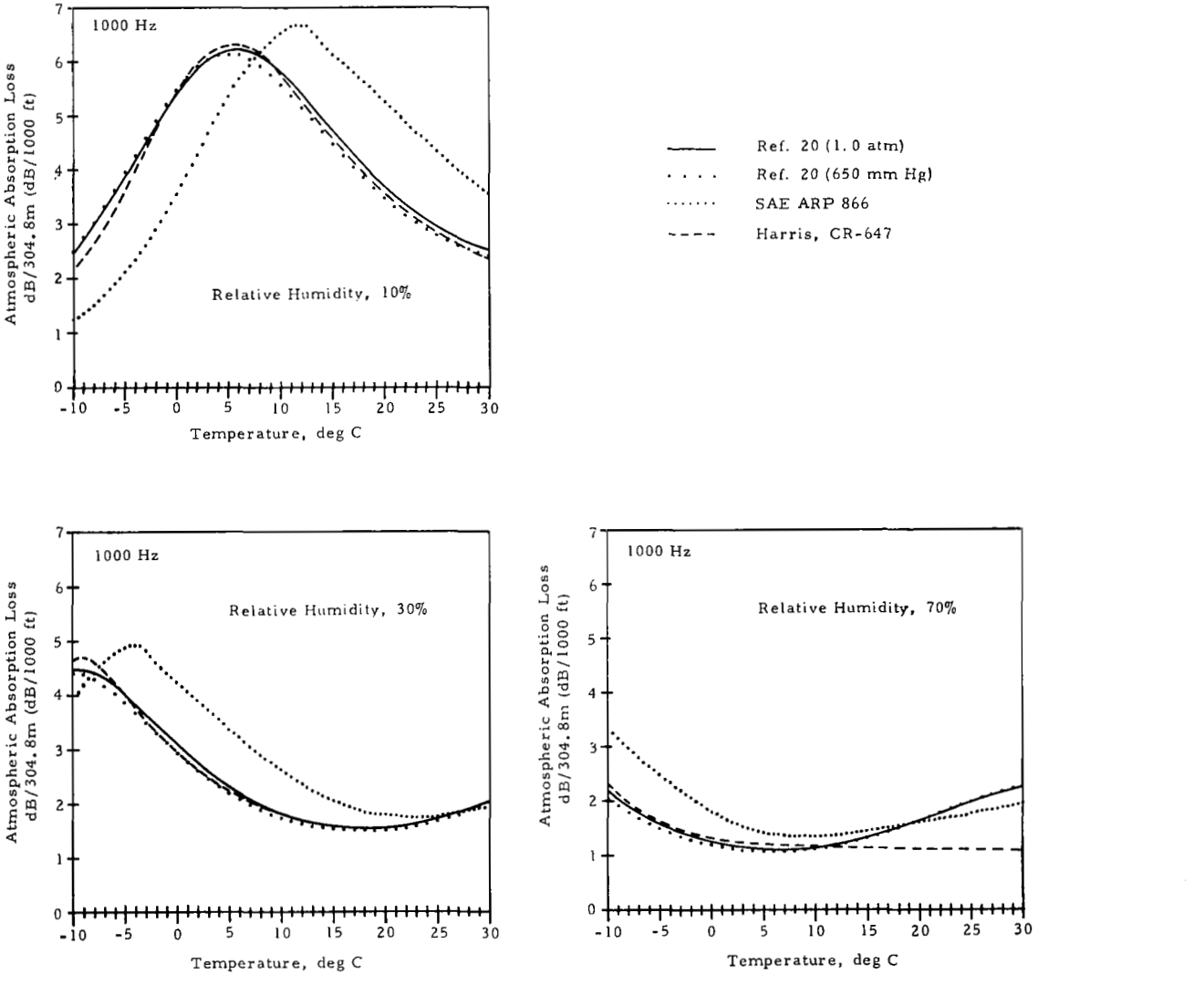

Figure A1. Comparison of Predicted Atmospheric Absorption Losses at a Frequency of 1000 Hz for a Range of Relative Humidity and Temperature Values Using Four Different Procedures

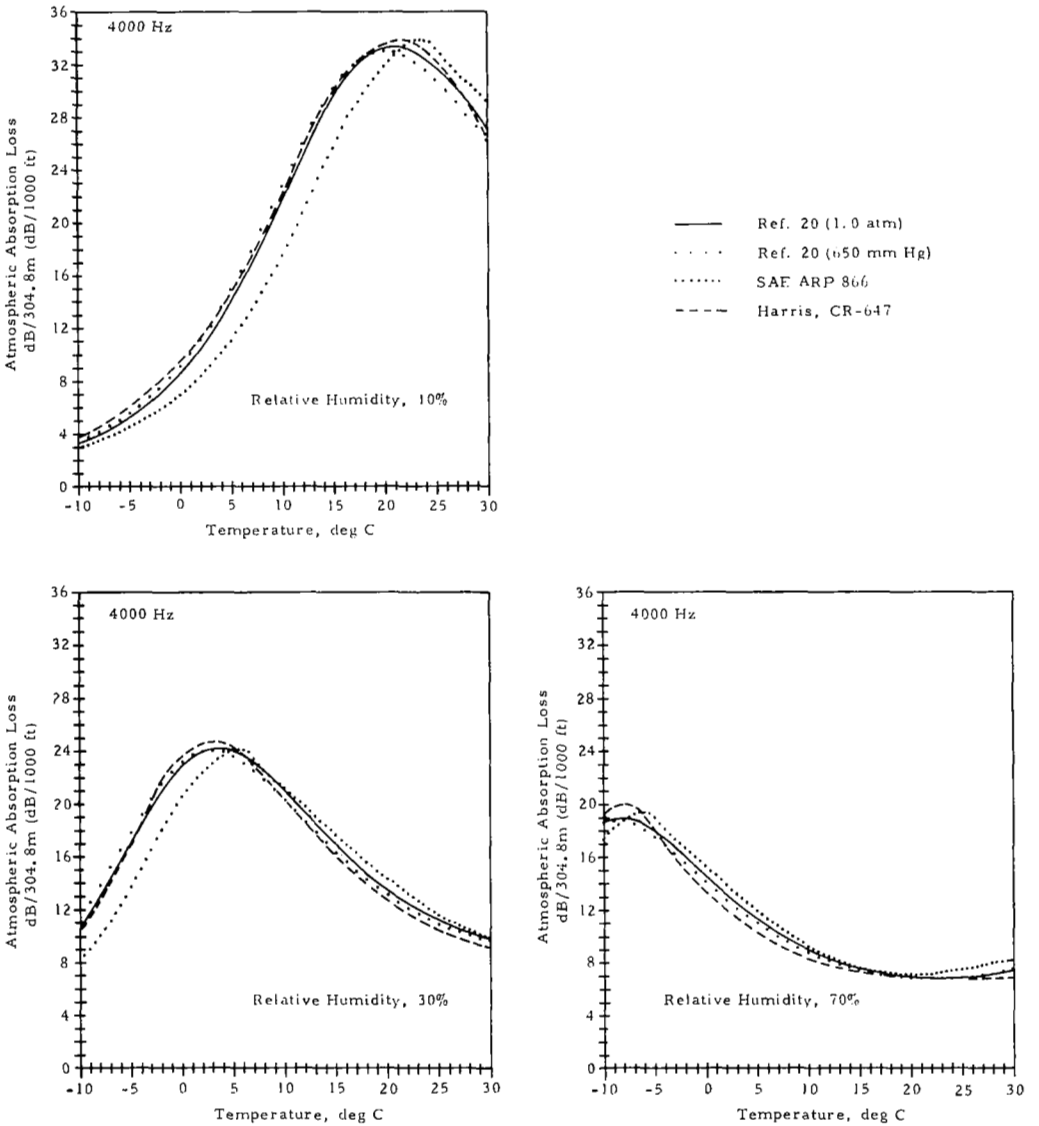

Figure A2. Comparison of Predicted Atmospheric Absorption Losses at a Frequency of 4000 Hz for a Range of Relative Humidity and Temperature Values Using Four Different Procedures

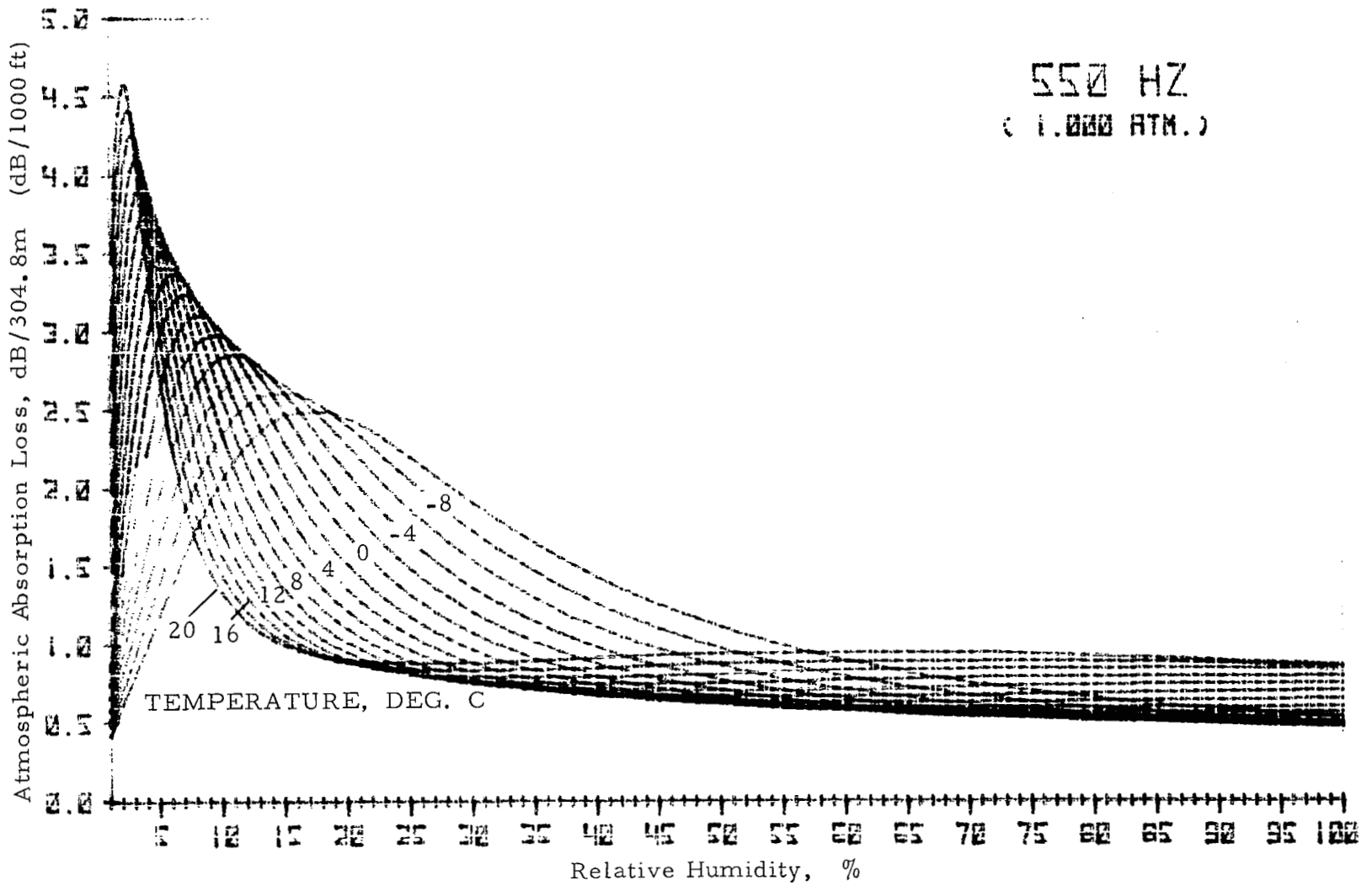

Figure A3. Calculated Atmospheric Absorption Loss, 550 Hz.

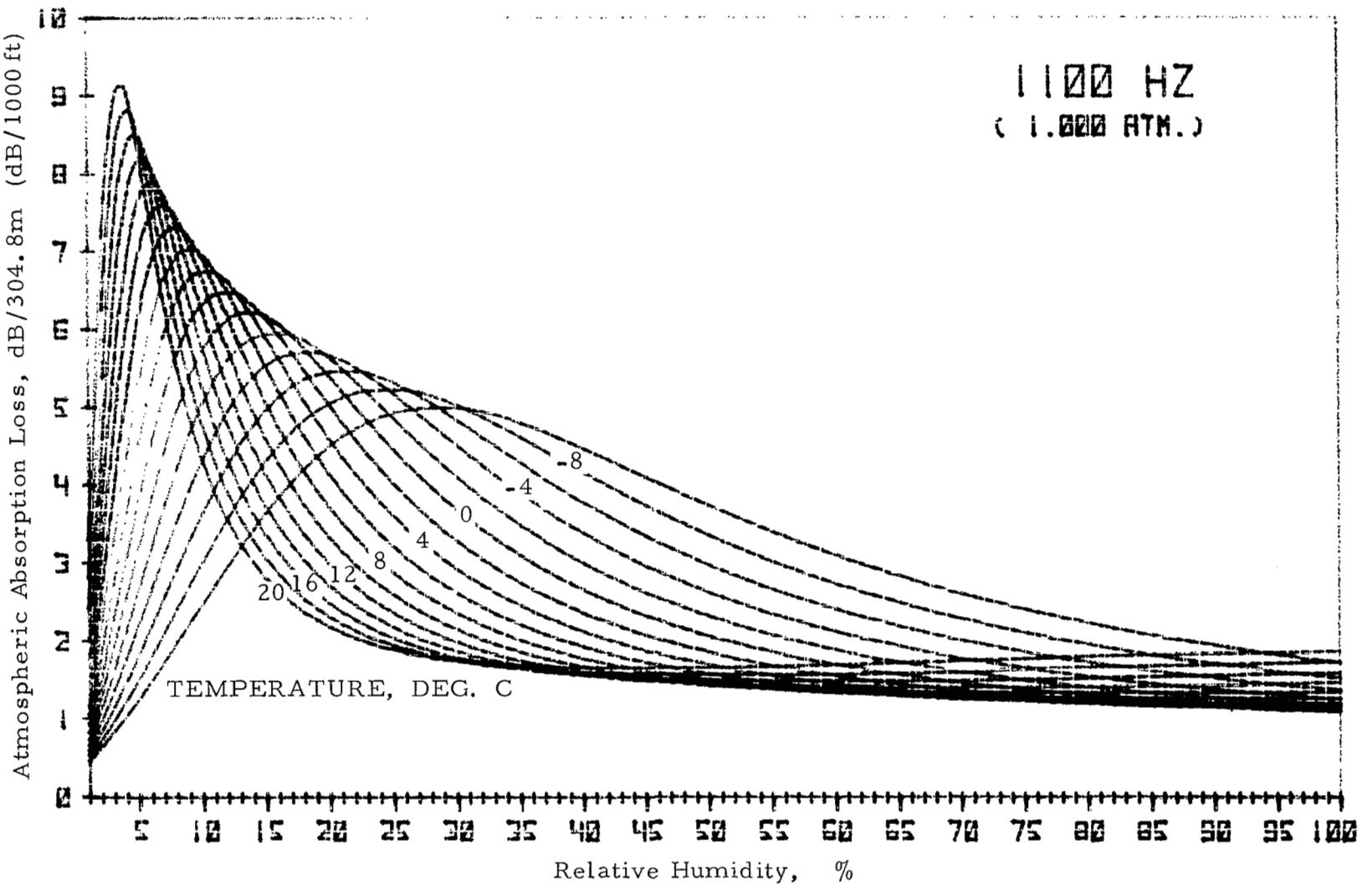

Figure A4. Calculated Atmospheric Absorption Loss, 1100 Hz.

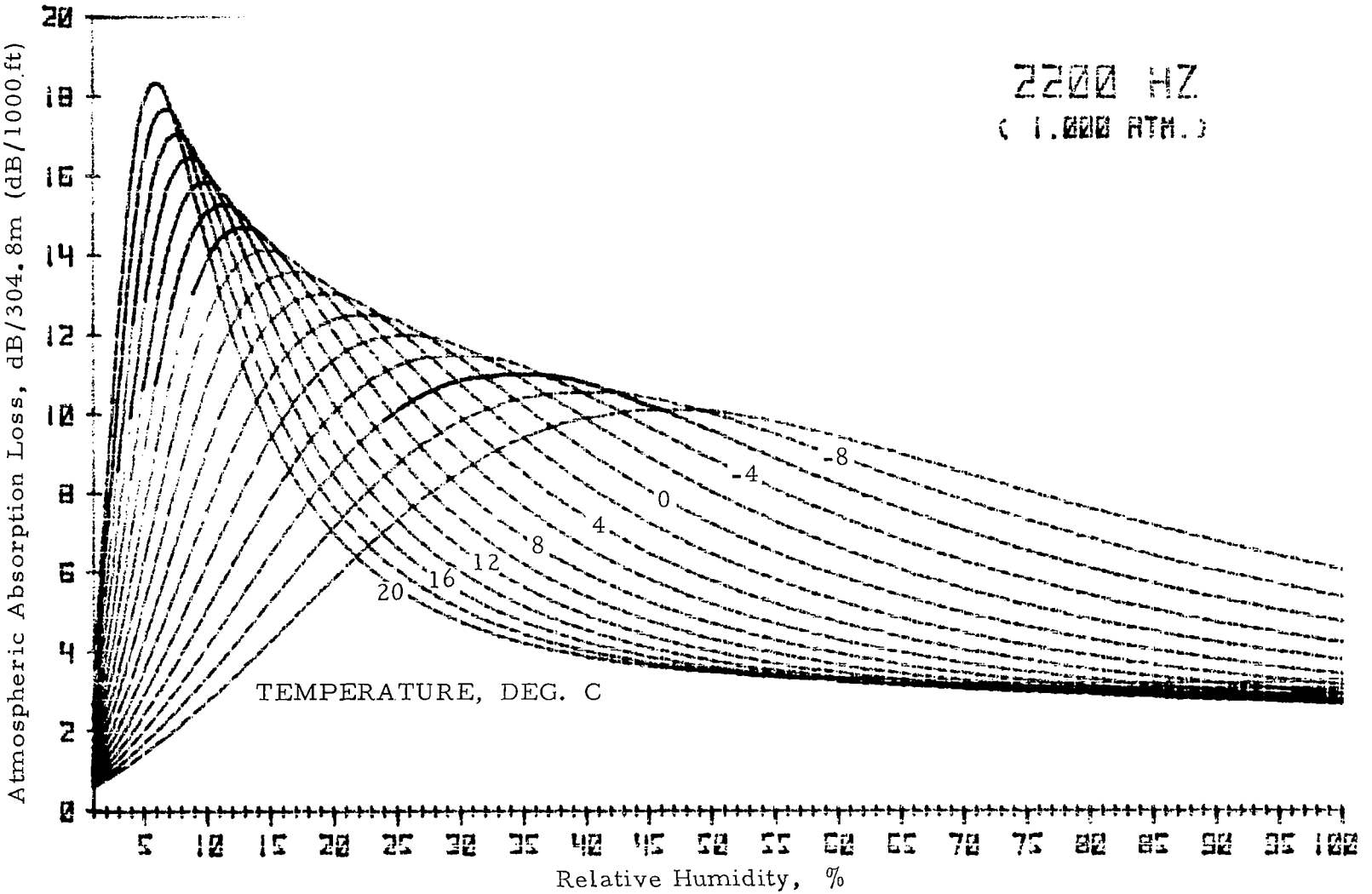

Figure A5. Calculated Atmospheric Absorption Loss, 2200 Hz.

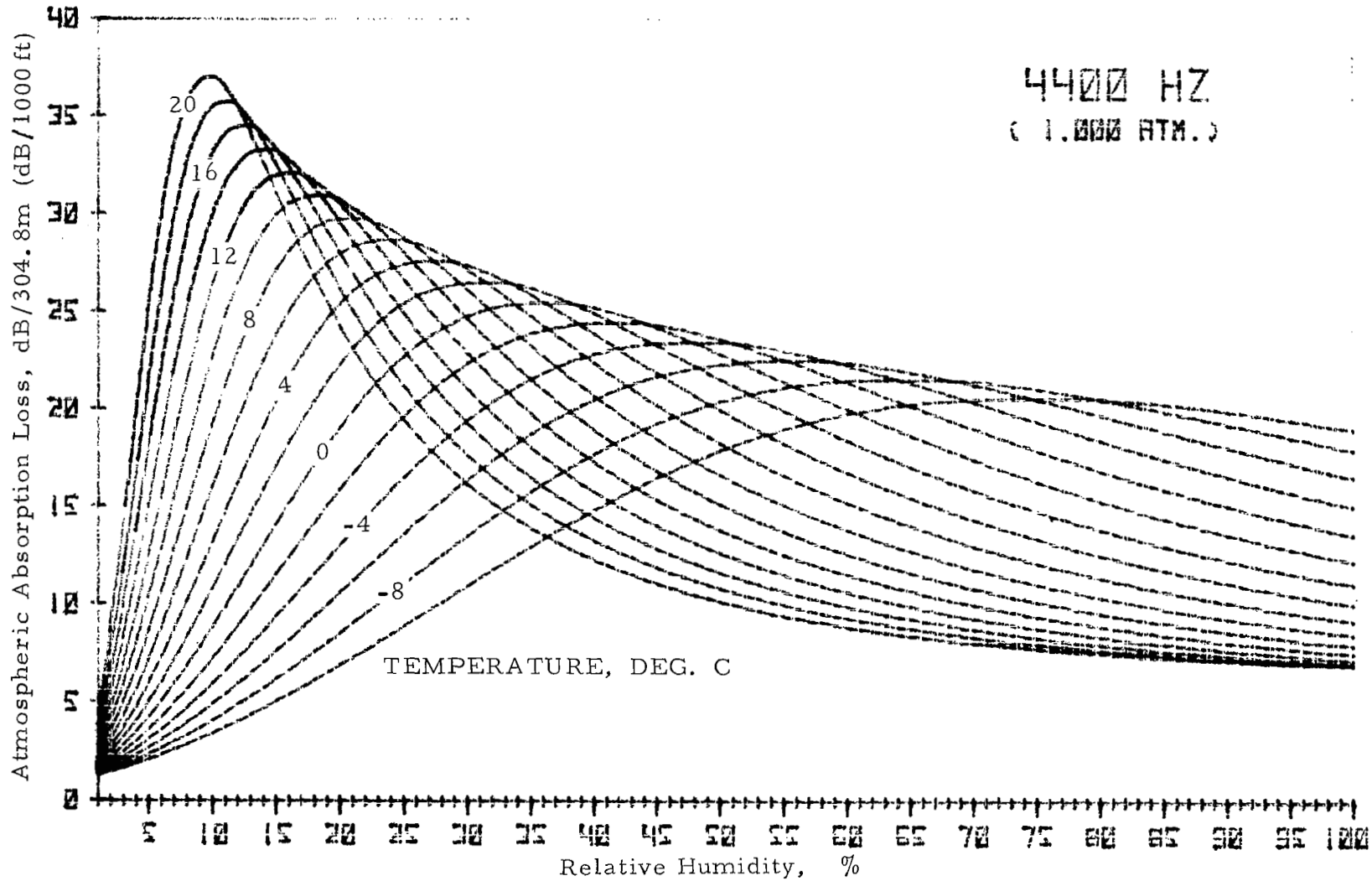

Figure A6. Calculated Atmospheric Absorption Loss, 4400 Hz.

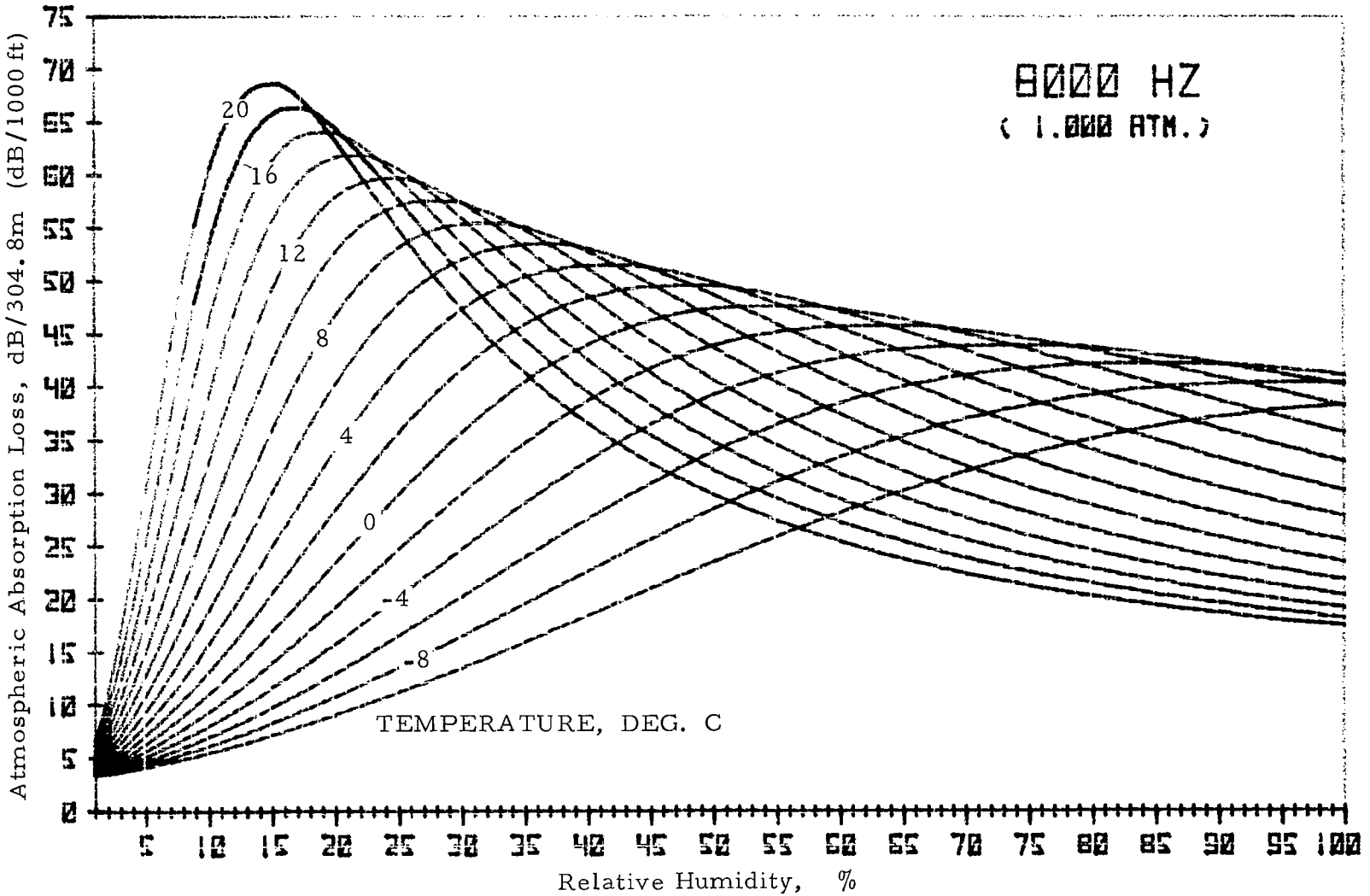

Figure A7. Calculated Atmospheric Absorption Loss, 8000 Hz.

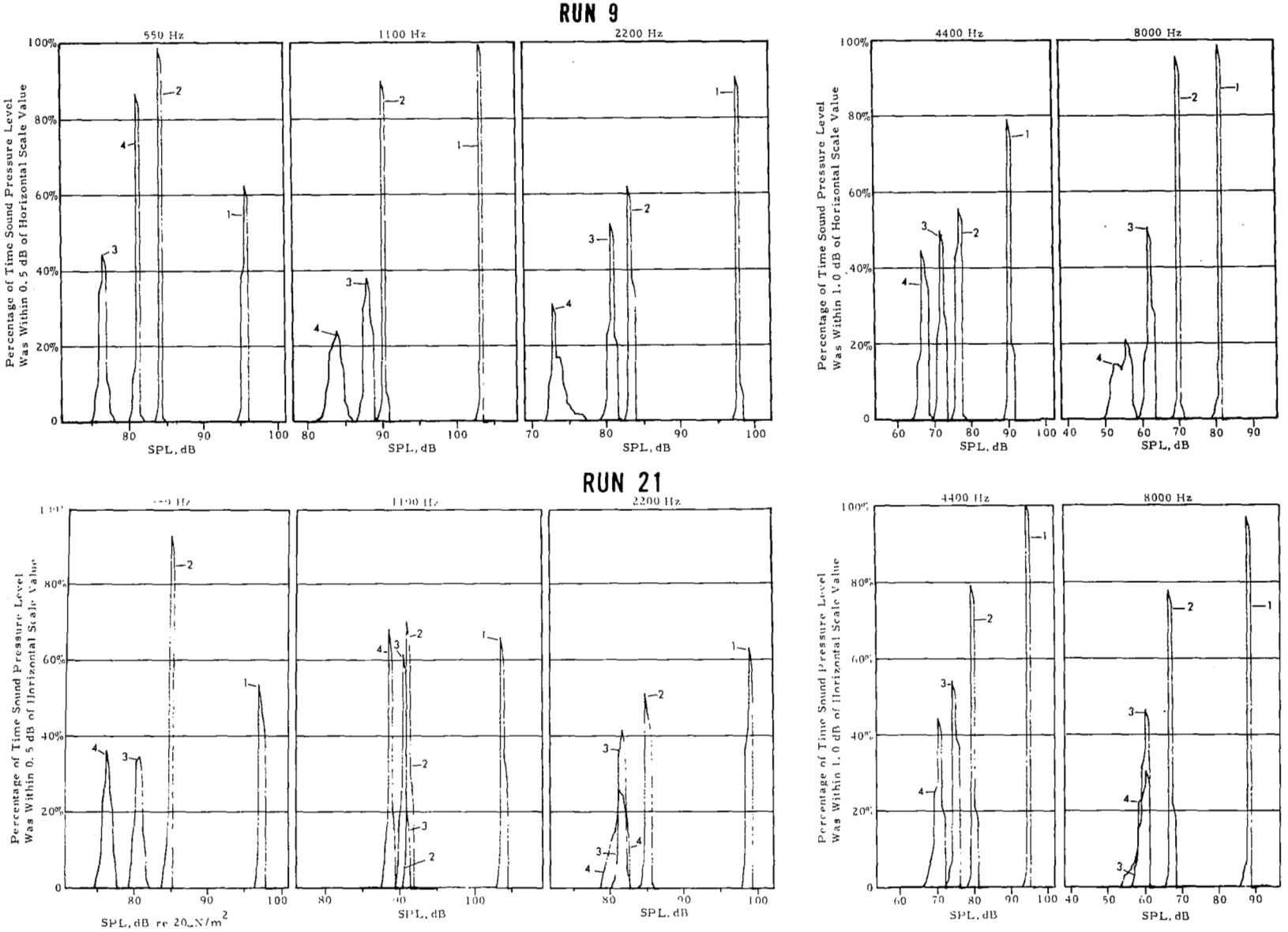

Figure B1. Measured RMS Sound Pressure Level Histograms for Test Runs 9 and 21.

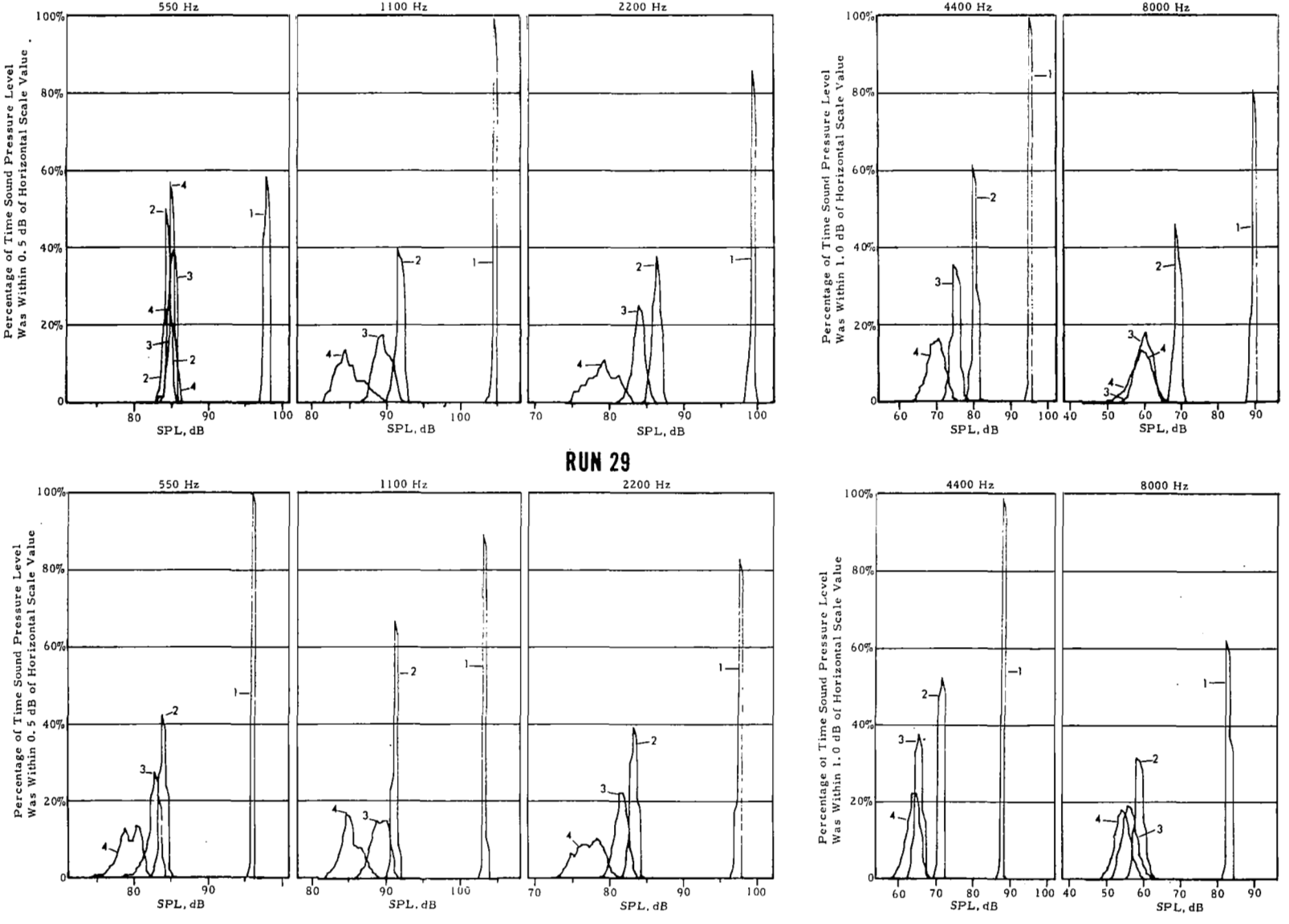

Figure B2. Measured RMS Sound Pressure Level Histograms for Test Runs 26 and 29.

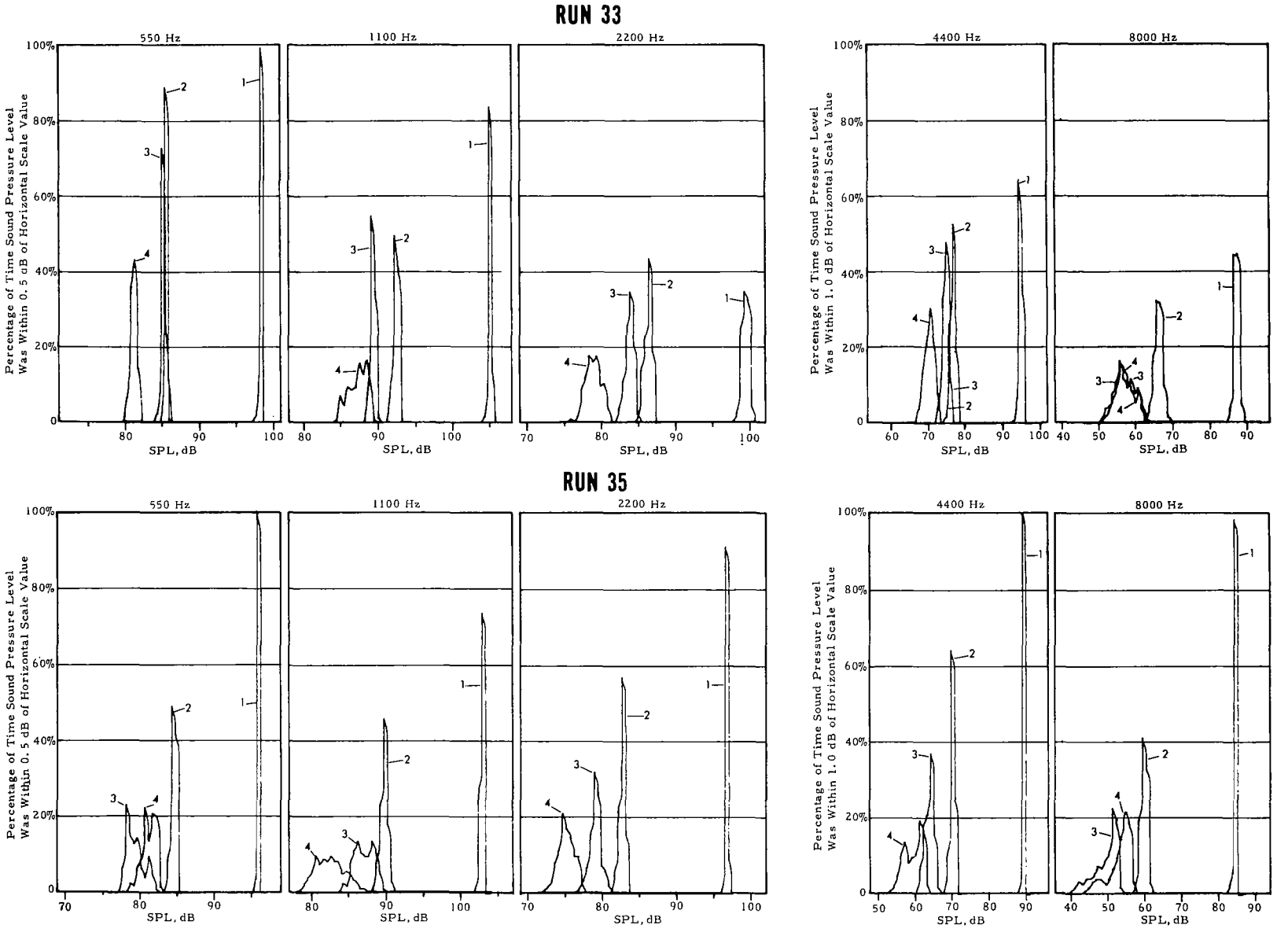

Figure B3. Measured RMS Sound Pressure Level Histograms for Test Runs 33 and 35.

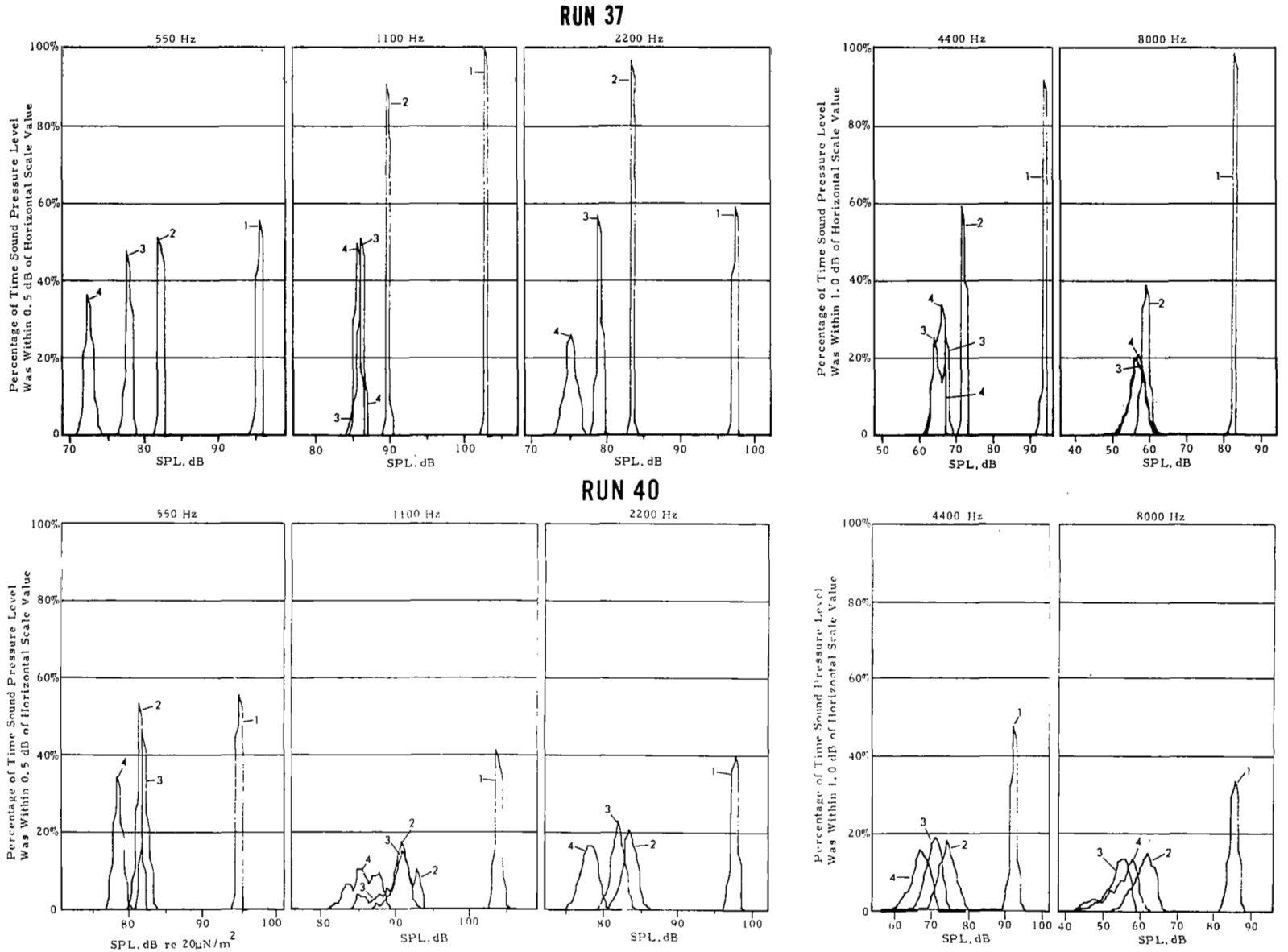

Figure B4. Measured RMS Sound Pressure Level Histograms for Test Runs 37 and 40.

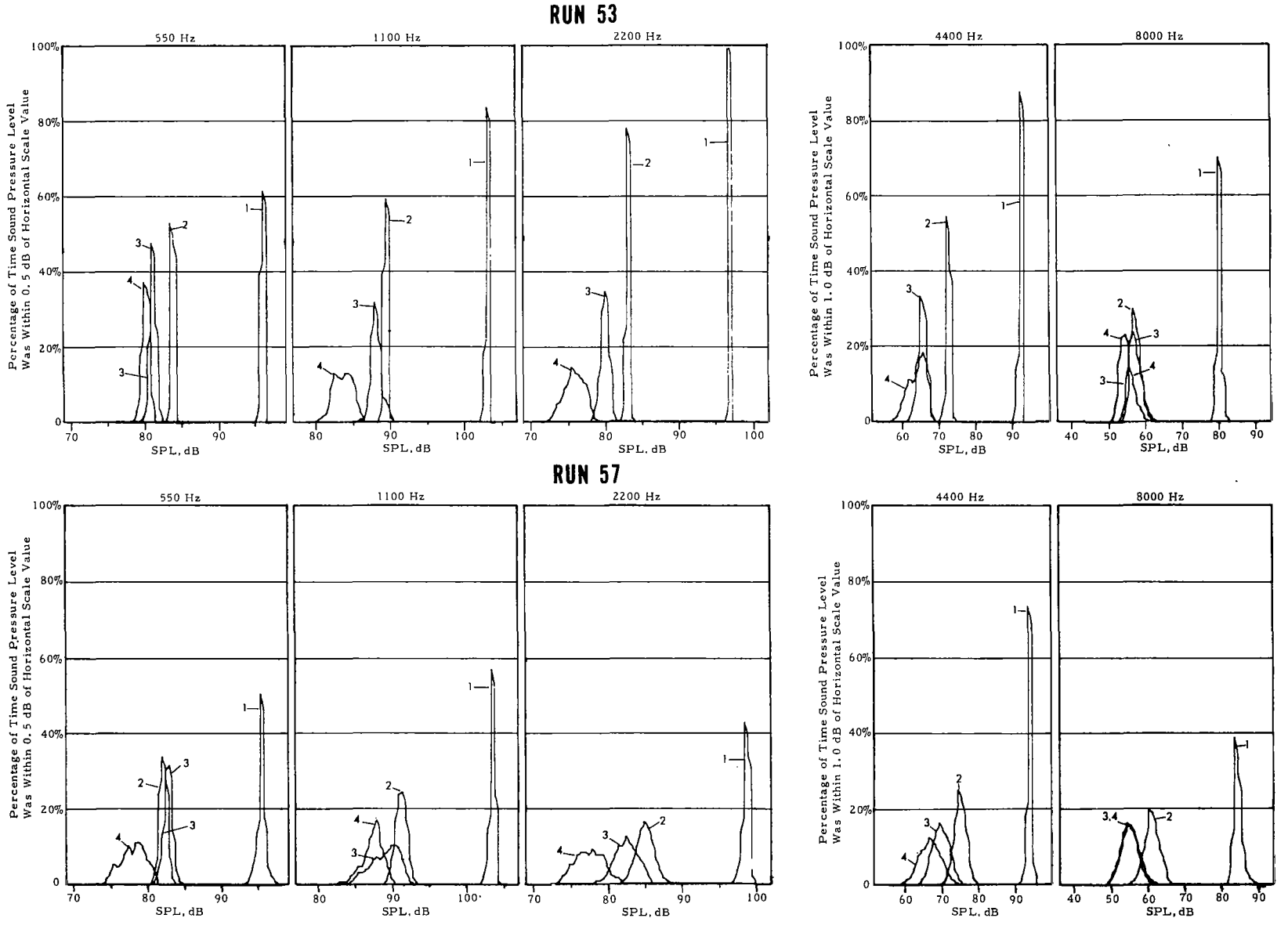

Figure B5. Measured RMS Sound Pressure Level Histograms for Test Runs 53 and 57.